Programmable Surfaces

by

Amy Sun

B.S., Purdue University (1996)
S.M., Massachusetts Institute of Technology (2006)

Submitted to the Program in Media Arts and Sciences
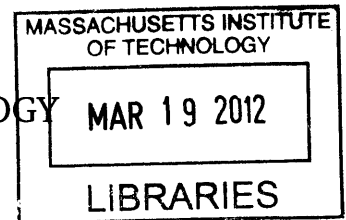in partial fulfillment of the requirements for the degree of

Doctor of Philosophy in Media Arts and Sciences

at the

MASSACHUSETTS INSTITUTE OF TECHNOLOGY

February 2012

Author . . . .
Program in Media Arts and Sciences
October 06, 2011

Certified by . . . .
Neil Gershenfeld
Professor of Media Arts and Sciences
Program in Media Arts and Sciences
Thesis Supervisor

Accepted by . . . .
Mitchel Resnick
LEGO Papert Professor of Learning Research
Academic Head, Program in Media Arts and Sciences

THIS PAGE INTENTIONALLY LEFT BLANK

Programmable Surfaces

by

Amy Sun

Submitted to the Department of Media Arts and Sciences
on October 06, 2011, in partial fulfillment of the
requirements for the degree of
Doctor of Philosophy

Abstract

Robotic vehicles walk on legs, roll on wheels, are pulled by tracks, pushed by propellers, lifted by wings, and steered by rudders. All of these systems share the common character of momentum transport across their surfaces. These existing approaches rely on bulk response among the fluids and solids. They are often not finely controllable and complex approaches suffer from manufacturing and practical operational challenges.

In contrast I present a study of a dynamic, programmable interface between the surface and its surrounding fluids. This research explores a synthetic hydrodynamic regime, using a programmable surface to dynamically alter the flow around an object. Recent advances in distributed computing and communications, actuator integration and batch fabrication, make it feasible to create intelligent active surfaces, with significant implications for improving energy efficiency, recovering energy, introducing novel form factors and control laws, and reducing noise signatures.

My approach applies ideas from programmable matter to surfaces rather than volumes. The project is based on covering surfaces with large arrays of small cells that can each compute, communicate, and generate shear or normal forces. The basic element is a cell that can be joined in arrays to tile a surface, each containing a processor, connections for power and communications, and means to control the local wall velocity. The cell size is determined by the characteristic length scale of the flow field ranging from millimeters to centimeters to match the desired motion and fluidic system.

Because boundary layer effects are significant across fluid states from aerodynamics to hydrodynamics to rheology, the possible implications of active control of the boundary layer are correspondingly far reaching, with applications from transportation to energy generation to building air handling. This thesis presents a feasibility study, evaulating current manufacturing, processing, materials, and technologies capabilities to realize programmable surfaces.

Thesis Supervisor: Neil Gershenfeld

Title: Professor of Media Arts and Sciences

THIS PAGE INTENTIONALLY LEFT BLANK

Acknowledgments

A very recent addition to the Physics and Media group asked how long I've been at MIT. On my reply, which must have seemed like a great long time, she said, "oh, so you did your undergrad here too?" No, I did not. But to have been so long in one place necessarily means contact with a tremendous number of people. I am indebted to so many for their math as well as muscle. At this wonderful place I have been surrounded by supportive, inspirational, and crazy people who persist in spite of the (perceived) absurdity of their projects. Their ideas, encouragement, assistance, and enthusiasm have led me to develop and understand my relationship with the world as an engineer.

Acknowledgements are noted inline with contributions but some fingerprints are not so obvious. In particular: My parents Samuel and Lo-chuan and my extended family whose struggles and successes have fundamentally shaped me. Sherry Lassiter who made it possible to research from far, far away and to come home again when it was necessary; she is all of these: travel agent, shipping agent, travel companion, editor, student, teacher, friend. Amon Millner who leads by example, taught me about people and communities, and who has conspired with me to take over the world through access and education. Keith Berkoben who not only put up with but even shared in my crazy, especially the stuff too tall for me to reach, while taking pictures the whole time. Paul Scearce who has stood sentry between me and the real world, offering encouragement to finish while allowing great leeway to pursue my every whim. Everett who continues to be an amazing source of unbounded happiness and energy, ever patient and uncomplaining.

I am especially grateful to my thesis committee for their time, guidance, and patience; in addition to my thesis supervisor Neil Gershenfeld, they are John M. Deutch (an institute professor who shaped my study on energy systems), John W. M. Bush (Mathematics), and Alexandra H. Techet (Ocean Engineering), all from MIT. In addition, Mark Drela from MIT's Aeronautics and Astronautics Department must be recognized as a virtual committee member although he is not recorded as a formal reader. Each visit with him was a high data rate burst of aeronautical engineering and his insights made this thesis more robust and interesting.

THIS PAGE INTENTIONALLY LEFT BLANK

Thesis Reader

John Deutch is an Institute Professor at the Massachusetts Institute of Technology. Mr. Deutch has been a member of the MIT faculty since 1970, and has served as Chairman of the Department of Chemistry, Dean of Science and Provost. Mr. Deutch has published over 140 technical publications in physical chemistry, as well as numerous publications on technology, energy, international security, and public policy issues.

Professor Deutch's research applies statistical mechanics to equilibrium and time dependent problems in physical chemistry. Emphasis is placed on developing techniques that permit the quantitative understanding of a wide variety of phenomena. Three distinct areas of research are under investigation. One area is the theory of dilute and concentrated polymer solutions with attention placed on understanding the frictional properties of these solutions, for example, diffusion and viscous flow. A second area of interest involves two-dimensional chemistry. This work includes study of the chemistry that takes place in constrained environments such as at fluid interfaces, inside cells, and in liquid crystal solvents, where the environment influences both the equilibrium distribution of particles and their dynamic motion. The third area concerns the theory of diffusion controlled reactions.

Read by:

John M. Deutch ....

Institute Professor
Department of Chemistry
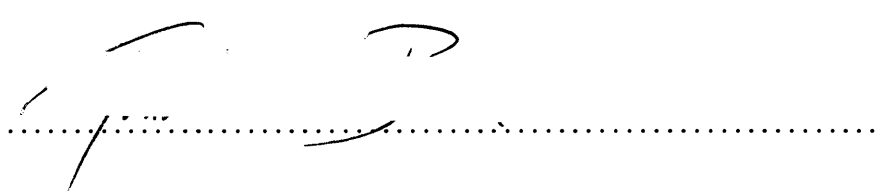Massachusetts Institute of Technology

THIS PAGE INTENTIONALLY LEFT BLANK

Thesis Reader

John Bush is a Professor of Applied Mathematics in the Department of Mathematics. He is interested in fluid dynamics problems that may be readily observed in a laboratory setting. His approach involves interplay between experimental and theoretical modeling techniques, and is focused towards identifying and elucidating new fluid dynamical phenomena.

Professor Bush's three principal research areas are Geophysical and Environmental Fluid Dynamics, Surface Tension-Driven Phenomena, and Biofluidynamics. He has over 60 publications and has been featured on the cover of Nature.

Read by:

John W. M. Bush..

Professor of Applied Mathematics

Department of Mathematics

Massachusetts Institute of Technology

THIS PAGE INTENTIONALLY LEFT BLANK

Thesis Reader

Alexandra H. Techet is an Associate Professor of Mechanical and Ocean Engineering at the Massachusetts Institute of Technology. Her research focuses on experimental hydrodynamics with naval applications and has been recognized by several APS Gallery of Fluid Motion Awards, and featured in a Discovery Channel episode of "Time Warp", as well as on the cover of Journal of Fluid Mechanics.

Professor Techet's research into multifaceted hydrodynamic phenomena has direct implications on the design of vessels and structures operating in the ocean, as well as other areas of fluid dynamics. Her work employs non-invasive two- and three-dimensional flow measurements and visualization methods coupled closely with theoretical modeling to yield improved insight into designing biologically inspired underwater vehicles, ocean surface vessels and offshore platforms, as well as ballistic projectiles for defensive weapon systems.

Read by:

Alexandra H. Techet..

Associate Professor

Department of Mechanical Engineering

Massachusetts Institute of Technology

11

THIS PAGE INTENTIONALLY LEFT BLANK

Contents

List of Figures

List of Tables

From Volumes to Surfaces

Chapter 1

Introduction

A *programmable surface* is a wall that can be dynamically commanded at arbitrary resolutions finer than the bulk motion of the entire wall. The surface may interact with another solid or a fluid. When in contact with other solids, the programmable surface may be used for mobility, eg, sliding over terrain, or the manipulation of objects across the surface, eg, a robotic floor. When interfacing with fluids the programmable surface can dynamically alter the flow around the object. This largely unexplored fluid dynamic regime has implications in drag reduction, controls without control surfaces, conformal means of propulsion, and synthetic geometries, leading to novel form factors, noise reduction, and the ability to create unnatural flow fields.

Programmable surfaces are an extension of work being done in programmable matter. Reconfigurable robotics, a subset of programmable matter that seeks to make self-reconfiguring volumes, has been progressing in the last decade to address the complete tool chain required to produce reconfigurable robots. Although there are several implementation schemes, all of the approaches must address geometry deconstruction and assembly planning, goal mapping and programming, internal and external communications, intra-node actuators and mechanisms, and power sources. At the moment, the cost and complexity of manufacturing, the necessarily large numbers of nodes to construct large objects at fine resolutions, and the density of forces required to move adjacent nodes with respect to each other have limited physical investigations to relatively small numbers of macro-sized parts. In contrast to reconfiguring volumes, pro-

grammable surfaces are only concerned with the interface of the outside edge of the object. There is no rearrangement of the internal volume of the object.

The approach to programmable surfaces implementation is similar to programmable materials. The surface is divided into small cells or nodes, each with the means to interface with the nearby fluid, computation, communications, and power. Nodes are arranged side-by-side in arrays and are connected to each other mechanically in a manner than may allow the entire array to flex. The nodes are individually addressable and controllable so that each can create a different surface velocity. The combined effect of cells working together is to alter the apparent stream lines of a fluid flowing about the solid object. The net result is the ability to set an arbitrary wall velocity at a small patch on a surface. When a flow is present over the surface, the surface no longer appears to be a simple fluidic "stick" condition but an alternative boundary layer between the free stream and surface is created.

In comparison to programmable matter, programmable surfaces are easier to realize with today's technological capabilities because substantially fewer number of nodes are required to cover the surface area of an object (rather than fill its volume) and allows for larger feature sizes (because resolutions required are much larger).

While techology and manufacturing are not quite ready to produce gallons of programmable materials to enter mainstream usage, this thesis presents a feasibility study of creating programmable surfaces using current manufacturing capabilities and technologies. I review recent advances in distributed computing and communications, actuator integration and batch fabrication for the sizes and quantities required to make significant impacts in energy efficiency, recovering energy, introducing novel form factors and control laws, and reducing noise signatures.

Chapter 2

Background

Programmable surfaces is an extension of work in programmable matter. It is a novel technology that builds upon recent progress in several key areas.

Fully realized, programmable matter is the *stuff* of science fiction. On command, it changes from something to something else. Sometimes it is self-aware, sometimes it is commanded remotely. A key characteristic of programmable matter is the ability for the material to respond to inputs by transforming shape or changing its other physical properties.

Toffoli and Margolus are credited with coining the term *programmable matter* to describe a "three-dimensional, uniformly textured, fine-grained computing medium" [55]. Rather than a collection of passive molecules, programmable matter is composed of uniformly interconnected identical computers, capable of data handling and processing. This synthetic "material" has bulk properties which are invariant to the amount (or number) or computers involved. Toffoli and Margolus' definition in 1991 called out four properties of programmable matter: 1) the material can have arbitrary size and infinite extensibility, 2) the interconnections among the computing units are capable of dynamic reconfigurability, 3) the programmable matter can be interactively driven by an external operator or event, 4) the operation of the programmable matter offered complete access to real-time observation, analysis, and modification.

The first hardware implementation of programmable matter was CAM-8, was a uniform, scalable, parallel computation machine intended for use as a general purpose

lattice-gas or similar simulations [33]. Physically, the CAM-8 machine was a Sun work-station host controlling STEP modules plugged into a common bus. In short, it was physically a "box" rather than itself a "material".

A 2004 Defense Advanced Research Projects Agency (DARPA) program investigating programmable matter emphasized the *physical* notion of physical matter. From the solicitation, programmable matter was defined as "[a] material that can perform several operations in sequence: upon activation by an external signal, decode and propagate instructions; translate information into action, transport particles and assemble shapes; interlock particles to form an object; perform error-checking and encode final state information, again activated by external signal; and disassemble into the starting material."

Programmable matter is often envisioned to be composed of millimeter or smaller scale microsystems, including speculation on programmably organizing quantum dots to emulate different materials from an atomic level[34]. A particularly active subset of programmable matter research is *reconfigurable robots* which can both change shape as well as move. Work in this area is generally focused on constructing large quantities of scaled-up elements which are connected through a variety of force mechanisms such as magnetic, electrostatic, or geometric latching. The term has become generally accepted to refer to a universal material which can be commanded to change its physical properties, in particular its mechanical properties such as shape. More recently, programmable matter is often described as a fundamentally "digital" material having computation, sensing, actuation, and display. Furthermore, these properties are continuous and commandable throughout the medium. DARPA's Programmable Matter effort[1] today "represents the convergence of chemistry, information theory and control into a new materials design paradigm - 'InfoChemistry' - that focuses on building information directly into materials". Infochemistry and its successor program, *Maxmimum Mobility and Manipulation*[2], renewed the emphasis on the reversibility of material assembly, analogous to Toffoli and Margulos' requirement of reconfigurability.

---

[1]http://www.darpa.mil/Our_Work/DSO/Programs/Programmable_Matter.aspx

[2]DARPA Maxmimum Mobility and Manipulation (M3) is the program under which a part of this research was funded.

In most cases, approaches aim to manipulate volumes rather than surfaces. In practice, significant challenges remain, in particular to shrink the size of computation, power electronics and force actuators. The smallest programmable matter nodes are approximately 1 cm in dimension[19] and their manufacturing complexity and cost have precluded creating large numbers of nodes sufficient for the "buckets of parts" vision[3]. To form volumes, nodes must be concerned with linkages and interactions in every direction surrounding them (i.e., for a cube-shaped node, there must be essentially six sets of sensors and bonding elements). Programming surface motion rather than volumetric shapes is an easier goal because there only needs to be interaction of the "outside" surface that is in contact with the fluid. Even if the overall cell size is the same, internal feature sizes can be larger. Additionally, as the size of the object grows, a much smaller number of nodes is required to cover the surface area rather than fill the volume. This allows us to make larger objects more quickly because fewer nodes need to be manufactured and assembled.

Toffoli and Margolus's CAM-8 machine was a step along the path to realizing universal computation using cellular automata. Dating from the 1940's, *cellular automata* is a discrete model of system dynamics comprised of discrete cells, arranged on a grid, with states that simultaneously update based on rules affected only by neighboors. CA's can be used to model many different physical processes including fluid dynamics. Furthermore, the models can be increased to cover more volume by expanding the size of the lattice.

As it becomes increasingly difficult to ensure that all sections of the lattice are updated at the same time, an asynchronous design becomes necessary; this is an *asynchronous* cellular automata. An "asynchronous *logic* automata" is a specific kind of ACA which is scalable like all ACAs but designed so that its behavior is always deterministic. As with CAs, the computational structure of an ALA mirrors its physical structure. Since computing modules are assigned to physical modules, there is a link between the

---

[3]For Butera's 2002 *Paintable Computer* paintable display, 1000 macroscale nodes were created and demonstrated. Each node had a light sensor, light emitting diode (LED), processing, and IR communication with neighboors. Although this demonstration involved a very large number of working nodes, they were 3.4 cm devices intended to represent 1 mm "particles" [7, 28].

network topology and physical topology.

With programmable surfaces, cells also have control of an actuator which can interact with adjacent fluid. These cells define a surface that is the same shape as the fluid so that the computational architecture mirrors the physical system. This approach is immediately scalable in number and portable across technologies. The following thesis investigates the maturity of current technologies and processes required to realize a programmable surface.

Programmable Surfaces

Feasibility Studies

Feasibility studies contents:

As with other programmable matter approaches, we expect to construct the programmable surface from many small cells or nodes. Although the implementation calls for a great number of nodes, each node is identical and simple. The aggregate effects of a large number of simple nodes can create a complex fluidic response; we need to understand streamwise fluidic coupling, thrust output and wake profile for these simple nodes when arrayed together.

Before we set about constructing a large scale object, we take a broad look at previous work in the target application areas, noting extensive literature in drag reduction and propulsion methods. These works typically considered larger size elements and much smaller numbers of actuators. Based on these works we make some estimates on expected behavior and performance of distributed surface actuators and when appropriate validate or investigate with benchtop experiments.

Chapter 3

Propulsion: Scaling and Wake Interactions

The general idea of adding more propulsive devices to a vessel to propel it more swiftly might well have been discovered before the wheel - simply put, two hands paddling are better than one. The focus of this section is the aggregate effect of many propellers operating together. It may seem intuitive that adding propellers with matched engines to a vessel would increase the total net thrust, but as there is an accompanying power draw, weight and volume increase (and thus more surface area for drag), the scaling laws governing multiple propellers is not immediately clear.

Other approaches to increasing output thrust are to increase the speed of rotation of the propeller (by adding power to turn the motor faster) and increasing the size of the propeller (which requires increasing the torque provided by the motor). In practice, aeronautical engineers have implemented combinations of all the above approaches. For example, most modern aircraft today have two or four very large propellers or jet engines and fuel is throttled to each engine.

The classic image of powered flight is a vessel with a single large propeller; a helicopter with a single rotor or a power boat with single engine and propeller. Instead of a single large propeller, distributing the propulsion system can lead to a long list of benefits: dynamic scalability, increased stability, (re)configurability, robustness, fault tolerance, increased safety for other aerial vehicles, a better balance of verical lift and

directional flight efficiency, reduced structure and less bending moment, noise abatement, simpler maintenance, and cheaper and simpler manufacturing. While this section is concerned with the technical performance of using multiple propellers, these benefits of a distributed propulsion system may outweigh any technical performance inefficiencies as compared to other approaches.

Distributed Propulsion

"Distributed propulsion" (DP) is a category of powered flight propulsion system for fixed wing aircraft in which airflows and forces are distributed about a vessel. Its goal is to increase performance in fuel efficiency, emissions, noise, field length, and handling performance as compared to the use of a single large engine, jet, or propeller. DP is typically accomplished by spanwise distribution of partially or fully embedded multiple small engines or fans across the width of wing. It may instead employ ducting of exhaust gases along the entire trailing edge of a wing.

Recent analytic and experimental distributed propulsion studies suggest several improvements in aircraft performance[13]. These include fuel consumption efficiency, noise abatement, steep climbing for short take off and landing (STOL), novel control approaches (in particular eliminating control surfaces for roll, pitch and yaw moments), and high bypass ratios. It has also been suggested that smaller propulsors will be cheaper to manufacture and easier to handle during assembly and maintenance.[27].

Any fixed wing aircraft with more than one propulsor can be considered a distributed propulsion aircraft. However, in common modern usage DP describes a propulsion system scheme with distributed exhaust, a large number of distributed engines (typically fully or partially embedded within the wing), or a large number of distributed fans with a common core[21]. These implementations are often proposed in conjunction with blended wing body (BWB) or hybrid wing body (HWB) aircraft.

Implementation approaches include jet flaps, transverse or cross-flow fans (CFF), multiple small engines (typically gas turbines), or multiple fans driven by a smaller number of engine cores. In the last case, the power transmission between the fans

and engines may be linked by ducting hot gas [1], mechanical gears[12, 23], or electric power lines[26].

While some of these concepts were tested on full scale aircraft in the 1960 - 1970's, such as the Hunting H.126, they were not fielded in production aircraft. More recently, several full-size and smaller unmanned aerial vehicle (UAV) projects have proposed DP approaches to meet noise abatement[22], fuel efficiency, and field length goals. Advancements in materials engineering, cryogenic cooling systems, novel fuels[50] and high fidelity computational fluid dynamics (CFD) modeling and analysis[10] have been credited for the renewed interest in DP approaches.

Conformal propulsion

The "conformal propulsion" vision is to replace large propellers with many smaller propellers, to the extreme of replacing the entire surface of a vessel with propellers. This allows completely novel airframe and hull designs and missions. Although the implementation calls for a great number of nodes, each node is identical and simple. The aggregate effects of a large number of simple nodes can create a complex fluidic response; we need to understand the thrust output and wake profile for simple propulsion blocks when arrayed together. This chapter investigates these effects.

The ideal actuator disk

First we need a basic relationship between the power input and thrust output of a generic propeller. This relationship depends on the density of the fluid, the propeller's diameter, geometry, and rotation speed. Our analysis is a mathematical exercise of scaling trends and not meant to be concerned with specific motor or propeller designs, so we can use the actuator disk model of an ideal propeller to relate the power and thrust force with propeller velocity and geometry.

---

[1] Some authors note in particular, Winborn, B. 'The ADAM III V/STOL concept', American Institute of Aeronautics and Astronautics 69-201 (1969)', which I have not been able to obtain.

The historical interest in developing a theory of propellers dates from the industrial revolution when screws were fitted on to ships. In 1865 Rankine proposed a theoretical basis for estimating the efficiency of a propelling screw given only the density of fluid (seawater, in his case) and the coefficient of friction of the fluid against the rotating disk blades[49], with high agreement from experimental data from two ships. More than 30 years later Froude described the infinitely thin "actuator disk" where "the whole of the acceleration takes place without the propeller; which last, so far as the water is concerned, may be regarded simply as an advancing surface of instantaneous change of pressure"[15]. Froude attributed half the additional speed imparted on the fluid to occur before the disk and half in the region after while considering the entire aperture disk to be uniform.

Although the initial application of propellers was hydrodynamic, by the first quarter of the 1900's the model of the ideal aperture disk generalized for different fluids (in particular, water of different densities and air) and was refined by viewing each blade as a separate lifting surface modeled as a wing [11]. Prandtl additionally refined the model with the lifting line wing theory which incorporated vorticity along the lateral length of a finite length wing[56]. The generalized actuator disk model is based on solving the Navier-Stokes or Euler equation with or without finite discretization of the volume and models continue to be improved for various solution methods.

The ideal actuator disk (see figure 3-1) is a theoretical abstraction used to analyze a simple flow that produces or is the result of a force on the disk. It is an infinitely thin device with force uniformly distributed about its area and through which there is a sudden jump in pressure. Although there is a discontinuous jump in pressure, the mass crossing the plane of the disk must be conserved so we can use conservation of momentum methods to relate the thrust force on the disk with the additional speed in the fluid.
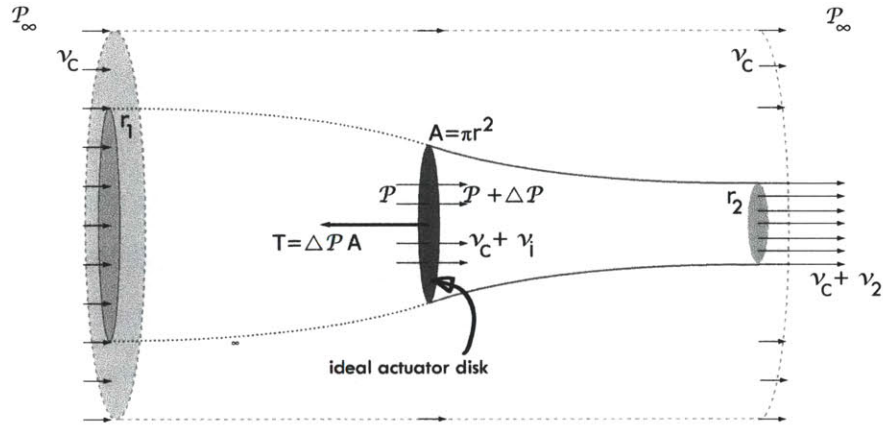
Figure 3-1: Sketch of an ideal actuator disk. r = radius, $\mathscr{P}_\infty$ = ambient pressure, $\Delta\mathscr{P}$ = pressure change, T = thrust force, v = velocity

Power and thrust for an ideal actuator disk:

(Rankine-Froude actuator disk theory)

$$T = \frac{1}{2}\rho c_T A(\omega r)^2 \qquad (3.1)$$

and

$$P = \frac{1}{2}\rho c_P A(\omega r)^3, \qquad (3.2)$$

where

ρ is the density of the operating fluid,

c_T is the dimensionless thrust coefficient,

c_P is the dimensionless power coefficient,

ω is angular speed,

r is the propeller radius, and

A is area which is swept out by rotation of the propeller about the motor shaft.

The programmable surfaces approach to scaling is to use many propellers and motors of a reasonable size and complexity to increase thrust. Instead of increasing the rotation speed ω or increasing the propeller length r, this approach fixes speed and size and only varies the number of propulsive units. (For flight controls, the programmable surface would likely vary propeller speeds within some range of efficient motor operation. However for this analysis we only want to examine thrust output.)

If there is some thrust force T for a give power input P with one motor-propeller unit, we would expect that an identical motor-propeller unit will also generate T thrust for P input. Adding more units does not change the rotation speed (ω), propeller geometry or size. Thus,

$$\boxed{P \propto T} \tag{3.3}$$

There is no apparent scaling limit for this approach, though there may be practical operational constraints such as available surface area for flight or landing. Additional possible scaling limitations include power distribution degradation over long distances and practical command and control of the flying sheet. Power distribution losses and aggregate effects of multiple wakes could degrade the performance efficiency. Section 3.2 describes a benchtop experimental validation of the linear scaling and investigation in these effects.

At the outset it wasn't clear what would happen when we put several spinning propellers together[2]. In section 3.1-3.5 I experimentally investigate,

- Section 3.2: Is there a linear scaling of thrust and power as units are added?
- Section 3.3: Do units positively help or negatively interfere with each other?
- Section 3.4: Is this effect exclusive to the spiral-shaped wakes from propellers?
- Section 3.5: For a set number of units, are there more or less beneficial geometrical configurations, especially in forward flight?

The conclusion from the experiments show that adding more units generate more

---

[2]I was unable to obtain a copy of a paper describing numerical simulations showing constructive wake interaction of multiple counter-rotating blades arranged coaxially and operating at Reynolds number of 200[51].

thrust, so that thrust output grows linearly with power input. This validates our expected behavior. Nonobviously, closer packing of units so that their wakes overlap generates more thrust, and as the forward speed increases greatly compared to the downward speed, a span-wise transverse layout of units generates significantly more thrust than other geometries.

3.1 Experimental Scaling Investigations

The goal of the benchtop experiments is to validate linear scaling when adding more propellers and to investigate interference effects of propeller spacing and layout. The exemplary embodiment of the nodes are a propeller directly coupled to an electric motor (along with some power electronics, computation, and communications circuitry), so the scaling law analysis models the same. A single propeller-motor pair is characterized in section C then additional propeller-motors are added in section 3.2. The interaction of wakes are recorded in section 3.3 and I discover that laying out the propeller-motor pairs in a line transverse to flight yields greater thrust in section 3.5.

This investigation began by characterizing a single propeller-motor pair. The intent of the benchtop investigation is to find the aggregate effects of several propeller-motors working at the same time rather than find, design, or acquire custom propellers. I matched a commercially available hobby propeller to a commercially available hobby motor. Because the experiments call for a large number of units, availability, cost, and simplicity of control were a consideration in selecting the brushed DC motors. Plastic hobby propellers in smaller diameters are offered in inch increments starting around 2 inches and available in one spin direction. The procedure to select and characterize the propeller-motor pair is: 1) Search for a reasonably priced, small, high speed brushed DC motor; 2) Experimentally match the motor with a small selection of commercially available propellers; 3) Characterize the propeller-motor pair to find the thrust coefficient (C_T) and power coefficient (C_P) of the pair. The motor and propeller used in the experimental work of this section is described in detail in Appendix C, in particular, see figure C-5 for a graph of C_P vs C_T.

For an experimental investigation of the effects of multiple propellers, I selected a matched propeller and motor pair (see Appendix C) and mounted seven pairs in various layout configurations (figure 3-2). The various configurations were intended to isolate or allow interaction of propeller wakes, and to align the propellers streamwise along or transverse across the direction of forward flight.

I measured input electrical energy and output thrust for different propeller rotation

speeds to characterize efficiency. I also recorded wind velocity profiles to visualize wake interactions. The configurations are shown in figure 3-2. Wind velocity profiles were recorded with a hot wire anemometer described in section B.2 and rotational speed was measured using a non-contact tachometer described in section B.3.

To evaluate the effects of different layout geometries, I selected a few layouts which were unambiguously different, near the extremes of their axes of configuration. Figure 3-2 shows the test geometries created from seven (7) propeller-motor units. A symmetric layout are the hexes in Figure 1a. While the frames are hexagonal, the propellers trace out circles which are packed into a larger circle. For clarity I refer to this test shape as a hexagon or hex but it should be understood that as the number of units grow in this layout the conglomerate shape comes closer to a circle. The units in Figure 1a-1 have minimal spacing, just enough to prevent propellers from hitting each other, which in Figure 1a-2 the spacing is increased significant by more than the diameter of one propeller. This pair of geometries will allow us to investigate the coupled effects from adjacent propellers.

The pair of layouts in Figure 3-2b maintain the same uniform spacing as the smaller hex in Figure 3-2a-1 but the units are arranged so the composite object is transverse to the flow (ie, maximally "wide and short", or streamwise (ie, maximally "skinny and long". This pair is used to gain intuition on the effects of frontal area exposed in the direction of flight.
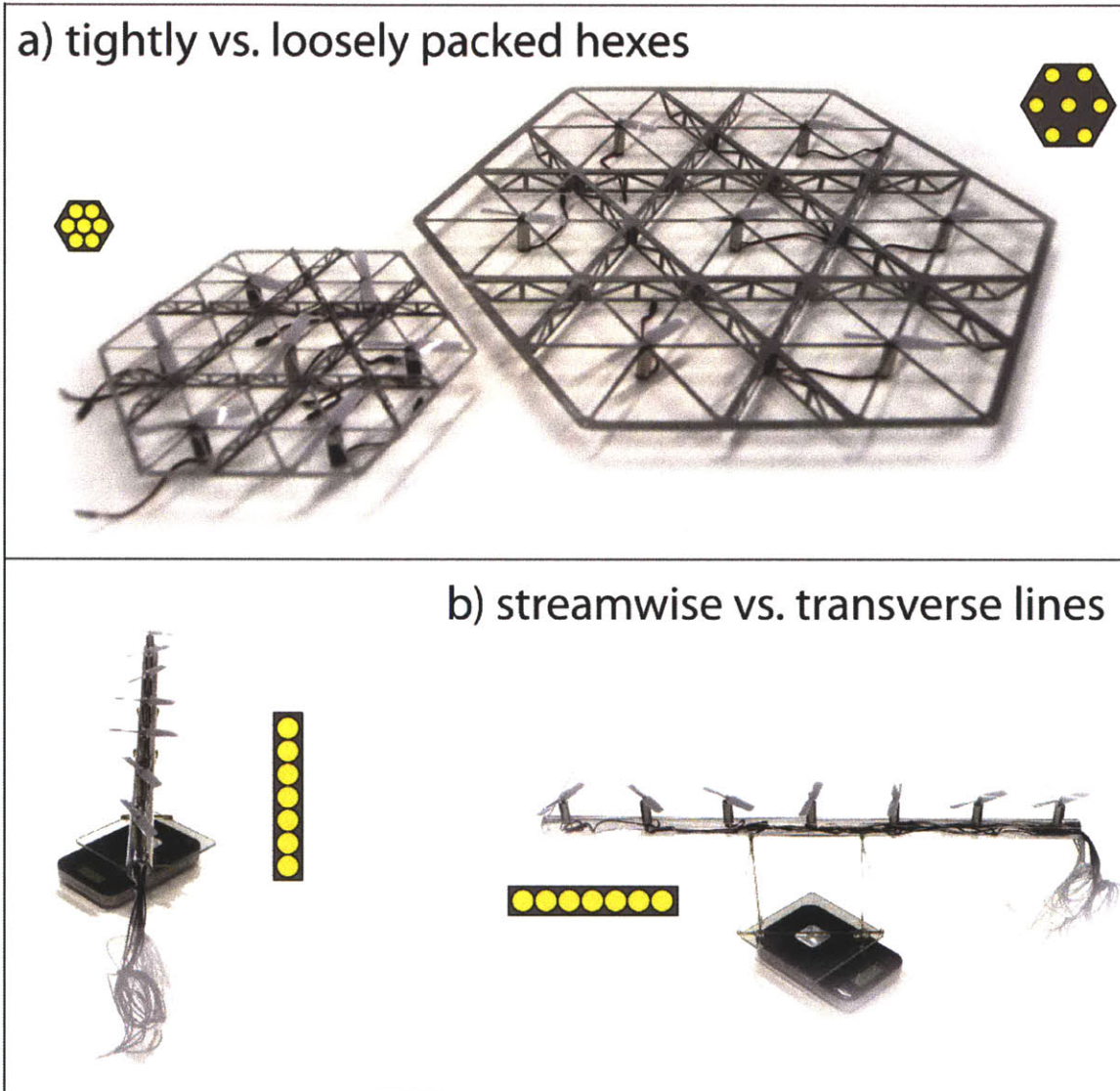
Figure 3-2: Test geometries. a) Propeller centers are laid out as if inscribed in a larger circle. b) Propellers are arranged in a line.

3.2 Linear scaling in hover

The effect of adding more units is comparable to an example with helium balloons. If one helium balloon provides L lifting force, adding another identical balloon is expected to result in a total of $2 \times L$ lifting force. Thus, the expected scaling is $nP = nL$. Propeller-motor units are expected to add similarly, as discussed in section 3. If power to each motor is held constant, we should observe equal thrust increments as new units are added. Interaction effects of neighboring propellers are not yet considered in the following experimental validation of a linear scaling law. The results in table 3.1 summarize the findings as units are added. They are consistent with linear scaling.

With the propellers spaced more than 1 propeller diameter apart, each motor was supplied with constant power. The total average thrust, thrust per watt, and thrust per unit are tabularized in Table 3.1. Inspecting the last two columns shows that there is a linear scaling effect on thrust with the number of units added and power expended.

Number of Units	Total Power (W)	Average Thrust (g)	Average Thrust (g) per Watt	Average Thrust (g) per unit
1	4.5	23	5.1	23
2	9.0	48	5.3	24
3	13.5	72	5.3	24
4	18.0	97	5.4	24.5
5	22.5	121	5.4	24.2
6	27.0	144	5.3	24
7	31.5	163	5.3	23.3

Table 3.1: Linear scaling of thrust with number of units added and power expended.

This experiment was repeated at several speeds. Propellers are noisy devices and thrust readings could vary as much as a couple of grams. Small manufacturing differences among the motors are to be expected which vary motor performance, in particular the resulting RPM for a given voltage level. Despite these sources of error, the plots in figure 3-3 show the addition of propeller-motor units is consistent with a linear scaling.
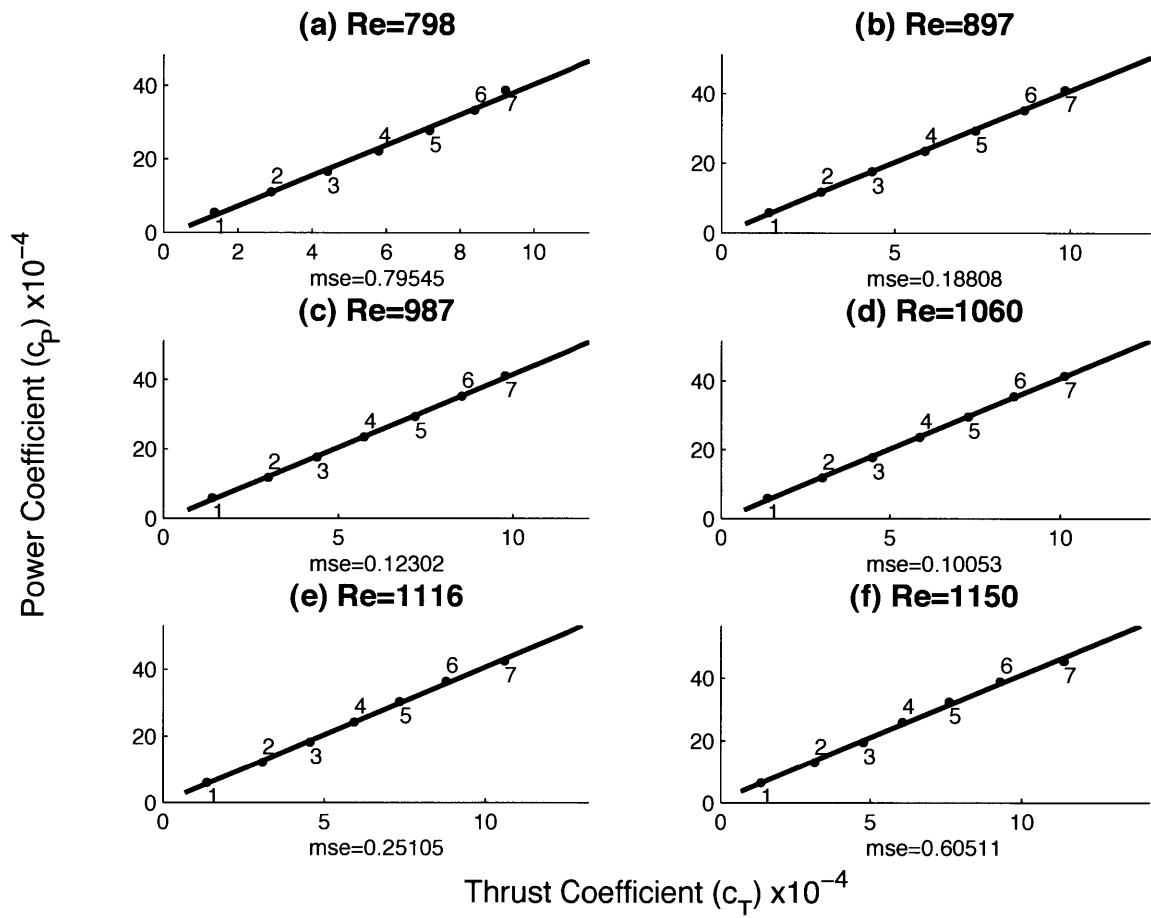
Figure 3-3: The addition of propeller-motor units at several speeds is consistent with a linear scaling. The numbers indicate the number of propeller-motor units active. Reynolds number is calculated using average propeller chord.

3.3 Interaction of propeller wakes

Although wind speed is fastest directly in front of a fan, wind is created outside of the imaginary cylinder projected from the circle traced out by the propeller tips. If I have multiple propellers, do I want to locate them far enough apart so that their wakes don't interact, or instead place the propellers closer together so that their wakes combine?

Measuring wind profiles of tightly and loosely packed hexes and comparing their thrust outputs reveals if either configuration is more effective. Figure 3-4 shows the velocity profiles of both hexes for a constant power per motor. The profiles shown were captured at a distance 11.25 inches away from the centerline of the propeller. They are a cross-section (as indicated by the dotted line on the hex-icons) and only measure the normal component of the wind generated; that is, the speed of air traveling in the direction perpendicular to the plane of the propeller. The velocity data was captured using a commercial hot wire anemometer mounted on a track so that the sensor was cantilevered above the propeller and could be accurately positioned in a plane parallel to the propeller. For more details on the instrumentation setup and experimental procedures, see appendix B.

Comparing figure 3-4b and figure 3-4c it is evident that a tightly packed arrangement leads to a more uniform velocity profile with a single broad peak while the loosely packed arrangement resulted in several distinct peaks. The same curves are overlaid for comparison in figure 3-5. We might suspect that there are shearing losses in the slower regions between propellers in the loosely packed hex (figure 3-4c) where the differences in fluid speed result in dissipative losses rather than contribute to useful work.

We now experimentally compare the thrust output of a tightly packed geometry to a loosely packed geometry. The two array configurations were attached to a scale that measured with a resolution of 0.1 grams. The motors and propellers were mounted such that they pushed down onto the table and the motors were on the intake side of the propellers. The assembly was mounted more than 3 propeller diameters from the
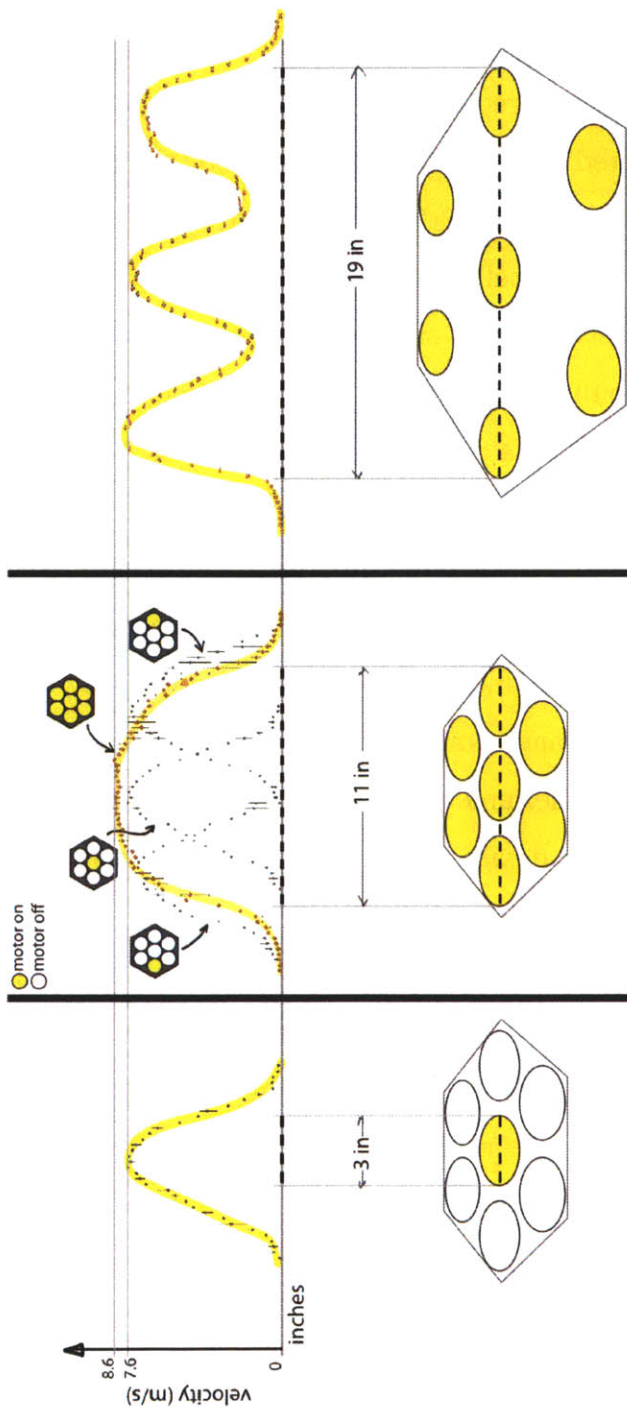
Figure 3-4: Combined effects of multiple units. (a) Velocity profile of one propeller. (b) Gray circles are profiles of propellers running one at a time. Yellow curve is the velocity profile with all motors on in a tight packing. (c) Velocity profile of all propellers running at once in a loose packing. Figure 3-5 overlays the yellow highlighted aggregate velocity profiles of (b) and (c).
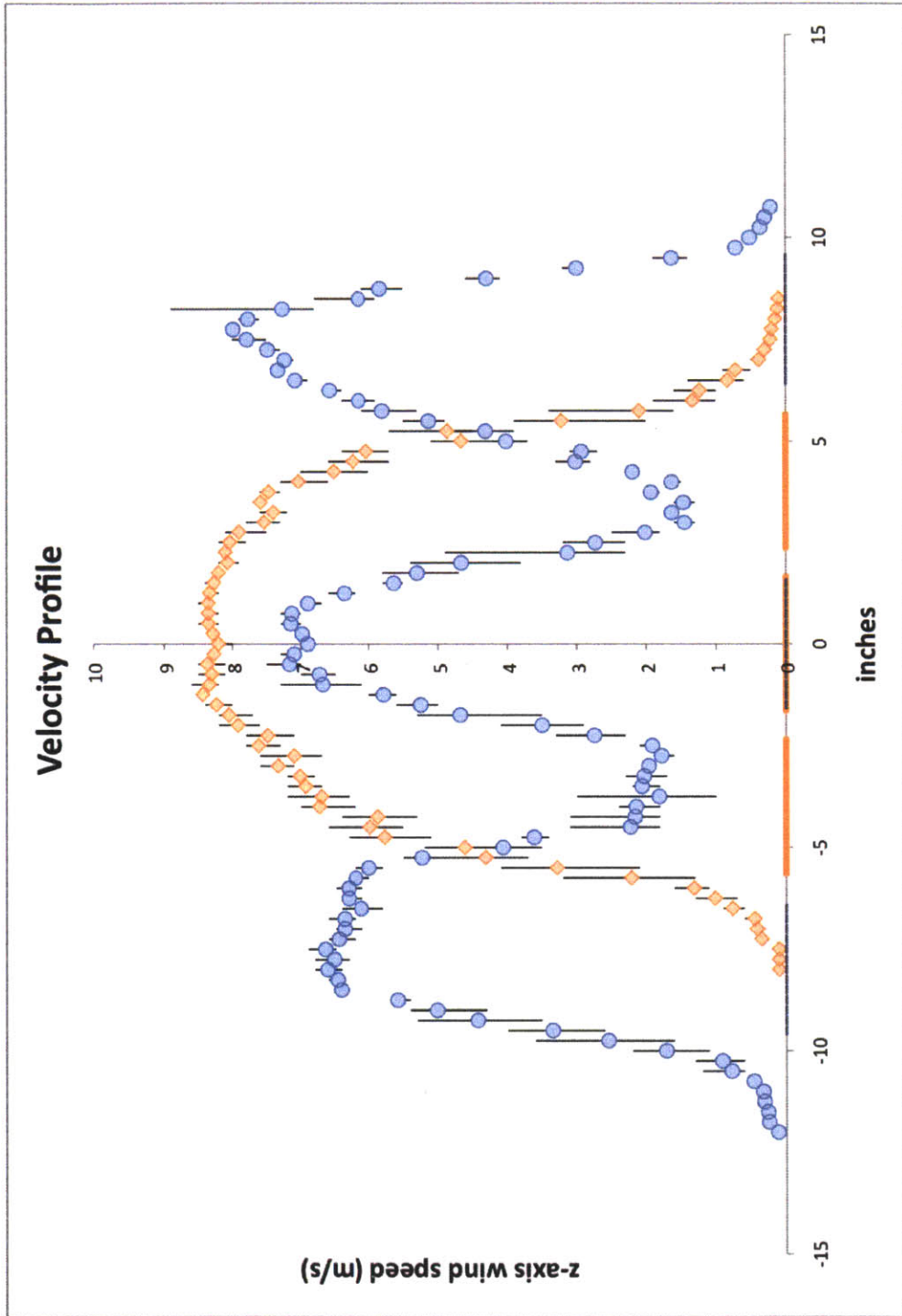
Figure 3-5: Tightly packed (orange diamonds) and loosely packed (blue circles) profiles overlaid for comparison. Both curves are with all motors on. The short lines on the x-axis indicate x-position of the propellers. Instrumentation and procedures for data capture are described in section B.2

.
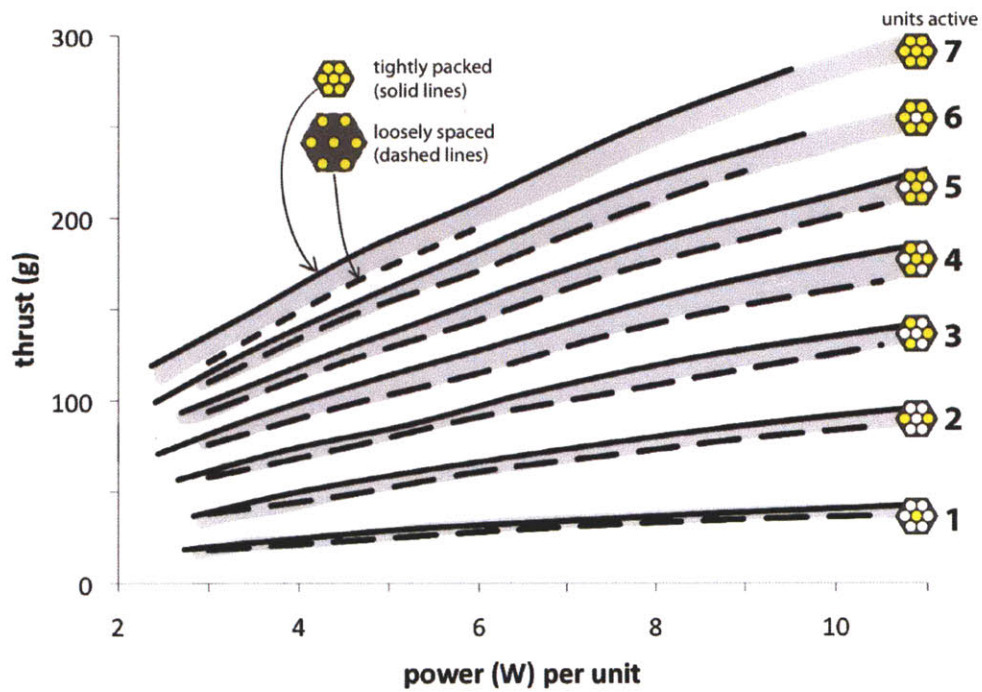
Figure 3-6: Thrust generated by the loosely and tightly packed arrays

.

surface of the scale so there would be no interference effects from the air near the scale plate. As motors were added, they were supplied with equal power (for several sets of power values) and the resulting RPM, total thrust, and total power consumption were recorded. Figure 3-6 shows that the loosely packed configuration yields less thrust than the tightly packed configuration and the difference grows as the number of units increase.

3.4 Interaction of jet wakes

In the previous section we found that overlapping wakes from propellers spinning in the same direction produced a beneficial aggregate effect, that is, more thrust was produced for the same input power. With the propellers rotating in the same direction I had been prepared for the opposite because at any point of overlap, the swirling wakes would be moving in opposing directions. On the other hand, as occasionally witnessed with tornadoes, two nearly overlapping spirals could be expected to form into one tighter spiral. I wondered if the spiral shaped "swirl" of the wake was a necessary component of this beneficial interaction. To investigate this, I used jets which have wakes without a rotation about the axis of ejection.

Water streaming out of a garden hose is an example of a continuous jet that might be used for reactionary propulsion. Fluid is supplied from outside of and added to the working system. In contrast, a *synthetic jet* is formed entirely from the working fluid of the flow system. Fluid is injested into a cavity then expelled quickly through a small orifice. With sufficient velocity, the ejected fluid forms a donut-shaped vortex ring. Interactions of a train of vortices create a jet by entraining surrounding fluid into the jet flow[20, 52]. Because the working fluid is taken from the system rather than supplied externally, these devices are also known as *zero net mass flux* (ZNMF) actuators.

There are many natural examples of synthetic jets among marine life, most notably the salp which ingest water at one end of its body and ejects it through an orifice at an opposite end. A recent doctoral thesis studied four species of salps and found that although salps exhibit a "fear" response by moving rapidly away from a threat, the jets were likely evolved for feeding rather than locomotion[54]. This may explain why the inlet and outlet orifices are distinct whereas in most engineered synthetic jets a single orifice is used for both injestion and expulsion of the fluid. This arrangement removes the need for valves to close off the inlet or outlet during the appropriate cycle. Without the requirement to feed, a synthetic jet employs only one orifice through which fluid is both injested and expelled, further simplifying the overall design. A long, slow intake

followed by a rapid sudden expulsion generates a net movement in one direction.

Synthetic jets have been an area of interest in recent studies in conjunction with electrically controlled piezoelectric actuators, simple chambers and orifices[59, 1, 48] for flow separation and drag control. The small displacements and high frequencies are well suited for boundary layer manipulation. In contrast we wanted to use the jets for propulsion. Our experiments with using solenoids to injest and quickly expel large quantities of fluids were of mixed success. The large forces were capable of creating well formed vortex rings that travelled a great distance. However the electro-dynamic device, consisting of a cylindrical magnet in a non-conductive, non-magnetic tube about which an insulated wire was wound, has a corresponding large displacement of the magnet (a large mass) and heat generation in the windings (driving the need to use a high current power supply). This was also noted in Cattafesta's review of ZNMF actuators[8].

Ocean biologists had empirically shown that a larger number of smaller jets in a train created more net thrust than expelling the same total volume in a single pulse, (though the larger number of pulses required more total energy). In part this is due to the vortex rings encountering the still-moving tube of fluid in the wake of the previous ring. Because this fluid is moving in the same the direction of desired motion, it is as if the relative speed difference is smaller, so less energy is lost at the outside boundary of the ring[30].

The intent of our experiment was to construct several synthetic jets and observe the effects of arranging them with vortex rings overlapping as well as isolated. The outer diameter of the vortex ring is larger than the orifice diameter required to create it; this and the nature of the motive force allowed the test object to be a single electromagnetic driver expelling fluid through a wall with multiple orifices. The final test object used employed an audio speaker driven by a digitally controlled periodic ramp-shaped electronic signal. Constructing and characterizing the synthetic jets with single and multiple apertures is described in detail in Appendix D.

A side by side comparison of very tightly packed apertures and very widely spaced apertures showed that a single jet is formed in the tightly packed case and the jet

travels a larger distance before its energy is dissipated. Both synthetic jet test objects were driven simultaneously in parallel and because the number and size of orifices is the same, the estimated backpressure, drag, and other frictional forces are nominally equal.
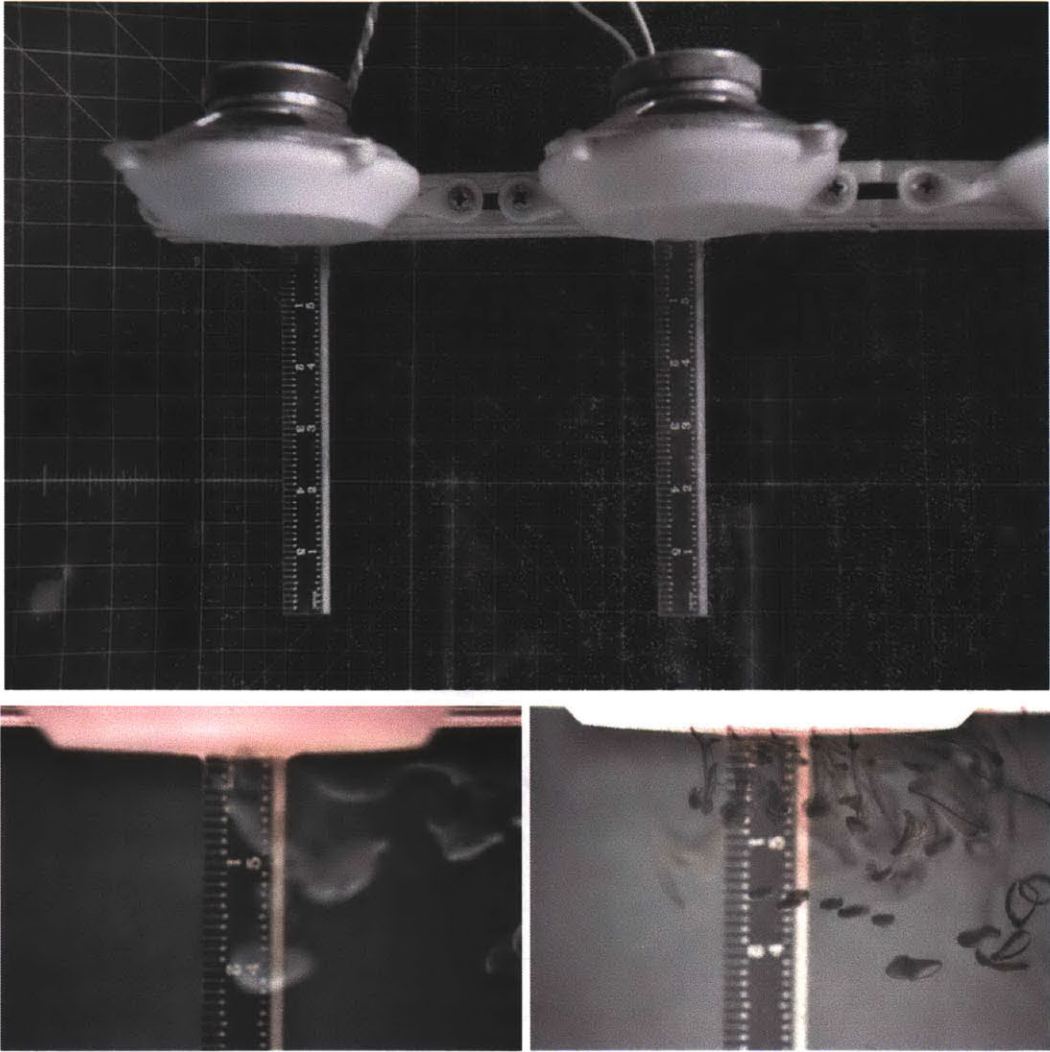
(b) Tightly packed jets   (c) Loosely packed jets

Figure 3-7: Side by side comparison of tight vs loosely packed jets
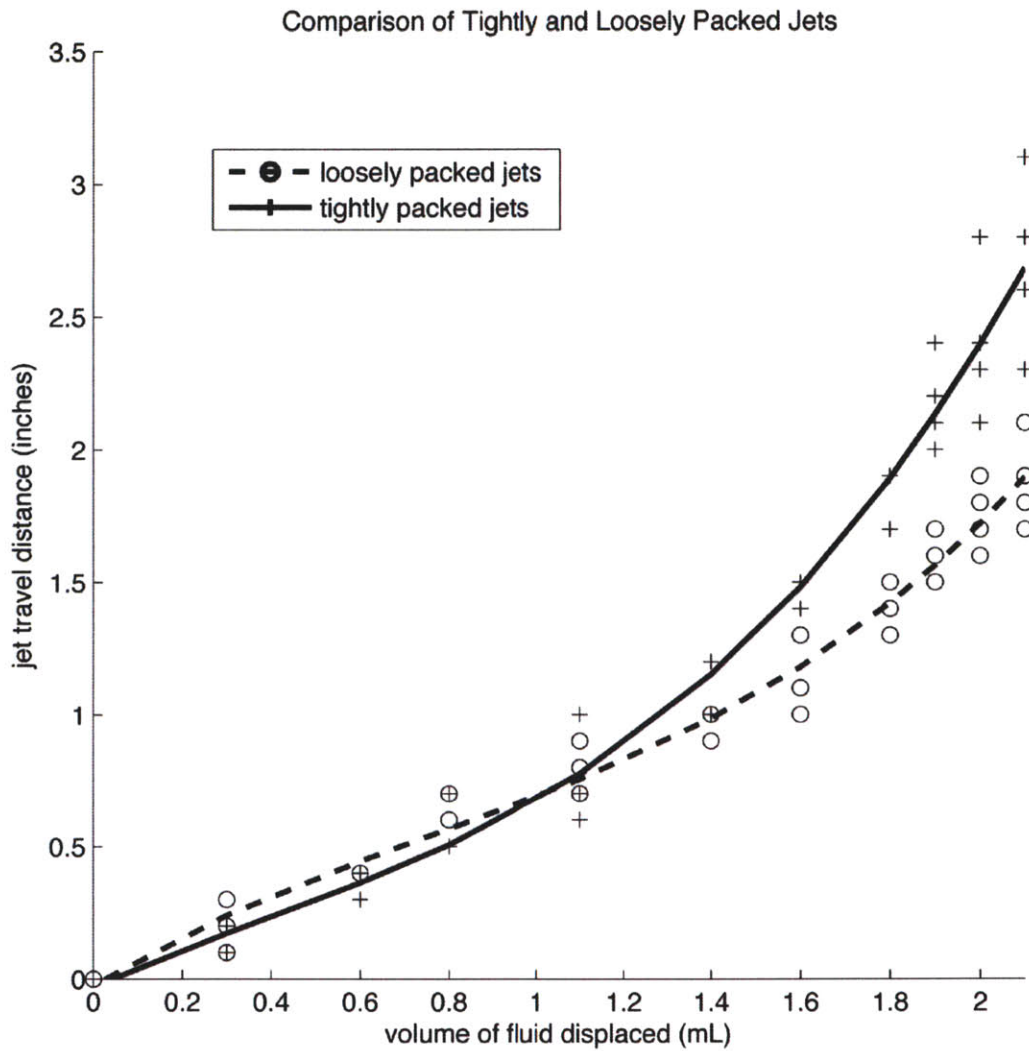
Figure 3-8: Comparison of packing distance on jet travel distance for several values of volume ejected

3.5 Layout Improves Thrust Generated in Forward Flight

When we began we couldn't help but think of the programmable surface as a 2D plane. A sheet of actuators, perhaps floppy, either passing fluid about on its surface as a fluid conveyor belt, or carrying a load about through the fluid as if a magic flying carpet. Changing the interconnection geometry among cells would create new, different structures. If "2D" connections on a grid make a programmable sheet, the "1D" connections (eg, connections only to "left" and "right" neighboors) can make a string or chain and "3D" might make (hollow) volumes.

The ball is an extreme limit of a programmable surface covering all or part of the exterior of a craft, such as an aircraft or marine vessel. Or, instead, the programmable surface may comprise the craft itself, and the craft may lack a conventional fuselage or wings (in the case of an aircraft) or hull (in the case of a ship). In this section, I experimentally show that the configuration of the propellers can positively improve performance in different enviroments. For example, we may easily imagine that we want our flyer to translate position, ie, fly "forward" in addition to "hover".

In forward flight, an incoming air stream provides additional mass that the propellers can interact with. If deflection angles are small, mass flow is dominated by the horizontal component. This suggests that a geometry which is maximally transverse to the incoming air flow will be more effective because there is more mass presented to interact with.

To investigate this in the lab, I constructed the widest and thinnest shapes with respect to the incoming air flow using the same number of propeller-motor nodes. These were in actuality the same test object, figure 3-2b, aligned streamwise along or transverse across the incoming wind. At a fixed power per motor, these units generated a velocity profile whose maximum, v, I recorded approximately 1 diameter from the plane of the propeller. To simulate forward flight, I fixed the test object on stand which was then mounted to a scale, and created an incoming wind with speed U with a wall of fans a great distance away from the test object. The propeller-motor units were tilted between 1 and 2 degrees away from the wind.
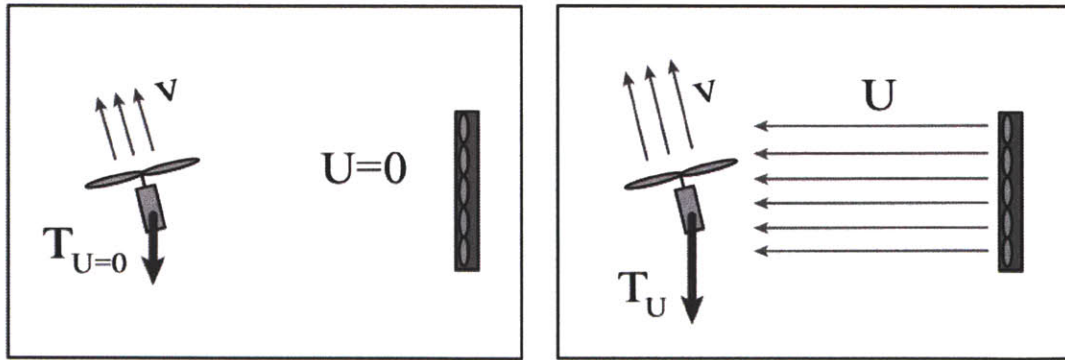
Figure 3-9: Forward flight is simulated by providing a wind speed U. The wind generated by the propeller-motor unit v is measured 1 propeller diameter away. The propeller is tilted 1.5-2 degrees away from the wind.

Figure 3-9 is a sketch of the system. Note that the propeller-motor unit is installed so that it is pushing down, a very convenient laboratory orientation. Data was recorded during three system states: wind only, propeller only, and both wind and propeller.
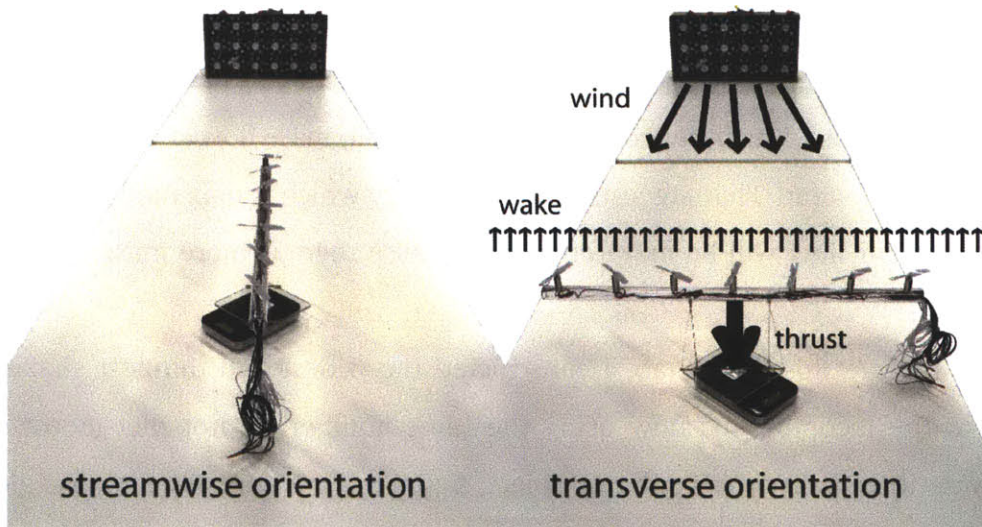
Figure 3-10: Photographs of the orientations with respect to the fan wall. In the course of the experiment, the actual fan wall was twice as large in both length and height dimensions and placed farther away from the test object. The handheld anemometer was used to verify that a uniform wind was presented to the test object.

The results in table 3.2 are graphed in Figure 3-12 with ratio of thrust (T) with wind vs. thrust without wind plotted versus the ratio of U/v. As the forward speed
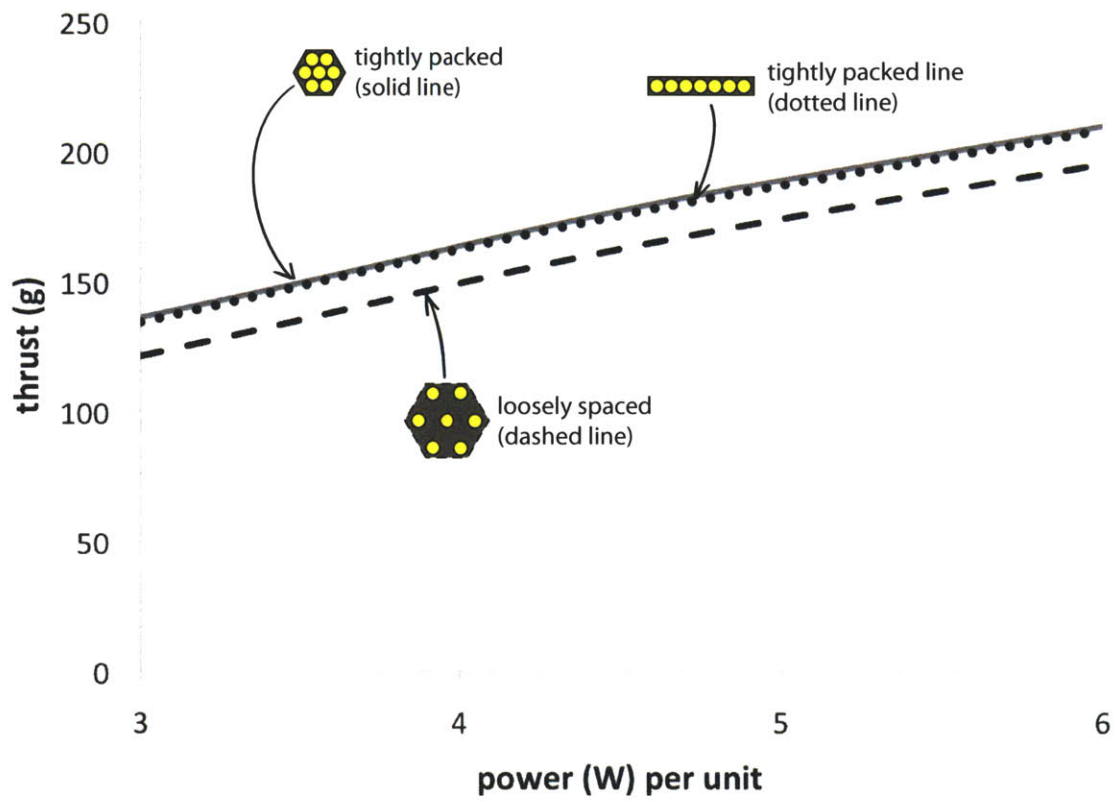
Figure 3-11: Performance of the line compared to the hexes.

Orientation	no wind (U = 0) $T_{\text{no wind}}$ (g)	with wind U / v	T_{wind} (g)	relative improvement in thrust T_{wind} / $T_{\text{no wind}}$
hex	7	4.2	12	1.7
hex	12	2.7	18	1.5
hex	20	1.9	29	1.5
hex	37	1.3	45	1.2
streamwise	6	4.2	8	1.3
streamwise	20	1.9	20	1.0
streamwise	38	1.3	42	1.1
transverse	5	4.2	20	4
transverse	10	2.7	18	1.8
transverse	17	1.9	22	1.3
transverse	36	1.3	43	1.2
transverse	57	1.1	64	1.1

Table 3.2: Effect of geometry and orientation in forward flight.

increases greatly compared to the downward speed, the transverse configuration does show significant benefit. When hovering or moving slowly, the hex was somewhat more productive than the lines.

configuration effect in forward speed

relative thrust (forward flight vs. hover)

relative speed (forward speed vs. propeller wake speed)

hex
streamwise
transverse
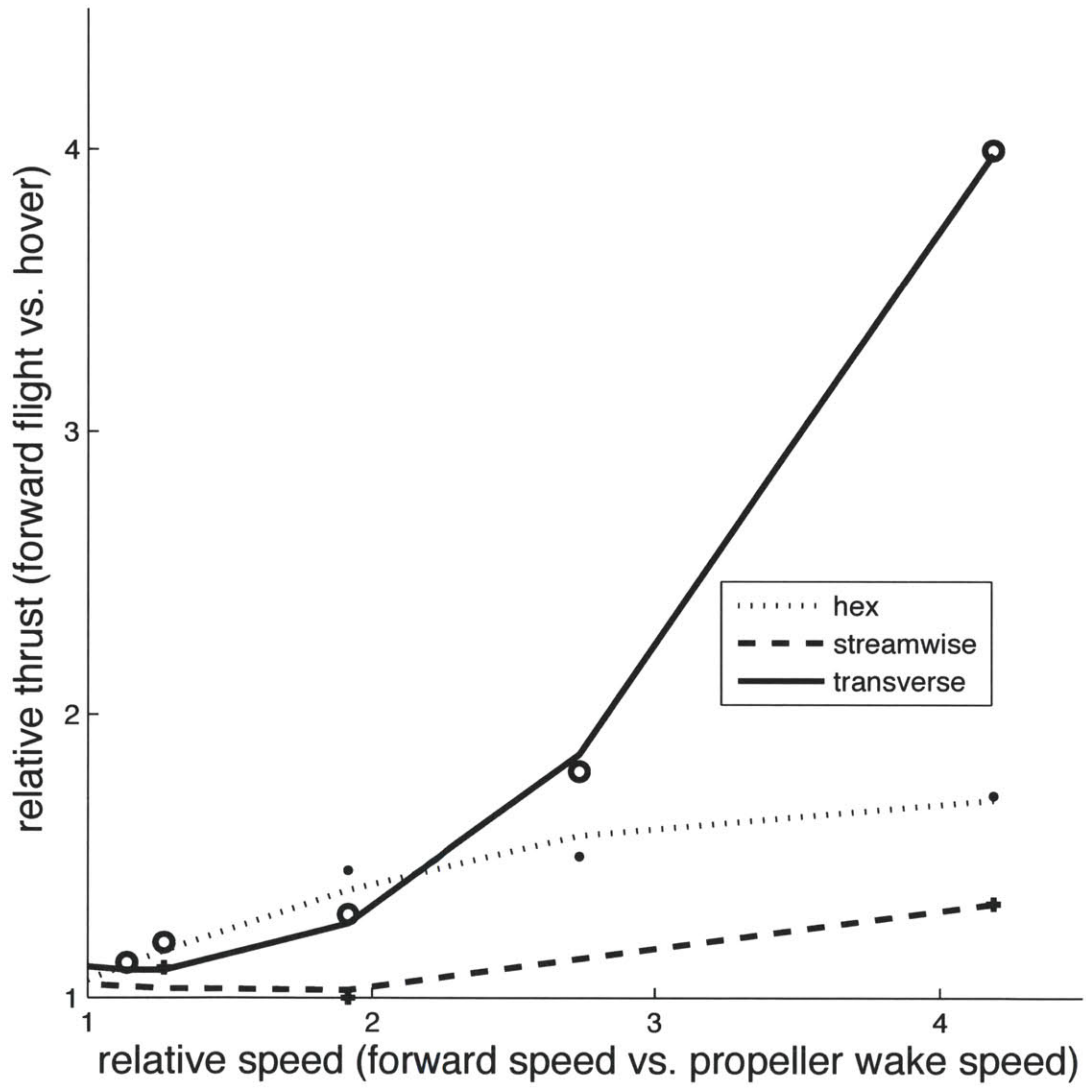
Figure 3-12: Effect of geometry and orientation in forward flight

3.6 Scaling summary

In the preceding sections I've experimentally verified that more propeller-motor units packed closer together generate more thrust for the same power (section 3.3 and 3.4), and as the forward speed increases greatly compared to the downward speed, a configuration transverse to the direction of flight can have significant benefit (section 3.5). When hovering or moving slowly, the symmetric tightly packed hex shape was somewhat more productive than the line of propellers, suggesting a dynamically reconfigurable shape to accommodate both efficient hovering and high speed forward flight.

In benchtop data collection I struggled with the effect of motor temperature on RPM and thus the thrust output produced by the propeller. Since coil resistance increases as temperature increases, the RPM decreases over time even if the input voltage is constant (see motor voltage constant equation C.1). As experimentation continued, the motors seemed to degrade permanently, ie, pausing to allow them to cool before resuming did not restore max speed. The most likely explanation for this is that low cost ferrite magnetic material lose their magnetic properties at high temperatures. Both of the possible contributors to motor heating, mechanical bearing loss and magnetic hysteresis loss easily resulting in temperatures over 80 °C which is the when permanent damage occurs to low end rare earth magnets.

Chapter 4

Drag: Boundary Layer Control

This chapter introduces the use of programmable surfaces to dynamically alter the flow around an object by moving the surface of an object creates a wall velocity that is decoupled from the bulk motion of the entire object. Programmable momentum transfer to the fluid through shear transport is a largely unexplored "synthetic hydrodynamic" regime which may lead to energy savings, drag reduction, novel vessel form factors, noise reduction, energy harvesting, and the ability to create flow fields which are not naturally occurring.

Technology exists in which boundary layers are manipulated primarily for the purpose of drag reduction. These are often passive approaches such as coatings and paints or textures like golf ball dimples. A well known active approach is to inject gas or gas-liquid mixtures into the boundary layer between the surface and fluid in order to lubricate the shearing interaction between the viscous fluid and surface. The gas may be moved through the surface in a variety of ways, including porous membranes, slots, and arrays of nozzles. However, this approach relies on bulk response among the fluid, solid, and injected layer and is not finely controllable at various locations of the surface, in particular along the streamwise length of the object. Nor is it finely controllable in time. It also suffers from manufacturing and practical operational challenges. Another actively driven method with similar limitations is to suck the boundary layer through a porous surface into the object so that the laminar boundary layer does not get too thick along the streamwise direction and separate. Handling and disposing of the fluid has

been the biggest challenge with this approach.

In contrast, programmable surfaces can create a dynamic, programmably controlled boundary layer. In "output" configuration, applications involving boundary layer manipulation include vessel propulsion, drag reduction, steering control, acoustical stealth, and synthetic profiles. In "input" configuration, applications include energy generation from low-head water bodies, stacked arrays of wind turbines, or sides of buildings, and regenerative energy recovery from vessel braking. Hybrid surfaces may be constructed to serve both modes.

4.1   Flow Control

When a free stream fluid moves past a solid surface the fluid's flow is distorted. Although the immediate distortion is very close to the surface, fluidic interactions within and beyond this thin, viscous *boundary layer* may induce large scale effects in the flow pattern. The nature of these large scale effects are dependent on a number of factors which include fluidic properties such as viscosity and density, surface properties such as surface roughness and geometry, and relative velocities of all components.

A particular effect of interest is the resulting fluid resistance or *drag*. Drag forces are those that oppose the motion of the fluid due to the object or vice versa depending on the observer's frame of reference. Drag forces generally represent inefficiencies in a system, ie, power lost to drag forces; however, dynamically controllable drag forces can be manipulated to produce braking or steering.

General approaches to manipulating the boundary layer is often termed fluid *flow control*. Methods for flow control encompass a large range of approaches including improved geometries and materials, the use of coatings and surface treatments, and various kinds of actively controlled actuators. Implementation of these approaches engages a wide range of disciplines in engineering, chemistry and materials sciences, mathematics, and controls. In all cases, the goal has been to suppress or eliminate turbulent flows near the surface of the object.

A significant portion of interest in flow control is the concerned with the detachment

of boundary layer from a bounding surface or wall. When this occurs, laminar flow become turbulent. The point (or region) of detachment is called the *separation point*. In most cases, delaying separation (moving the separation point streamwise aft) results in improved performance such as increase lift or reduced drag. These approaches are often termed *separation control*.

Drag reduction research has evolved in tandem with the development of water and air vessels which themselves tracked closely with war-time and peace-time consumer interests. Motivations have shifted from reducing uncomfortable vessel-wide vibrations in passenger steamships, to low acoustic signatures in submarines to evade detection, to fuel efficient and low noise commercial passenger aircraft. Drag reduction affects both performance (in the sense of top achievable speeds) as well as efficiency (from the perspective of the expense of fuel for the prime mover).

Several reviews have been made in this area, beginning with Goldstein in 1938 [1]. Early reviews of drag reduction methods are presented as a component of fluid mechanics following Prandtl's work in the early 1900's. The literature notes in particular Goldstein (1938), Lachmann (1961), Rosenhead (1966), Schlichting (1968), and Change (1970). Flow control methods of drag reduction research in the 1970s and 1980s were primarily concentrated in passive methods because of the relative ease of implementation and high payoffs[47]. By the 1990's reviews by Gad-el-Hak[16], Modi[38], and Pack[47] focused on active controls specifically while passive approaches continued to dominate drag reduction uses due to difficulties encountered in large scale employment of actuators with moving parts and complex signaling. In 2001 an Australian review reported that turbulent control research in the USA, Russia, Europe, and to a lesser extent Japan achieved up to 80% drag reduction by employing polymers, surfactants, coatings, or bulk injection of microbubbles[57]. The most recent review of moving surface actuators in 2011 by Cattafesta[8] found piezoelectric composite flaps and electroactive dimples to be the most commonly used active control actuators among a variety of applications. These technologies require the smallest mechanical displacements among active control approaches.

---

[1]Reported by Chew and Modi; I have been unable to retrieve Goldstein's review.

Active control of fluid flow have been investigated in America after the end of World War II; some full scale (successful) experiments were performed in the 1960's and 1970's, followed by a relative lull in the field for several decades. The advent of small sized digitally controlled electronic actuators and new materials reawakened interest in dynamic flow control using actively driven elements, in particular for weight reduction and radar signature reduction in high-performance aircraft. However, as noted by Pack [47], while most of these methods have been demonstrated to be effective, they have generally not been employed due to system concerns such as actuator robustness and system control complexity.

In a 2011 review Cattafesta organizes actuator types in to four functional classes. [8], They are: fluidic, moving object/surface, plasma, and other (a category he intended to include electromagnetic and magnetohydrodynamic approaches which were not reviewed). In considering actuators for programmable surfaces, the *moving surface* approach provides a reversible method of momentum transfer between fluid and solid.

4.2 Moving Surface

Momentum transport with moving surfaces is primarily accomplished through frictional, dragging force in the boundary layer. When the surface moves, the a thin layer of fluid closest to the surface is dragged along with it. The Tesla boundary layer pump operates on this principle, using a stack a large number of finely spaced disks to maximize surface area.[2] The inverse, Tesla "bladeless" turbines are commonly used today to recover energy from the smoke stacks and cooling towers of large power plants and factories.

The simplest moving surface is a rotating cylinder and the literature is rich with simulations, numerical studies, and empirical work with cylinders. The rotating cylinder develops fluid *circulation*, or a flux of vorticity. In the flow around the rotating cylinder,

---

[2]A common modern use is in oil - water separating skimmers where a disk or belt is partially submerged in water on the surface of which there is a film of oil. As the disk is rotated, the oil clings to the surface of the disk, lifted away from the water, and scraped off by a blade before that section of disk returns to the water.

streamlines are squeezed closer together and have higher velocity on the side of the cylinder moving in the same direction as the flow. The opposite half, which is moving against the flow, slows the streamlines which are farther apart. Like any object with circulation From Bernoulli's equation, there is a higher pressure on the side with the flow than against the flow. A resulting force, known as the *Magnus effect* after Heinrich Magnus, is generated towards the side moving in the same direction as the flow. The relationship between the "lifting" force (depending on direction) generated and the circulation was independently generalized by W. M. Kutta in 1902 and N. Joukowski in 1906.[58]

The resulting force of the Magnus effect alone (it is responsible for "curve balls" in baseball and ball "bending" in soccer) has been investigated for use as a motive force, most notably by Anton Flettner who constructed and successfully sailed a transatlantic schooner with two large vertical rotating cylinders driven by a diesel engine. Several other devices were proposed and some constructed that utilized the "Flettner rotor" including bomblets and heavier-than-air airplanes but the increased relative complexity of driving a large rotating mass is not justified by a corresponding increase in performance as compared to driving a propeller and using aerodynamic wings as lifting surfaces. A series of 1959 NASA Langley wind-tunnel experiments on circular cylinders (with rocket engines in mind) at subsonic and Mach 1.9 speeds (corresponding to Reynolds numbers from 355,000 to 1,600,000) found that lift could be generated throughout the range of Mach numbers but decreased with higher Mach numbers as the drag of the circular cylinder increased rapidly[31].

If the anti-flow portion of the cylinder is shielded from the flow then fluid "above" a wing can be speeded up and directed "down" to produce greater lift, especially if employed in the slip stream of a main propeller[5]. This is of particular interest to short and vertical take-off lift (S/VTOL) aircraft. One of the earliest examples of the use of rotating cylinders in S/VTOL aircraft was by Alvarez-Calderon[3, 4] who in 1961-1965 described a rotating cylinder near the trailing edge of a wing on a conventional single wing aircraft. A pusher propeller was attached to the streamwise aft end of

the wing and could be rotated downward to direct flow downward[3]. This design was improved on by MacKay[32] for tiltrotor aircraft use by rearranging the rotor to be streamwise ahead of the rotating cylinder so that high speed air would be directed over the cylinder. Mackay notes in a 1993 patent application that NASA tests showed rotation speeds between 6,000 RPM and 9,700 RPM was sufficient to prevent boundary layer separation on the airfoil surfaces. Mackay[4] was previously involved in 1972-1973 NASA flight tests of an North American Rockwell YOV-10 fixed wing aircraft modified with a rotating cylinder in the slipstream of the propellers[9] (see figure 4-1). In those series of flights, a high lift coefficient was found when during cylinder operation.
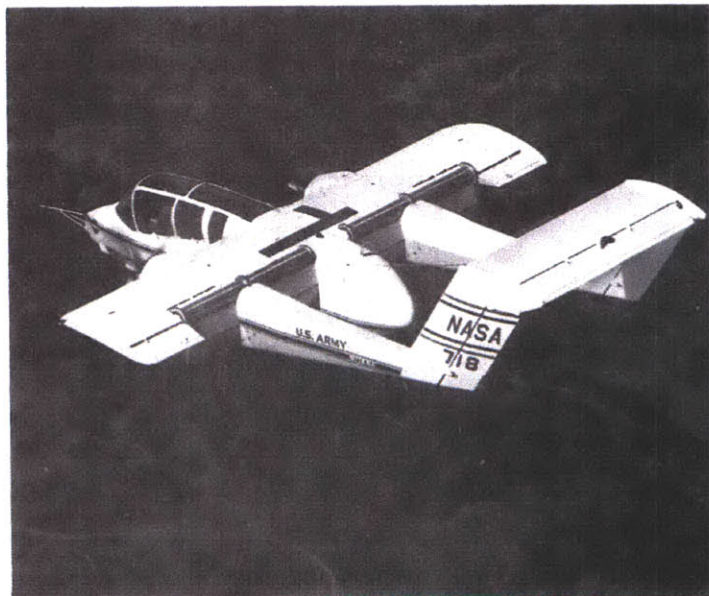
Figure 1.

Figure 4-1: NASA / Rockwell YOV-10 aircraft with trailing edge rotating cylinder[9].

The field of experimental investigation in using rotating cylinders partially shielded by a vessel's structure goes quiet until around 1989. Led by V. J. Modi's research group at the University of British Columbia and subsequent partnerships with Chew at the National University of Singapore, the 1990's was a prolific decade of rollers of var-

---

[3]Modi[39] reports that this system was flight tested by the Aeronautics Division of the Universidad Nacional de Ingenieria in Lima, Peru, but I was unable to obtain any references that describe these tests.

[4]A 1973 NASA report spelled his name *McKay*, though the 1972 report and the 1993 patents show *MacKay*.

58

ious sizes installed in various configurations, operating in various fluids and speeds. Target applications spanned leading and trailing edges of airplane wings[39, 40, 36, 44, 42] to the leading edges of rectangular container trucks and ships[2, 43, 36, 45], buildings[45, 29, 41] and even other cylinders[35]. In all cases, the wake was found improved by the use of rotating cylinders and the separation point moved downstream.

Of note, in a 2002 experiment on a rectangular barge-like model in water, Modi found a 24% reduction in drag with the use of two vertical rollers installed at the front leading corners of barge. The cylinders were driven by electric motors and the drag savings corresponded to an 8 Watt reduction in power for every 1 Watt expended to rotate the cylinders[37]. See figure 4-2 for a diagram of Modi's structure. With Munshi, Modi had previously visualized similar structures; see figure 4-3.
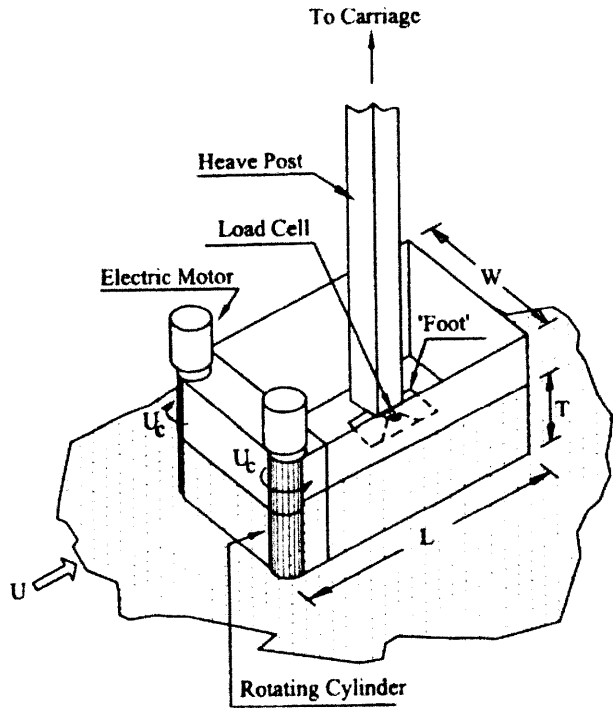
Fig. 2 Diagram showing test set-up during the tow-tank experiments.

Figure 4-2: Modi's barge-like structure with rotating vertical cylinders at the leading corners[37].

59
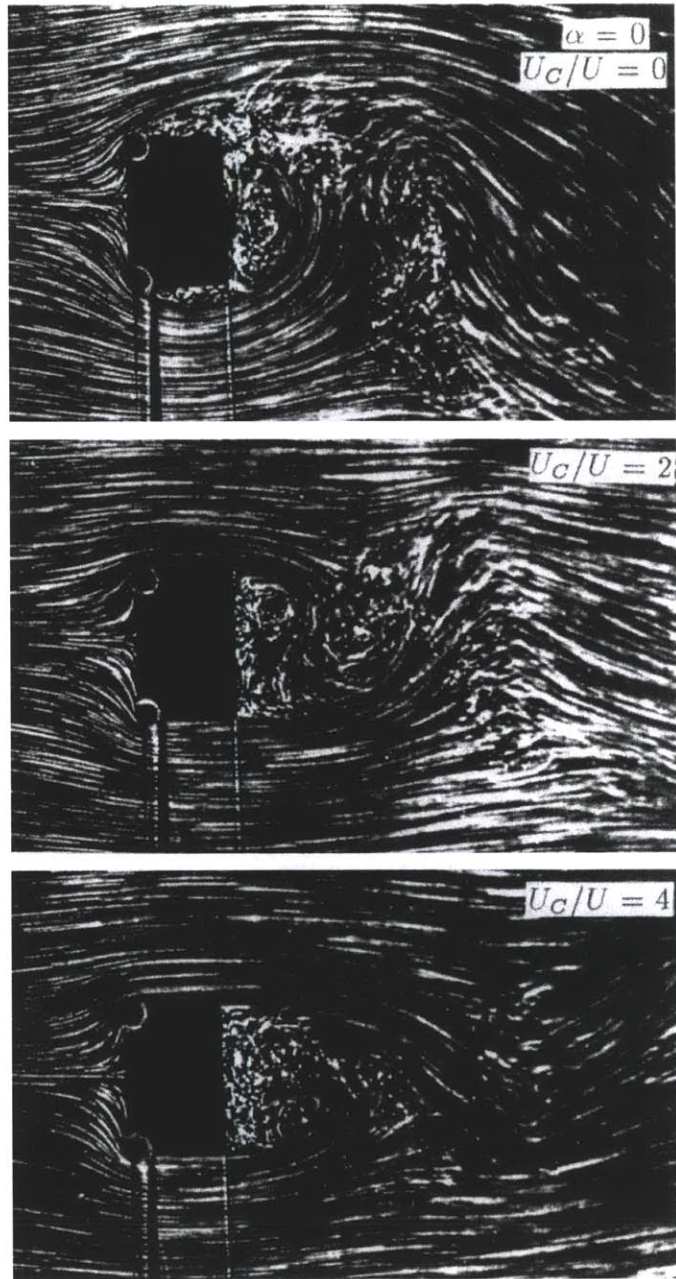
Fig. 16. Effect of momentum injection on the characteristic features of the wake and the shed vortex system associated with the rectangular prism (AR = 0.5) as observed during the water channel flow visualization study.

Figure 4-3: Munshi's flow visualization of a rectangular prism with rotating cylinders[45].

4.3 Programmable Moving Surfaces

The goal of moving surface boundary layer (MSBL) control is to physically move the solid surface to create a wall velocity which may reduce or increase the difference with the velocity of the free stream fluid. Unlike previous MSBL approaches which employed large rotating cylinders or belts to move large parts of a surface at once, a programmable surface is divided into a multiplicity of small cells called *ergos*[5]. Each ergo interacts with a small region of fluid nearest its surface. Because the fluid is a continuum, the combined effect of individual ergos working together is to alter the apparent stream lines of a fluid flowing about the solid object.

The entire wetted surface of an air or ocean-going vessel can be employed for reducing drag and generating propulsion by covering the surface with driven cells. Drag reduction with programmable surfaces is based on expending energy on the surface to reduce or eliminate energy consumed by frictional losses. Internal losses of the ergos, such as bearings friction and flow recirculation must be kept small. While there are many design options to address these losses, the worst case outcome is that there is no net energy savings. However programmable surfaces will still have mobility applications, including effecting control without control surfaces, reducing noise, and expanding performance envelopes.

A programmable surface may be also used to control the motion of a vessel. Controllability is influenced by the thrust-to-weight ratio and fraction of flight surfaces used for control. Conventional control surfaces change the profile of the aerodynamic wing or rudders by physically deforming, moving, or changing the geometry. If payload aiming is involved, a stand-alone pointing system is often employed to make course path solutions simpler. The surface of a vessel may instead be covered with individually controllable cells that allow for fine-grained complex flows surrounding the vessel. In this approach, the entire external surface may be involved in small manipulations of the fluid flow and pressures immediately adjacent to the walls. A full range of bulk control motions can be accomplished by driving cells independently; a few are shown

---

[5]*Ergo* is from *erg*, a unit of work, and *Lego*, a modular construction toy.

in figure 4-4. Additionally, by mismatching "top" and "bottom" surface velocities in the presence of fluid flow, a net lifting force is generated which can be used for additional non-traditional controls.
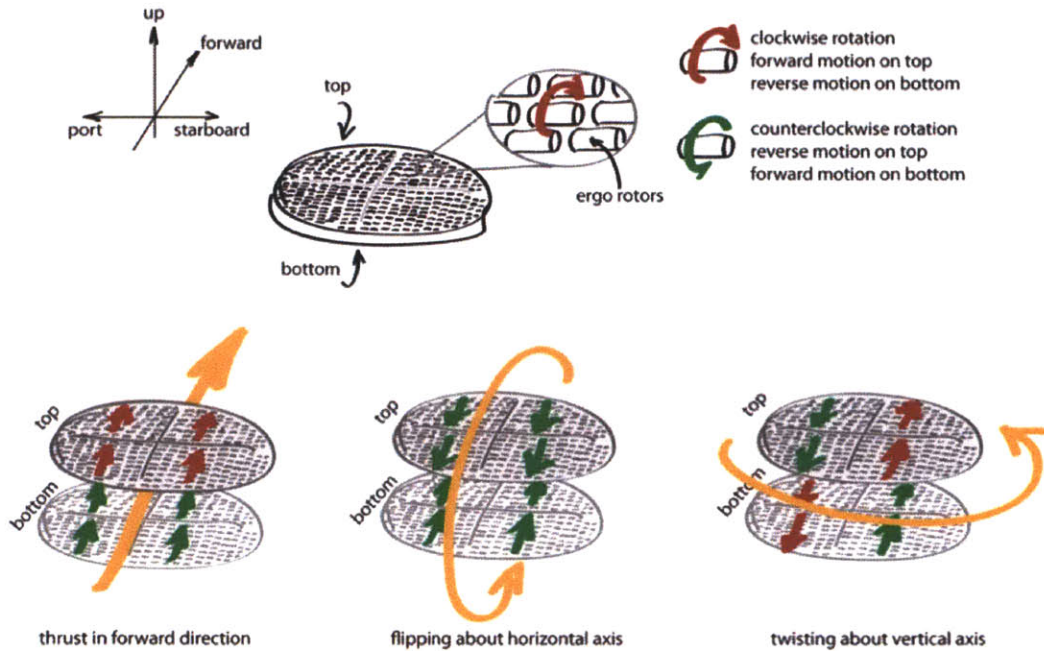
Figure 4-4: Individually addressable moving surface regions can be used to control the motion of a vessel.

Another consequence of active manipulation of the boundary layer is the ability to generate synthetic geometries, that is, to project a boundary layer shell into the flow and appear to be a different shape to the flow. Turned inward, these surfaces can be used to create flows with novel flow profiles.

"Hello World" - propulsion and controls with an underwater double belt

Achieving propulsion will require adequate momentum transfer through shear transport from the surface. The Reynolds numbers required for this may limit thrust to water or granular media, rather than air. To reassure ourselves that there is sufficient momentum transfer through shear transport in the boundary layer, I constructed a test object which had smooth moving belts on the top and bottom (or left and right) sides.

The belts were driven by spinning rollers which were powered by electric motors. A 60 fps high speed camera recorded belt movement to determine the velocity of the belt. With this "underwater double belt sander" I verified that 1) moving the belts was sufficient to propel the vehicle and 2) mismatching the belt speeds caused the vehicle to turn.

Figure 4-5: Underwater test object with moving surfaces.
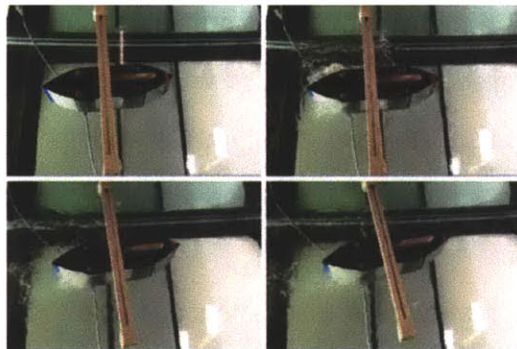
Figure 4-6: Moving belts for propulsion and steering.

The construction used readily available steel shafts and bearings which quickly rusted in the water tank. The rusting moving elements on the test vehicle contributed additional power loss due to friction and was not suitable for future quantitative experimentation and was retired after demonstrating forward/reverse propulsion as well as turns.

63

4.4 Modeling, Prediction, and Numerical Simulation

To develop control laws that can be used in full-scale applications it is necesssary to understand the temporal and spatial evolution of the flow response to active control. The research of Joslin[24, 25] in flow control theory have demonstrated that instability suppression without a priori knowledge of the disturbance is possible. However, the methodology requires "sensing" of the system (which is necessarily beyond the immediate reach of the controllable object) and system coefficients must be solved for all space and all time. In contrast, programmable surfaces are based on cellular automata and the idea of local neighboorhood sensing, computation, and actuation.

In nearly all reviews, it was noted that 3 dimensional analytical solutions have proven to be particularly difficult and in the case of predictive computer aided finite element modelling (FEM) inaccurate outside of a narrow range. This is important because a mathematical control model is required in order to fully control a dynamic boundary layer. Pack and Joslin report in a 1998 review of activities at NASA Langley that solutions obtained with 3 dimensional direct numerical simulation and control theory methodology yielded desired control features without prior knowledge of the forced instability[47]. However, they note an enormous quantity of coefficients necessary to represent the entire system state at all times and all spaces and long computation times due to the iterative solver.

In Gad-el-Hak's 1991 review is a discussion of the difficulties of determining an exact, rigorous analytical model for separation of unsteady 3 dimensional flows despite a large body of qualitative flow visualization data collected over many decades.[16]

Active control design tools and performance scaling laws for use in full-scale applications will require the construction of computational fluid dynamics (CFD) simulations. Although I constructed some crude and simple simulations in COMSOL, serious CFD was outside the scope of this thesis that was driven by experiments.

A small number of exemplary embodiments of the cells were constructed for evaluation. Ergo performance was investigated in a recirculating water tunnel using seed particle flow visualization techniques. Future work required to characterize the behav-

ior of the cells is to align CFD results and experimental results so that variations of the flow patterns and geometries can be simulated and predicted by the design tool.

Ultimately, CFD should be used to resolve the boundary layer flow along an ergo array as well as the flow evolution downstream from the array, then lift and drag forces would be calculated directly by integrating the simulated flow pressure and shear stress over the test section surface. The calculated forces along with the flow-field retrieved for certain planes from the simulation results would be compared with their counterparts from the experimental results.

THIS PAGE INTENTIONALLY LEFT BLANK

Chapter 5

Control and Programming: Asynchronous Thrust Array

This chapter considers the methods of programming a surface made of a large number of discrete identical nodes. It is clear that a conventional centralized approach, which essentially wires all sensor inputs and actuator outputs to a central computation unit, would not be suitable for the programmable surface described in this research because there may be thousands or tens of thousands (or more) units. Each time the configuration changes, the controller's physical interface as well as software would need to be reconfigured as well.

To maintain inherent scalability, we have two important requirements for the inter-operation of the nodes: 1) each node is self-contained, such that a special controller is not needed whenever the number or configuration of parts change, and 2) nodes are capable of coordinating with other nodes so that one may act on sensor information gathered by another node.

5.1 Approach: Asynchronous Thrust Array

A programmable surface will have thousands to millions of degrees of freedom which would be impractical to implement with traditional dynamic behavior control systems. Computationally, traditional control systems are created with a systems viewpoint. Feedback parameters are assumed to be available wherever they are needed in a calculation, i.e., global parameters available to all nodes at any time. Mirroring this system frame of reference, the physical implementation of a control loop generally takes the form of a central processor that is connected to all sensor inputs and all output actuators, and stores intermediate values in local memory. Although computational capacity per time and space increase each year, as the degrees of freedom increase the number of coefficients that must be computed and stored become intractable. For very large vessels, simple signal delay times from one end of vessel to a centrally located "brain" would be too long to compute or signal the proper actuator response.

To program the surface of a 747 or an oil tanker will require control that scales with the object being controlled. Distributing computation physically to local nodes limits the use of conventional control algorithms and increases complexity at each node. While it requires a radically different control algorithm, distributed control can scale arbitrarily beyond the limits of conventionally centrally wired systems. Wiring for avionics is already a major challenge despite the comparatively limited number of actuators. An important consequence of distributed control is redundancy and system reliability.

A specialized area of programmable materials research has been focused on their organization and control, in short, the *program* part of *programmable matter*. Because the number of individual parts is very large, *amorphous computing* assumes that the organization and topology of the material will be irregular, unknown, and time-varying (in particular, individual parts may break). A 2008 symposium brought together various approaches under the name *Avagadro Scale Computation*. The name recognizes that a variety of computing systems are approaching a limit of thermodynamic complexity, in which the number of information-bearing degrees of freedom becomes comparable

to the number of physical ones. At this point it is no longer possible to separate the physical and computational descriptions of enormously complex computers.

In order to program programmable surfaces we also need a high level spatial programming language to describe surface motions. From amorphous computing research, Bachrach created a high level language for motion programming where each node executes the same program built out of spatial primitives such as synchronized time, gradients, pointwise operators, and conditionals[6]. *Flo*[1] allows the designer to procedurally abstraction surface motion as high level declarative programs of systems goals solved by online optimization. These programs can be implemented in the surface cells by mapping a primal-dual decomposition onto a graph of the cells and their links, with local message-passing of state and constraints variables performing the global optimization of the desired system motion.

The interconnection and routing of the programmable surface is inspired by work on RALA (Reconfigurable Asynchronous Logic Automata)[17, 18]. RALA is a programming model that ties the spatial structure of programs to the spatial structure of the computer hardware. RALA uses a 2D or 3D grid of cells that perform logical operations on tokens that are asynchronously passed between neighbors. The spatial structure of the cells ensures that they can be embedded in the surface to provide more computation for larger surfaces. Local communication avoids global communication buses which would need to scale their bandwidth to the number of cells. Asynchronous token passing allows synchronization locally as needed for consistency in computations without maintaining a global clock. By adjusting the ratio of surface cells to RALA cells, an adjustable amount of computation required for different applications is possible.

Control programs developed in RALA can be used to directly synthesize non-reconfigurable hardware that performs the same function with only a few dozen transistors per cell. Because the spatial structure of a RALA program is directly mapped to spatial structures in hardware we can use a small library of cells that perform the fixed functions and directly map them to grid locations with no additional synthesis or compilation. The primary consequence of this for programmable surfaces is that the program is portable

---

[1]*Flo* was previously named *Proto*.

across manufacturing technology lines changes during a development cycle or system lifetime. Second generation hardware would, at least from a programming perspective, interoperate seamlessly with previous generations.

5.2 Simulation of a minimal distributed control law using Flo

As part of the Center for Bits and Atoms' work in DARPA's InfoChemistry program, a simulation of a distributed control law was created to show that global effects could be achieved with only near-neighboor local communications and distributed local-only actuator control. The simulation can be thought of as a "flying carpet" comprised of individual thrust nodes. Collectivelly, the goal of the flying carpet is to remain flat and aloft at a constant altitude.

Flo (Proto) is a high level language for motion programming where every node executes same program. Nodes were tied together to their neighbors on a square grid and given one dimension of control - their own thrust. A "greedy controller" algorithm required each node to strive to maintain its altitude despite external perturbations such as wind or other nodes failing and becoming dead weight.

In Flo, each aperture node is represented as a disc with four attachment arms sticking out at right angles from each other in the plane of the aperture. The arms are rigid rods attached to each node as if with a servo, or driveable, multi-direction hinge. Normal to the plane of the aperture is the thrusting force, as if the cylinder was a rocket engine tube. Nodes are able to control the magnitude but not direction of their thrusting force, and the force is uniform and perfect (meaning no dissipation losses or rotational torques). Each node has a sensor which constantly reports absolute altitude.

Bachrach coded the nodes' behavior and simulated their interaction in what he calls a "cartoon physics" world. By itself, a node wanting to achieve a particular altitude adjusts the magnitude of its force vector, slowly overcoming the effects of gravity, until it reaches the target altitude. It will have some force needed to maintain its altitude

which is equal to its weight. If an additional mass is attached to this node, it will perhaps initially drop until it has a chance to add enough force to counter the new total weight. This additional mass might be a neighboring node failing and becoming dead mass, not contributing to lifting the collective assembly. The additional force might be transient, such as the force of wind pushing up or down on the sheet.
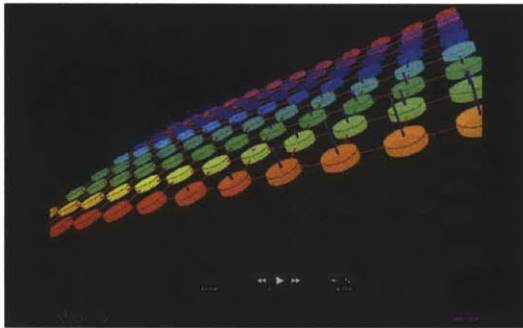

Figure 5-1: The Flo simulation showed that a simple "greedy controller" approach was sufficient to keep the carpet flat and aloft despite a variety of pertubations. Depending on the assumptions of lift generated per node, only the complete failure of a very large number of nodes would cause the carpet to fail to meet its goal. *Image courtesy J. Bachrach, 2010*

5.3 Fault tolerant (robustness) behavior of an asynchronous nearest neighbor lattice of thrust cells

Inherent to programmable surfaces composed of independent cells is increased reliability and robustness. This experiment aimed to show that routing redundancy can preserve global communication despite local failures.

Figure 5-2: The test array was made of nodes arranged on a grid. Each node had an 8" composite propeller, outboard brushless motor, pulse width modulated (PWM) electronic speed control (ESC), an integrated processor and inertial measrement device, four universal asynchronous receiver/transmitter (UART) ports, and a battery. All components were readily available from hobby supply stores.
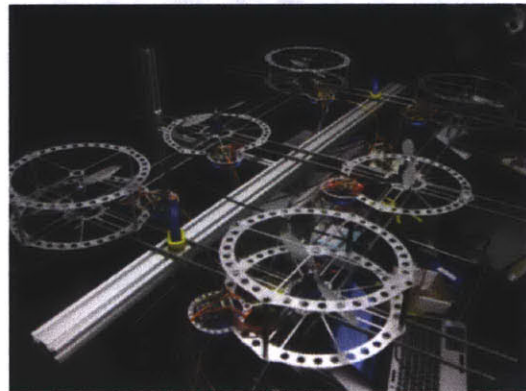
The processing and communications speed were chosen to match the mechanical response time of the system, which used a pulsing fixed voltage to regulate the speed of the propeller. Nodes were connected to their nearest neighbors in cardinal directions, also known as a Von Neuman neighborhood. Communications between nodes was mediated with a simple Asynchronous Packet Automata (APA) routing protocol, described in appendix E.

An additional component to integrate is a routing strategy which is an approach for selecting the payload route through the nodes. There are several possibilities from brute force broadcast (which isn't scalable) to dynamic optimal path discovery. There are numerous algorithms from established practice which offer various benefits such as robustness, speed, or avoiding local congestion.

We designed and implemented a system showing a method to handle redundant routing through a grid in an asynchronous fashion. Nodes were shown acting on information from far away nodes using only nearest neighbor communications and doing so correctly in the face of small numbers of failures.

The choice of a routing algorithm depends heavily on the control law's requirements and failure modes. There is a substantial body of (ongoing) research in routing, much of which can be applied above the APA layer. Here we implement the simplest with the understanding that more sophisticated routing can be done. We use redundant hard coded paths to show system robustness in the event of node failures.

For a physical demonstration we invented a goal of symmetry preservation. Each node is (conceptually) associated with an another node about an arbitrary line of symmetry. For a given node, if its opposite pair fails, the node should shut off too to preserve balance across the entire system. We could imagine that this occurs by physically dropping out of the array - perhaps as communication paths or nodes fail, the isolate or broken nodes to remove themselves by decoupling from the grid. There needs to be enough routing through the array to be able to discover if your pair is alive and responding. Since there are redundant paths through the grid, single "road" (intranode pairwise connection) failures do not cause pairwise shutdown.

The demonstration was done with 6 nodes. The propellers served as a visual indication of pair-wise connection status; however, our initial design did not sufficiently shield and isolate motor drive signals and the back EMF noise occasionally caused packet errors beyond what the system could handle. Either better designed power electronics (such as the use of bypass capacitors, improved and separate ground planes, shielded cables, and signal isolation) or a more robust protocol would have made this work. We were able to reprogram on-board LEDs to accomplish the same status indication.

In the case of communications between any pair of nodes, there are multiple paths of communications possible. For this demonstration the routing table was manually generated, though autodiscovery, ad hoc routing schemes could be implemented and is a well understood problem. As long as there is one path between the pairwise nodes is availble, the motors will stay on. When a node can no longer communicate with its pair, it turns itself off. Because all nodes are running the same code, both nodes in a pair will turn off (as in the case where both propeller-motors are not broken but all
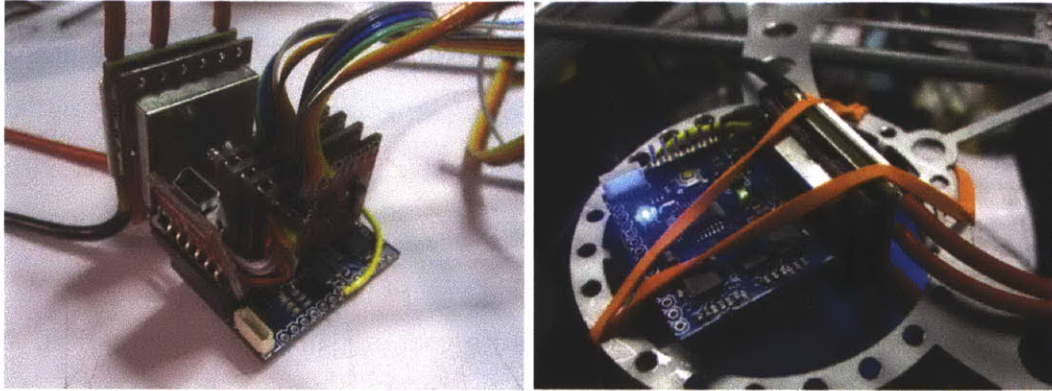
Figure 5-3: We used a commercial development board with an Atmel 328 processor and IMU with UART daughter boards to quickly prototype node controllers. Nodes were laid out on a grid. The processors perform the tasks of communications management, computing control law coefficients, and sending commands to the propellers. Pulse width modulated signals from the processor were connected to commercial electronic speed controllers (ESC) which provided power electronics and drive circuitry for the brushless DC motors driving 8" diameter propellers.

communications paths are severed).

5.4 Locally Sensed Global Parameters

The motivation here is to allow for a non-homogenous distribution of sensors in the grid and for nearby actuator cells to utilize this information in their own behavior. The simple experiment is to have a cantilevered chain of cells with strain gauges in the connections between cells. The goal of the ensemble is to become and stay level with an anchored cell at one end.

To date we have designed a custom circuit (replacing the prototype in figure 5-3) using an STM32 processor and Omega strain gauges. These "hub" boards included daughter board connections for UARTS and the analog front end for strain gauges. Lessons from the fault tolerant demonstration in section 5.3 were incorporated into a hardware rebuild with a larger propeller and motor and isolated power electronics. 50 controller boards were fabricated and work to come is to experimentally develop and optimize an algorithm where nodes utilize sensor information shared locally to build a global approximation.

5.5 Future Control and Programming Work

The end vision is reel-to-reel fabrication of integrated thrust cells which are assembled by a parallel, programmable robotic assembler. In this work we used readily available technology to physically implement an APA network to demonstrate communications robustness among cells and integrated the APA network with readily available propellers, motors, and controllers. It is a long way from the greedy controller to a distributed mathematical algorithm. It will be essential to understanding the performance needs of the distributed algorithm. In particular, we must answer these questions: a) how much computation is required on each node, b) the communication bandwidth required between nodes, c) the fault sensitivities of the algorithm, and d) the mechanical response time needed for overall system performance.

The greedy controller and more sophisticated algorithms can be immediately mapped to the existing nodes for evaluation. The current motor control implementation drives

the motor via 50Hz PWM signals while the circuit design utilizes 60 MHz processors allowing for a fairly complex amount of computation to occur between motor commands. These nodes can be used for algorithm development and evaluation to come.

Creating the physical, programmable, CA flying nodes has been demonstrated to be easily achievable with commericially available hobby parts. However, converting from the standard hobbiest architecture of a single controller sending control signals to a small number of propeller-motors to a distributed, asynchronous CA requires an as of yet undeveloped tool chain for distributed mathematics and programming distributed control laws.

Chapter 6

Energy Generation

Modern windmills come in a wide range of rotor sizes from a few feet in diameter to several hundreds of feet. They may provide individual and residential needs as small as 200W up to 700 MW for municipalities. Generally most common windmills have two or more blades rotating about a single hub which is connected to a shaft. The shaft is directly coupled to a generator and inverter or battery. The generator and electronics are covered by a nacelle to minimizes drag. Interaction of turbine wakes is a well studied field and manufacturers are able to provide guidelines for standoff distance among turbines for different blade configurations and wind profiles[14, 53, 46].

For power generation, many renewable sources (e.g., wind turbine, tidal generator, geothermal vent) supply a variable amount of energy with time, requiring an expensive variable-ratio gearbox in order to achieve high efficiency. Instead each of the independent propellers on a programmable surface could be allowed to spin at different speeds than its neighbors. The smaller size of the propellers means that they would be able to spin significantly faster and the smaller combined mass of the propeller and generator rotor would respond to more gentle breezes.

Instead of complicated gearboxes and charging circuits, each power generating *ergo*[1] would have an electromagnetic motor coupled to a super capacitor. The capacitor is left to charge to a predetermined level which trips a gate. The capacitor is then

---

[1]An *ergo* (from *erg* le*go*) is a single, asynchronous node comprised of a charging circuit, communications, processor, dynamo/generator, and fluidic interface actuator.

quickly discharged as a pulse to a neighboring ergo. More complex analog approaches can be applied to make the pulse passing more efficient.

Instead of approximating an aperture disk with one large propeller, using several smaller propellers can offer several benefits which, taken as a whole, may make the proposition of creating energy from flowing fluids suitable for a greater range of situations. There are two distinct topics here, one is the purely technical topic of component performance efficiencies such as the generator, propeller, or bearings which are usually presumed to be limited by a theoretical maximum assuming perfect component efficiencies. Known as the Betz limit, its derivation has several important limitations the most relevant which is the assumption that a windmill interacts only with an incoming stream tube no larger in diameter than the cross-sectional diameter of the propeller.

Another way to talk about efficiency emerges once we consider a system as opposed to a widget. Now we must bring in end-to-end, system-wide considerations such as funding, policies, and legalities such as rights-of-way. In the context of the real world, technical component-wise efficiencies can be misleading; there are other considerations which on the whole may be just as or more important. For example, a wildly expensive maximally efficient turbine is no match for a moderately priced but slightly less efficient turbine. This simple example hints at the complexities once dollars and time are brought into the equation. Appendix F shows a simple example of why sometimes "many small" can be a better choice than "a few big" when years and dollars come to play.

Chapter 7

Feasibility Summary and An Implementation

In chapter 4, a literature review and some benchtop experimentation show that using moving surfaces can make a significant effect on the overall flow pattern around and behind the object. However, 3-dimensional prediction required to compute the necessary wall movement poses a significant processing challenge, as current mathematical models require global system knowledge which could not be measured by the object.

In chapter 3, I experimentally verified that more propeller-motor units packed closer together generate more thrust for the same power (section 3.3 and 3.4), and as the forward speed increases greatly compared to the downward speed, a configuration transverse to the direction of flight can have significant benefit (section 3.5). When hovering or moving slowly, the symmetric tightly packed hex shape was somewhat more productive than the line of propellers, suggesting a dynamically reconfigurable shape to accommodate both efficient hovering and high speed forward flight.

From drive signals to flight controls, motors to propellers, batteries to power control, all components for a distributed flyer were available to purchase from commercial hobby sources. Propellers were available from 1 inch to 24 inches in diameter, along with correspondingly sized brushless DC motors, drive controllers, and lithium ion batteries. When investigating the programming and flight controls, an asynchronous cellular automata (CA) scheme was be implemented using small, inexpensive micro-

processors integrated with inertial measurement units and serial bus communications. Routing among CA nodes was determined manually, however, autodiscovery and dynamic routing is a well-understood and well-researched area. A simple example of global behavior with only nearest neighbor communications was demonstrated by simulation.

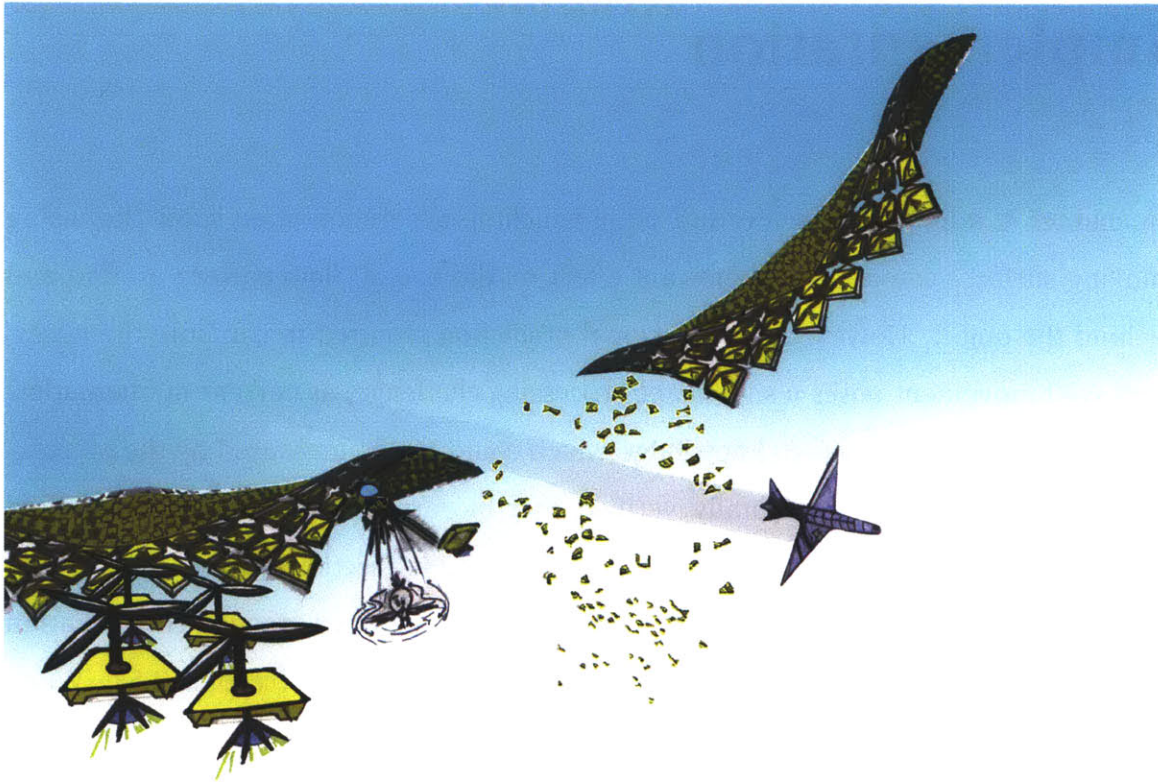## F5: Fungible Flexible Friable Frangible Flyer

Figure 7-1: F5: Fungible Flexible Friable Frangible Flyer

It seems clear that the first programmable surfaces to realize should be flyers, based on the availability of components and the depth of research in the various supporting areas. Today, there are a large number of unmanned aerial vehicles (UAV) fielded for a wide variety of tasks, from long range attack like the 300 mph, 10,500 lbs General Atomics MQ-9 Reaper UAV, to surveillance like the 81 mph, 20 lbs Honeywell RQ16A T-Hawk micro-UAV.
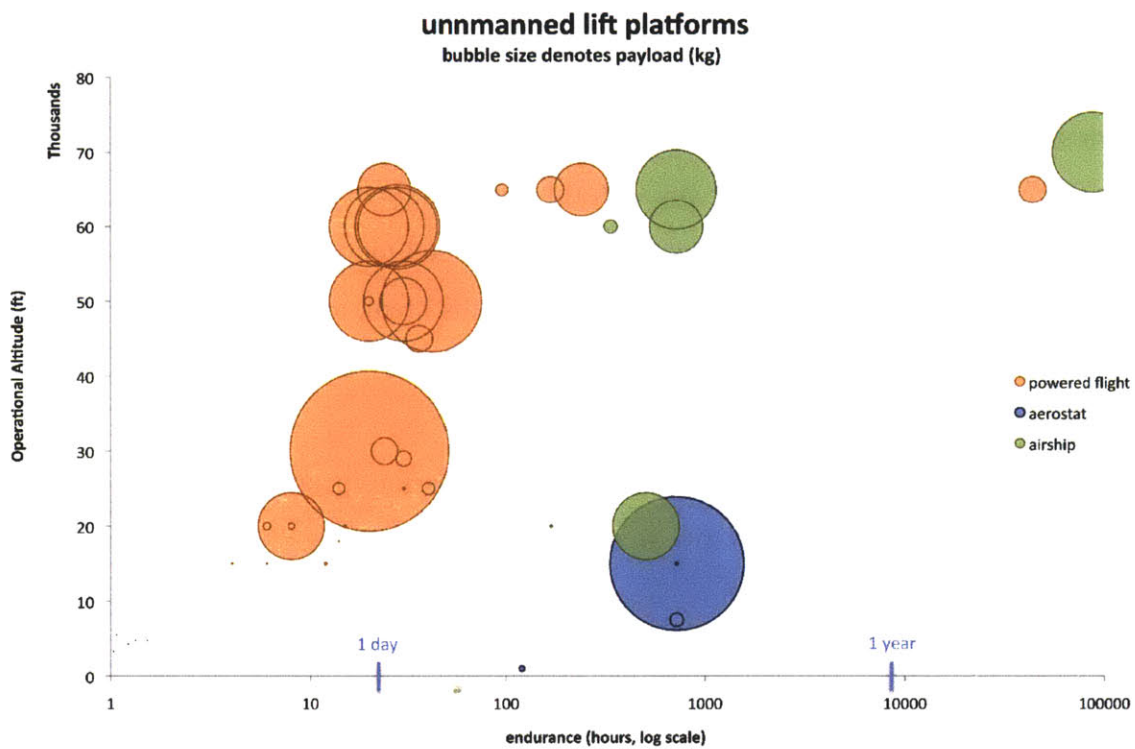
Figure 7-2: UAV's fielded or under development span a wide range of altitudes, endurance, and payload capacity. Unlike an F5 UAV, these platforms are not scalable to match the mission.

Most technical parameters can be designed to meet mission needs, however, a distributed flyer has two particular inherent advantages. The distributed nature allows efficient mission matching so that the platform can be sized in the field to match the range, endurance, or payload while minimizing the need for unique spares and specially trained personnel. The second advantage addresses a challenge to fielding UAV for general use in public airspace: regulatory forces that might prevent the systems

from operating out of concerns for safety. The distributed flyer, with loads distributed among the thrust units, could employ length-wise stiff but otherwise floppy interconnections among them. These connections could be designed to break or release as part of a detection and avoidance scheme. If the array were to be struck by another aerial vehicle or sucked into an engine, it could disintegrate into small parts which might cause less harm to the other vehicle.

The notional exemplary embodiment of a distributed flyer is the "F5". The F5 is a unmanned aerial vehicle (UAV) flier comprised of cells each containing the capability of generating lift, processor, power, communications, and a fundamentally distributed payload. It is *fungible*, that is, adding more cells gives more net lift and more payload. It is *flexible*, so that on landing it might drape over terrain or be rolled up for storage or transport. It is *friable* or easily broken apart into small pieces so that it does not pose a threat to other aircraft, and *frangible* so that cells break apart in a predictable way to protect the rest of the structure. Hence its name "F5", a Fungible Flexible Friable Frangible Flyer.

These features together provide an affordable, mission reconfigurable, systems efficient, fault-tolerant, safe alternative to conventional UAVs. The F5 builds on additional areas of research including additive asssembly of digital materials and spatial programming models.

Appendices

THIS PAGE INTENTIONALLY LEFT BLANK

Appendix A

Nomenclature

Symbol	Units	Definition
A	$(\text{meters})^2$	area
D	meters	diameter
c_T	*dimensionless*	thrust coefficient
c_P	*dimensionless*	power coefficient
i, I	amps	current
k_V		motor constant
k_τ		torque constant
l	meters	length
L	Newtons	lift force
$\mathscr{R}$	ohms	resistance
Re		Reynolds number
RPM		revolutions per minute
r	meters	radius
P_e	Watts	electrical power
P_s	horsepower	shaft (mechanical) power
$\mathscr{P}$	$\text{newtons}/\text{meters}^2$	pressure
T	kilograms	thrust
V	volts	voltage
u	meters per second	free stream velocity
$\mathscr{V}$	meters^3	volume
v	meters / second	linear velocity
ρ	density	
ω	angular speed	
τ	torque	

Appendix B

Instrumentation

B.1 "Benchtop" Water Flow Tank and Instrumentation

Tank: The flow tank is a 72 in long x 24 in wide x 25 in high, 180 gallon glass tank on a custom extruded aluminum frame with an attached instrument rack. The recirculating water flow was moved with a 1/4 HP utility water pump (later replaced with a 1/3 HP pump), rated for 20 (29) gallons per minute at 5 feet of head. 2 in diameter plastic pipes carried water from one end of the tank to the other where a flow laminarizer baffled and straightened the flow before the flow encountered the test object. The laminarizer was constructed with lengths of large diameter plastic pipe packed with wool, mesh, and straws. Additionally, a drinking-water rated filter system and surface skimmer were installed to help keep the water clean. Power strips attached to the equipment rack were outfitted with ground fault interrupter circuits (GFIC) which cuts main power if electronics are accidentally wetted or submerged.

Power: Two Hewlett-Packard power supplies were used to provide independent power to the propeller motors, rollers ("ergos"), speakers, or solenoids, as each experiment required. Each power supply could be commanded to a specific output voltage level and queried for the total voltage and current via null modem serial cables from a computer.

Displacement Instrumentation: A laser goniometer (angle measure) was constructed with a 5mW red diode laser pointing to a graduated wall outside the tank.

The position of the laser dot could be manually read. on a quad photo diode target mounted on the dry side of the tank wall. The laser was attached to the arm on which the test object was mounted. A compliant flexure at the base of the arm where it connected to a tank cross piece allowed the test object and laser diode to swing forward and aft in the flow with little movement in other axes. See figure B-1.
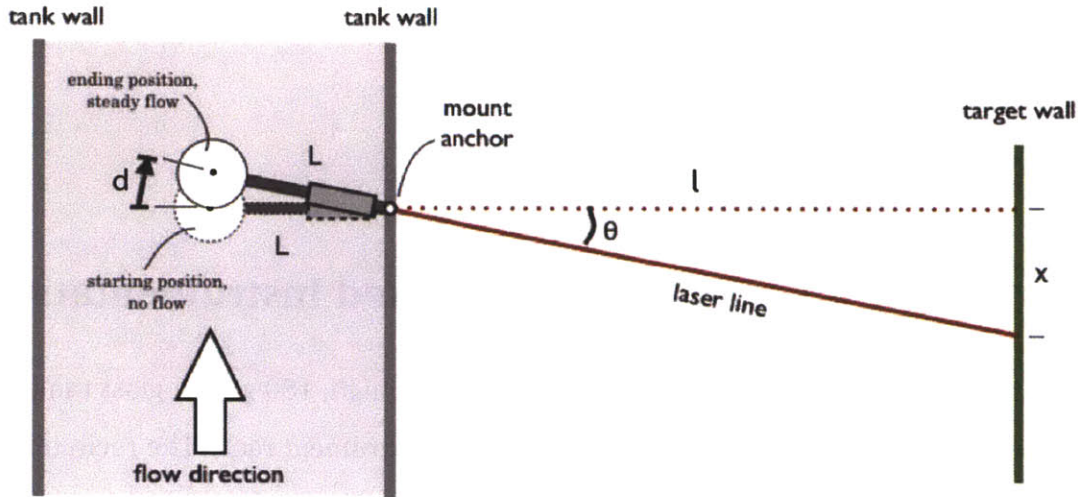

Figure B-1: Sketch of a laser goniometer used to measure displacement. View from top of tank looking down. Since $\tan(\theta) = \frac{d}{L} = \frac{x}{l}$, then the streamwise displacement of the object is $d = x\frac{L}{l}$.

Flow Speed Instrumentation: A Nikon D90 digital SLR camera with 60mm macro lens recorded particles entrained in the fluid flow. The camera was capable of high definition (1280 x 720 pixels) at 24 frames per second video or 4.5 frame per second still frame shooting. A green 5mW laser was mounted behind a glass rod to make a laser sheet. The sheet was aligned with the test object so that the laser sheet illuminated a streamwise cross section above the test object. Several types of particles were tested, from inexpensive, very fine glitter to glass and plastic microspheres, to the most expensive silver coated glass microspheres. All particles were certified as safe to dispose of through the building water drain, entrained with the waste water.

Flow and Wake Visualization: Drinking water safe fluorescent dye was injected into the flow or seeded on various parts of the test object for naked eye flow visualization. This was particularly striking when experimenting with synthetic jets.

B.2 Wind Speed Profiles Measurements Using a Hot Wire Anemometer

Wind speeds were measured using an Extech 407119 hand held hot-wire anemometer. The anemometer probe is a very fine metal wire which is heated by an electric current. The air flow to be measured causes convective cooling about the wire. The wire's resistance is dependent on its temperature; the anemometer internally measures the resistance of the wire to determine its temperature and thus deduce the air flow speed. The Extech 407119 has a range of 0.2 to 17 m/s with 0.1 m/s resolution and +/- 5% accuracy. The small size of a hot wire anemometer probe and its method of operation (in particular, having no moving or spinning parts such as common turbine or "cup" anemometers) resulted in minimal back-pressure or other impacts on the flow being measured.

The anemometer was mounted on an arm so that it could be positioned downstream from the propeller and moved through space in a plane parallel to the plane of the propeller. In some data gathering sessions, the probe was mounted on an arm which swung about a pivot point and the angle was recorded. In other sessions it was mounted to a Γ-shaped arm which slid along a linear track and position along the track was recorded.

The wake of a propeller is a spiral shaped sheet of high velocity flow. It it neither laminar, constant, nor aligned with the stream-wise direction. The anemometer has a baffle about the wire probe which I aligned with the stream-wise axis. The more turbulent or misaligned the flow, the greater variation in readings while more laminar flows were less varied. The wind speed profiles presented in section 3.3 represent a minimum of 6 data samples at regular time intervals for each data point. Error bars drawn in figure 3-4 and figure 3-5 represent maximum and minimum values while the data marker is placed at the average. Motor power consumption and propeller rotation speed were recorded simultaneously. In some cases, thrust force against a load cell was measured simultaneously as well.
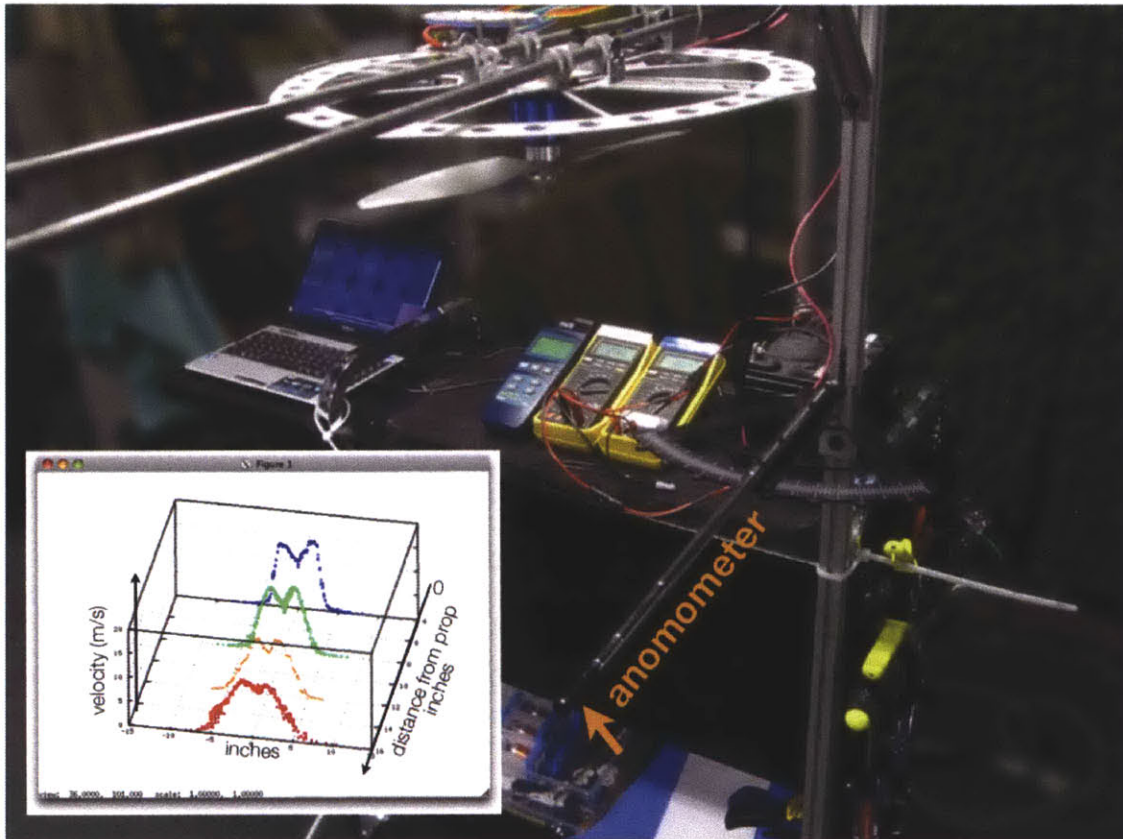
Figure B-2: Hot wire anemometer mounted on a plate marked with degrees. The propeller (at top of photo) is blowing "down". Inset is a scatter graph of velocities at different distances from the propeller.
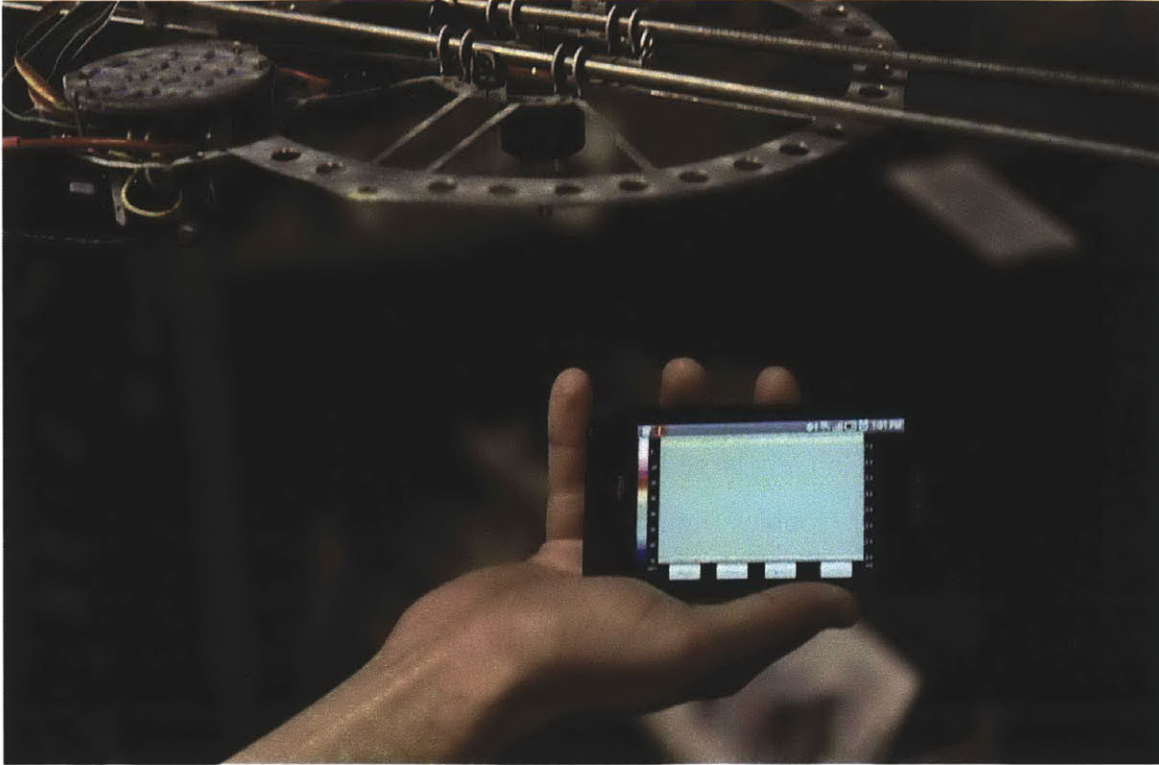
Figure B-3: Using a spectrum analyzer "app" on a smartphone to measure revolutions per minute (RPM).

B.3 Rotational Speed Using A Non-contact Tachometer

There are many inexpensive commercial tachometers available to measure the RPM (revolutions per minute) of propellers. The two methods I used most commonly were a hand-held no-contact photodiode meter intended for RC airplane hobbyists and a smartphone, laptop, or similar device with a microphone with freely available spectrum or frequency analyzer software intended for musicians.

Since whirling propellers produces an audible sound, a frequency or spectrum analyzer commonly available for music and sound work can "hear" the rotation speed. Each time a blade moves through and displaces a fluid, an observer hears a "whoosh". The rate of the displacements are displayed as a frequency inversely proportional to the whooshes per second. If n blades were mounted on a hub, one complete revolution of the hub would result in hearing n whooshes or n times the hub rotation speed.

Thus, to find revolutions per minute (RPM),

$$\left(\frac{1}{\text{frequency measured}}\right) \cdot \left(\frac{60\text{sec}}{\text{min}}\right) \cdot \left(\frac{1}{\text{number of blades}}\right) = \frac{\text{revolutions}}{\text{minute}} \qquad \text{(B.1)}$$

It can be difficult to isolate the effect of a single propeller when several are running at the same time. In those cases the non-contact photodiode tachometers are preferred. Some require a piece of reflective tape to be attached to the propeller which was difficult because most of the propellers used in this study were quite small and would be unbalanced with the relatively large and thick reflection target. The tachometer I used most often was a Tower Hobbies Digital LCD Mini-Tachometer. Its operating range is 0-32,000 RPM and automatically reports RPM after the user selects the number of blades on the propeller. It uses a photodiode to detect when the passing propeller blade obscures a light source. The Tower Hobbies device, and similar competing models from a very large variety of sources, were less than $20.

Appendix C

Characterization of a Single Propeller-Motor Pair

This chapter describes matching a commercially available hobby propeller to a commercially available hobby motor. Because the experiments call for a large number of units, availability, cost, and simplicity of control were a consideration in selecting the brushed DC motors. Plastic hobby propellers in smaller diameters are offered in inch increments starting around 2 inches and available in one spin direction.

Procedure to select and characterize the propeller-motor pair:

1. Search for a reasonably priced, small, high speed brushed DC motor. (C.1)

2. Experimentally match the motor with a small selection of commercially available propellers. (C.2)

   - Determine operating region for motor.

   - Measure no load motor speed in the expected operating region.

   - Experimentally find a propeller that loads the motor between 75 - 80% of the no load speed in the expected operating region.

   - Sample several operating points with the candidate propeller to refine operating region. (C.3)

3. Characterize the propeller-motor pair. (C.4)

   - Record power, thrust, and speed of the propeller at several points in the operating region.

   - Non-dimensionalize and relate power to speed (C_P vs Re) and thrust to speed (C_T vs Re).

C.1   the motor

The motor internal resistance $\mathscr{R}$ is too small to measure directly so it is calculated by measuring the voltage and current when the motor is stalled. I recorded several values

stalled volts	stalled amps	resistance (ohms)
1.00	0.2	1.01
2.00	0.9	1.11
3.00	2.5	1.20
4.00	unable to stall motor	
average internal resistance		1.11

Table C.1: Measured voltage and current of stalled motor with calculated internal resistance.

at different voltages to find an average $\mathscr{R}$, as recorded in table C.1.
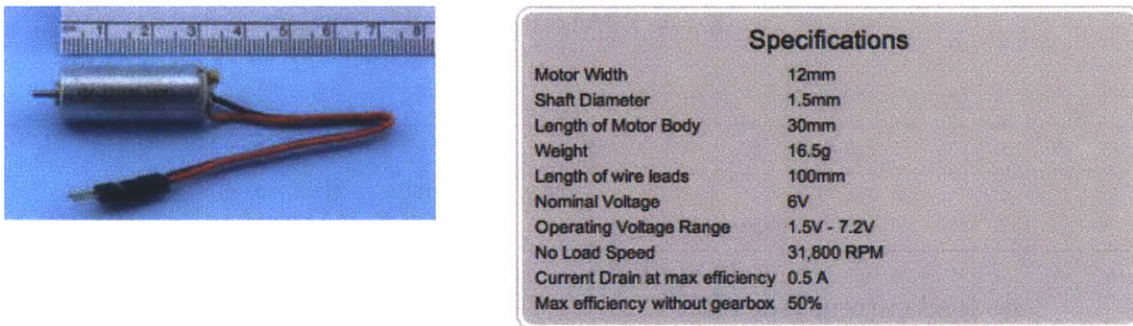

Figure C-1: Manufacturer data on the motor.

The manufacturer's specifications for the small, brushed DC motors (figure C-1) indicated a no load speed of 31,800 RPM (revolutions per minute) but it was unclear if this was at the nominal operating voltage (6V) or at the maximum voltage in its operating range (7.2V). I thought I could quickly verify the manufacturer's information by measuring the no-load RPM at the nominal and maximum operating voltages. I used a no-contact tachometer that requires a 1 cm x 1cm reflective target on the rotating part. I made a small flag out of reflective tape, however, the motor was not truly unloaded because the tape flapped around like a paddle. Table C.3 records the motor characteristics at the expected voltage for the scaling experiments.

The motor speed constant, K_V is the ratio of unloaded RPM to the voltage at the

volts	amps	RPM max	RPM min	RPM avg
1.00	0.156	3967	2275	3958
1.00	0.162	3846	3827	3834
2.00	0.216	8228	8215	8225
2.00	0.222	8280	8237	8239
3.00	0.376	12091	12006	12055
6.00	0.601	20497	19364	19560

Table C.2: Measured no load motor RPM at different voltages.

terminals minus the voltage loss inside the motor. It is calculated by,

$$K_V = RPM/(v - i_0 \mathscr{R})$$
(C.1)

measurement	Manufacturer @ ?V	Measured @ 6V	units
no load RPM	31,800	19,560	rev/min
no load current (see table C.2)	0.5	0.2	amps
internal resistance $\mathscr{R}$ (see table C.1)	(not provided)	1.11	ohms
motor speed constant k_V (see eq C.1)	(not provided)	3,384	RPM / volt

Table C.3: Motor parameters summary (Measurements at 6V).

C.2 selecting a propeller

The purpose of measuring the no load RPM is to guide the selection of a suitable sized propeller. An ideal loading is 75% to 80% of the unloaded speed, or 14,670 RPM to 15,648 RPM for this motor. A propeller operating close to its peak efficiency in this range would be the best match for this motor. I attached several differently sized plastic hobby propellers to the motor by press-fitting them on to the shaft and measured their RPMs while applying 6V to the motor. The results are recorded in table C.4.

propeller name	diameter (inches)	pitch (inches)	RPM @6V
GWS 2008	2.0	0.8	
GWS 2508	2.5	0.8	22,800
GWS 3020	3.0	2	14,981
GWS 4025	4.0	2.5	11,100
GWS 5030	5.0	3	stalled motor

Table C.4: Rotation speed at 6V of several propellers of different lengths.

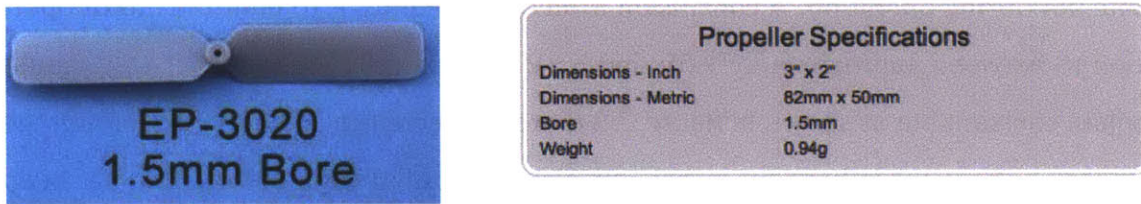At 14,981 RPM, the 3" propeller fell best within the loading range.

Figure C-2: Manufacturer data on the propeller.

diameter	3.23 inches
pitch	2.0 inches
chord min	0.45 inches
chord max	0.49 inches
chord avg	0.47 inches
thickness at tip	0.0335 inches
thickness at root	0.0560 inches
weight	grams

Table C.5: GWS EP3020 propeller parameters.

C.3   the motor with propeller load

With the 3" propeller directly attached to the motor shaft, I recorded the total power and RPM for several different voltages in table C.6.

| | power | RPM |
volts	(watts)	avg
1.00	0.2	3774
2.00	0.9	6904
3.00	2.5	9595
4.00	5.0	11855
5.00	8.0	13781
6.00	12.6	15488

Table C.6: RPMs of GWS 3020 Propeller at Different Voltages. These are plotted as K_V in figure C-3 and as C_P in figure C-4.

Above 5V, fluttering of the propeller was observed and the motor would become quite hot during operation. A conclusion from these findings is to limit the motor operation to between approximately 1.5V and 5.5V. Theoretically the RPM per volt should remain constant but as shown in figure C-3 there is a decreasing resulting K_V as voltage increases. The value in brackets is the equivalent amount of input voltage that has been lost. If the decrease was due to increased heat and thus internal resistance I would expect the loss to be non-linear and much larger at the bigger voltages where more heat is generated faster. Instead, the increase seems to be fairly linear and dependent on speed.

Two possible sources for the additional loss are mechanical bearing losses and magnetic core loss, both of which are dependent on speed. The inexpensive motors selected for the experiment used brass bushings rather than bearings; clearly as rotation speed increased, friction and heat at the bushing increased. Magnetic core losses are energies lost within the high permeativity magnetic material that guides the magnetic field in the motor. A well-understood source of core loss is a resistive loss due to eddy currents, this is primarily a geometric and materials composition effect and not strongly tied to frequency of operation. A second source of loss arises is known as hysteresis loss, which arises from defects in the crystalline structure of the core material that prevent a smooth change of the magnetic field through the material. The amount of energy lost is repeated each time the magnetic field change is cycled; hence hysteresis losses increase with higher frequencies because of the number of times the magnetic
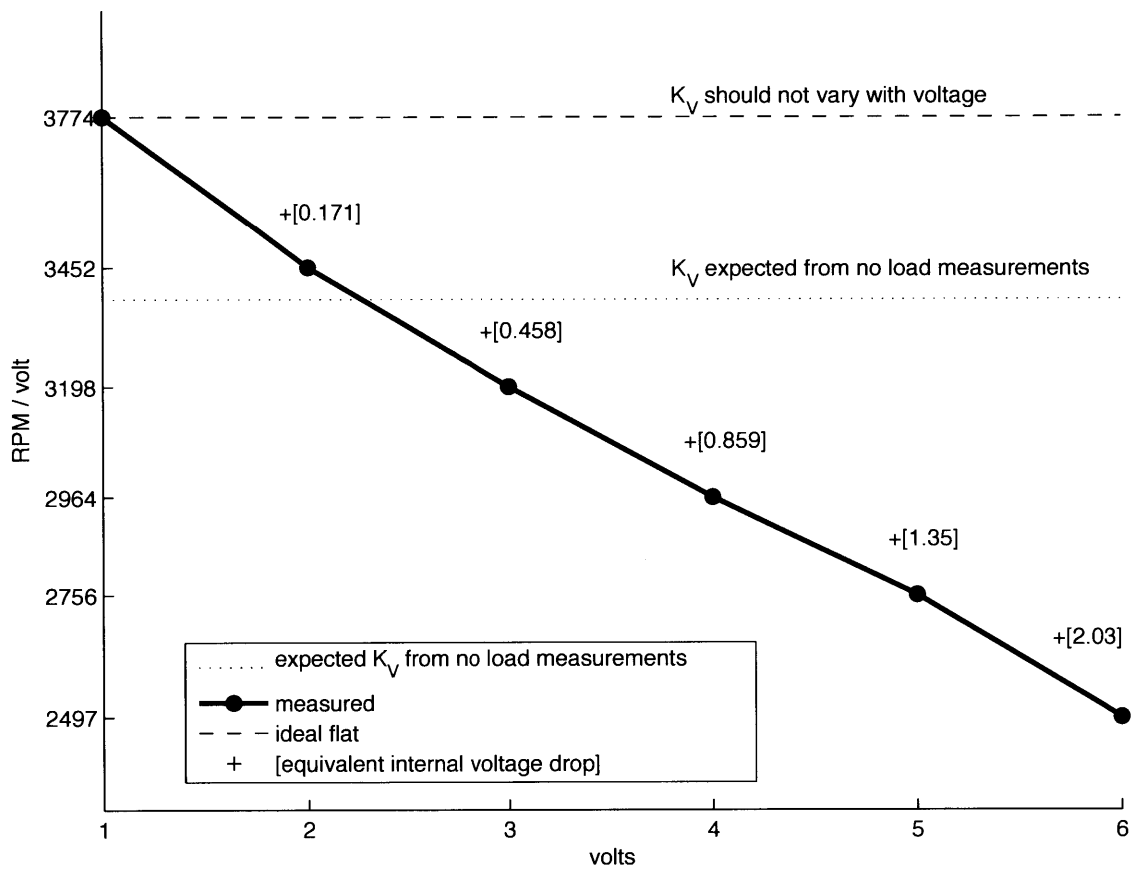
Figure C-3: Loaded K_V is not flat. See data in table C.6. Equivalent voltage loss is shown in brackets.
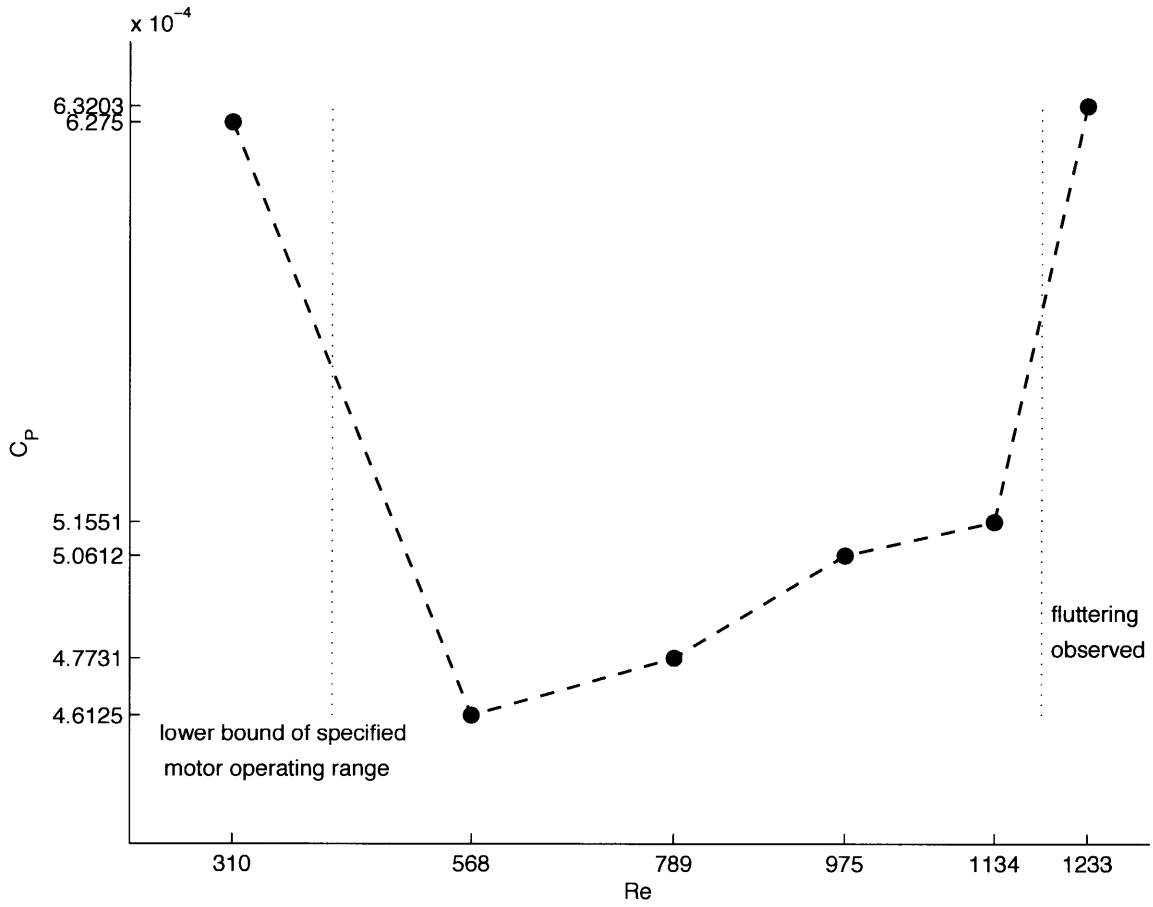
Figure C-4: Power coefficient of A 3" x 2" plastic propeller direct coupled to a 12mm brushed DC motor.

field changes.

A back of the envelope calculation to estimate possible core loss is to multiply the volume of steel times the energy loss per pound times the switching frequency and voltage:

$$\mathrm{P_{core}} \approx \underbrace{\mathrm{pi} \cdot (0.17\,\mathrm{in})^2 \cdot 0.745\,\mathrm{in} \cdot 30\%}_{\text{volume of steel}} \times \underbrace{\frac{1.74\,\mathrm{W}}{\mathrm{lbs}} \cdot \frac{8000\,\mathrm{kg}}{\mathrm{m}^3}}_{\text{power loss per volume}} \times \underbrace{\frac{15000\,\mathrm{Hz}}{60\,\mathrm{Hz}}}_{\text{commutating frequency}}$$

(C.2)

$$= 8.50\,\mathrm{watts}$$

$$= 0.43\,\mathrm{amps}\ @\ 6\ \mathrm{volts}$$

This is a reasonable possible explanation of the voltage dependent loss observed in figure C-3.

C.4   characterizing the pair: relating power and thrust to rpm

To fully characterize the chosen pair of propeller and motor, I recorded the power consumption, rotation speed of the propeller, and output thrust at several different voltage settings. The motor was rigidly mounted to a large block of metal set on a scale. The propeller was press-fit on to the motor shaft and oriented so that the wake pointed "up", pressing the test object "down" into the scale on the table. A benchtop power supply was connected to the terminals of the motor. The power supply can be set to a voltage and simultaneously reports the voltage and current draw on the digital front panel. For the low end of voltages I chose a value within the motor's intended operation region. Still wanting to characterize behavior in the higher range, I attached a large heat sink to the motor casing and waited for the motor to cool to room temperature in between samples. Flutter still occurred at the higher speeds. I used a non-contact tachometer that did not require the addition of a reflective tape which might have altered the performance of the thin propeller. A total of 70 data sets

were recorded. Using the physical geometry parameters from table **??**, equations for C_T (equation 3.1), C_P (equation 3.2), and a Reynolds number calculated using the chord, I plotted these data in non-dimensional terms on Figure C-5.
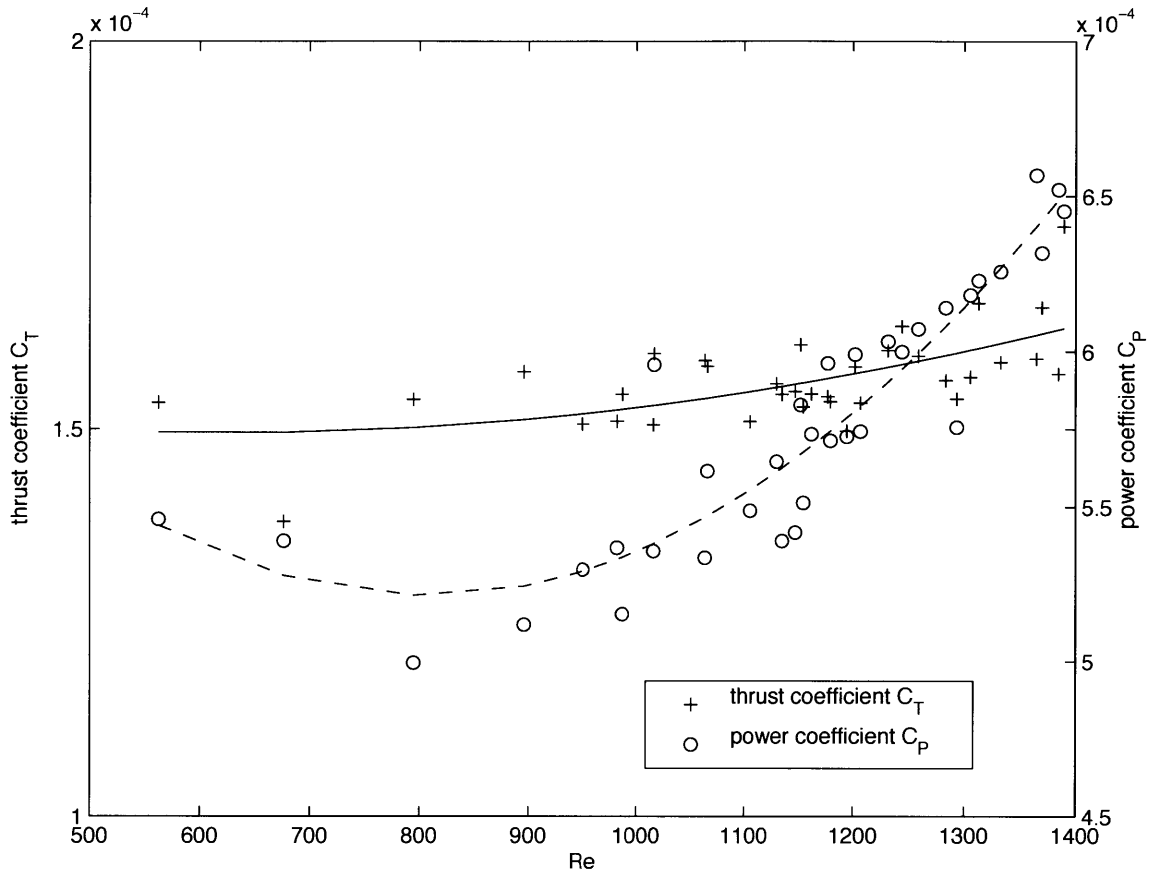

Figure C-5: Thrust and power coefficient of a 3" x 2" plastic propeller direct coupled to a 12mm brushed DC motor.

Appendix D

Making Synthetic Water Jets Using Audio Speakers

D.1 Experiments with a synthetic jet made from a speaker and plastic cups

These images are from a speaker driving a quick-and-dirty synthetic jet. Synjets suck fluid in and push it out of the same hole. I took a speaker, jammed it tightly into a plastic cup, and poked a hole in the bottom of the cup. The internal volume of the cup was filled with water and dye and the contraption was submerged in room temperature tap water.

The diameter of the base of the cup is just less than 1.6" (2.5oz/75ml cups; the internal wetted volume is about half of the cup). The aperture hole was made with a soldering iron and isn't terribly smooth; the hole is approximately 0.018" diameter.

I drove the speaker with a frequency generator and experimentally found the nicest looking jets from a ramp wave which has a sharp voltage transition in one direction and a smooth transition for the return. Each push of the speaker made a little jet pop out through the hole. To make the photos, the frequency was turned very low, around 1Hz or one pulse per second, so that the dyed ring would have some chance to drift
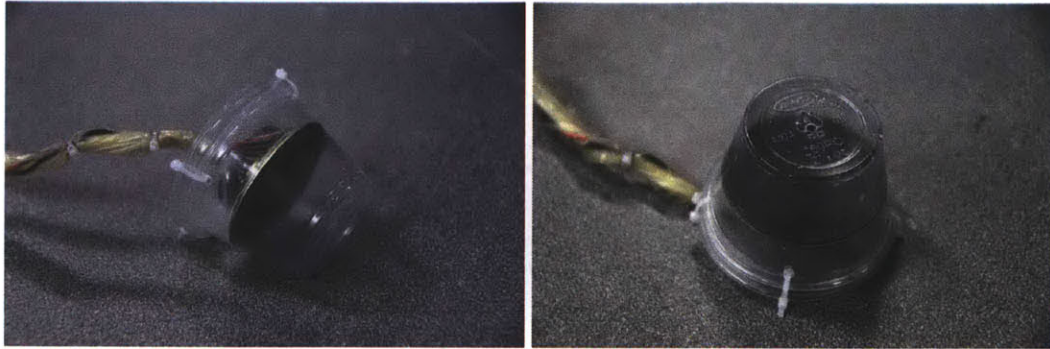
(a) a

(b) The aperture hole is approximately 0.018" diameter.

Figure D-1: Prototype synthetic jet.

away before the next pulse.

Sweeps through frequency (<1Hz - 60Hz), waveform (sine, square, triangle, ramp), amplitude (0V - 10V peak to peak), duty cycle (20%-60%) were performed to develop an intuition of their effect.

A rigid body synthetic jet was made by sealing a speaker into a preformed carbon fiber tube. An acetal copolymer disk with a small laser cut aperture is press fit into the front of the tube. The volume in front of the speaker is filled with dyed water and several different waveforms were applied to the speaker using a frequency generator. The rigid body jet behaved similarly to the jet made from a plastic cup.

D.2 3D Printed Multi-aperture Synthetic Water Jets

In a quiescent tank, once the vortex rings lose energy they stay in place, drifting only slightly, and new rings join the spent cluster (see the lower right area in images in figure D-8. The distances traveled from the front plane of the orifice were recorded as the location where the rings stop moving; this was a sharp transition. The collection of images in figures D-8 and D-9 were captured at 4.5 frames per second using a Nikon
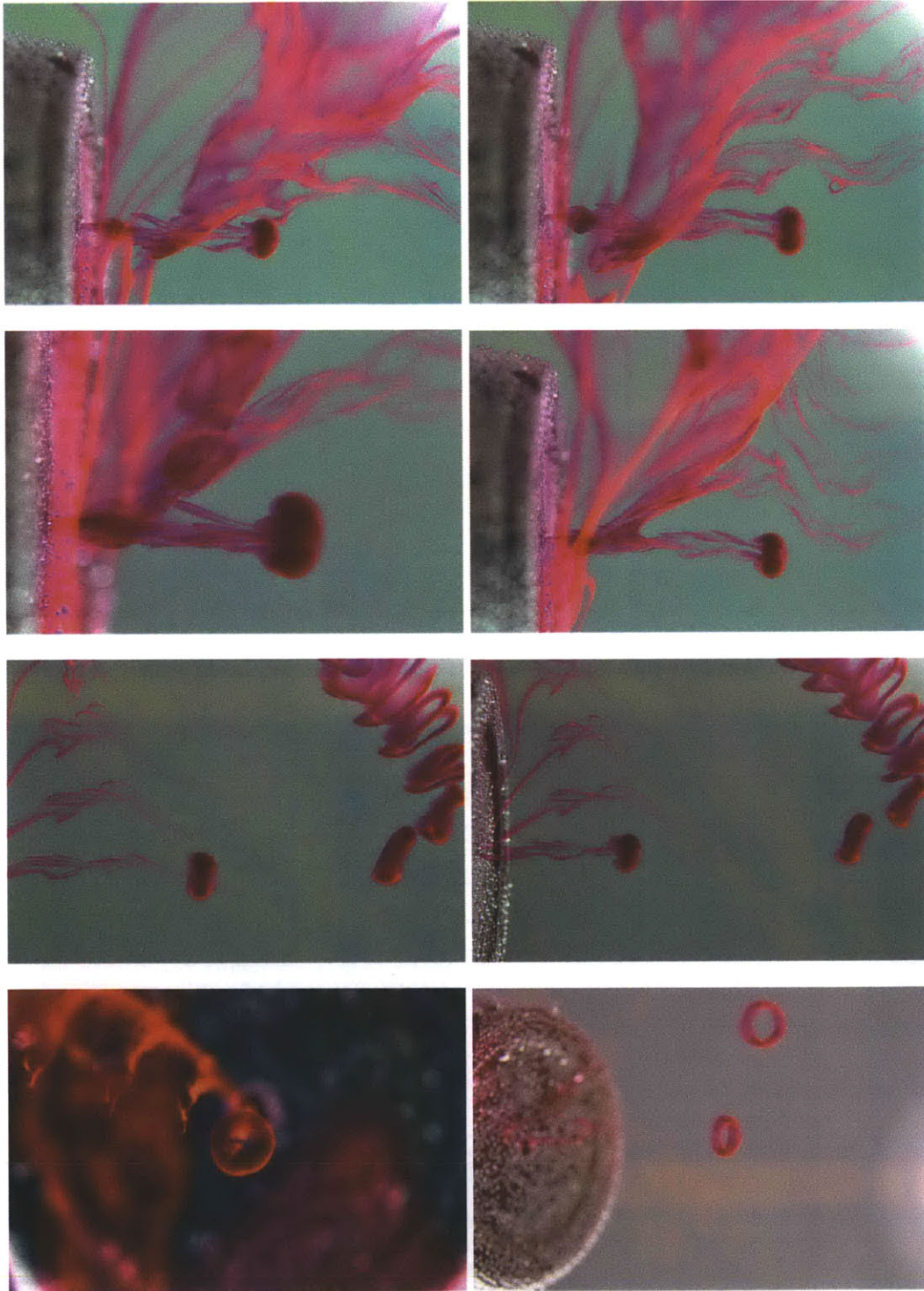
104

Figure D-2: Synthetic jet producing vortex rings. These images and videos were made with a Nikon D90 and a Nikkor 60mm micro lens which has a minimum focus distance of 8.64 inches.
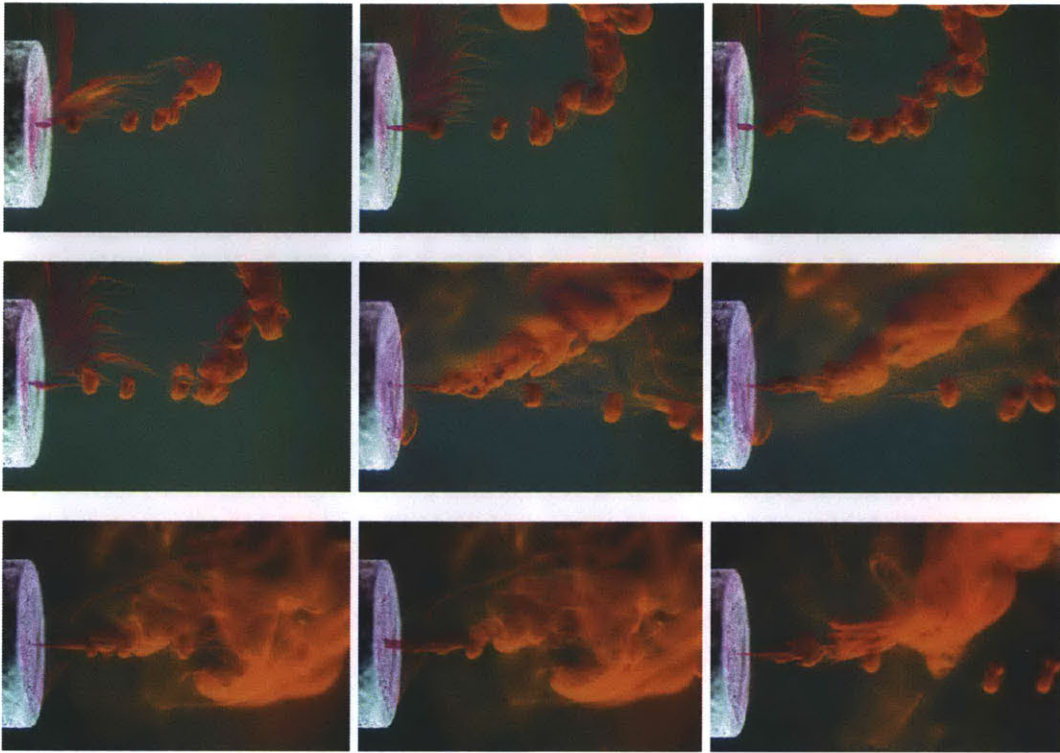
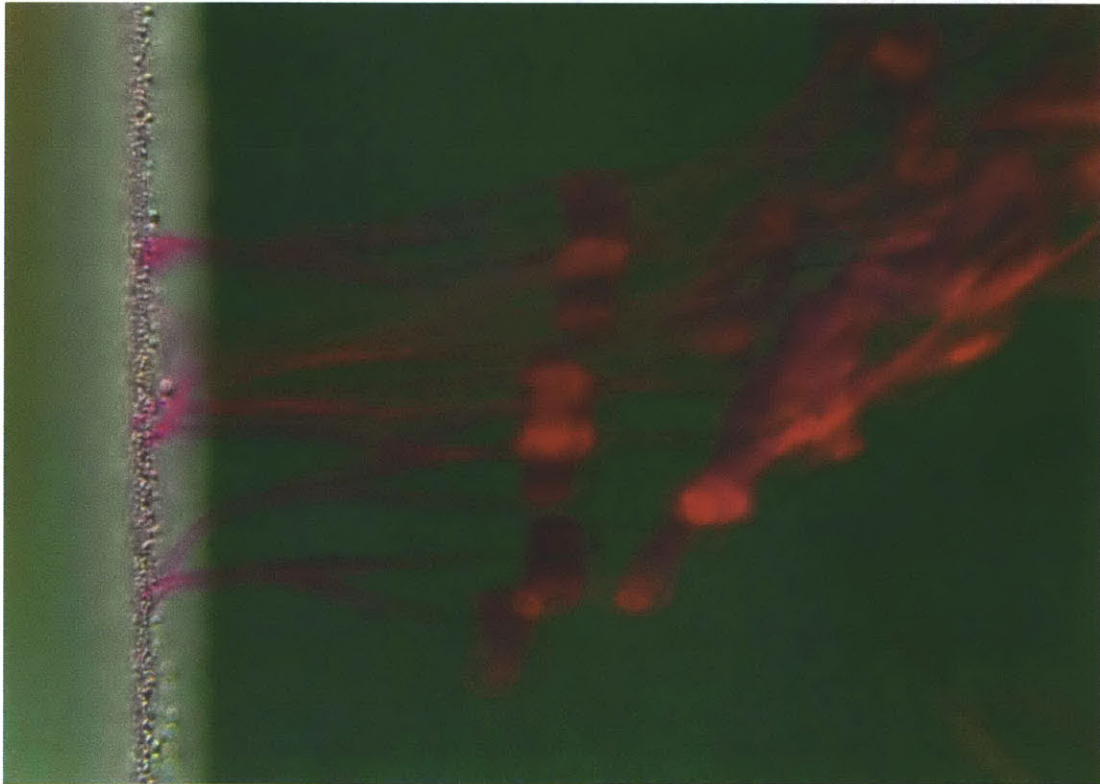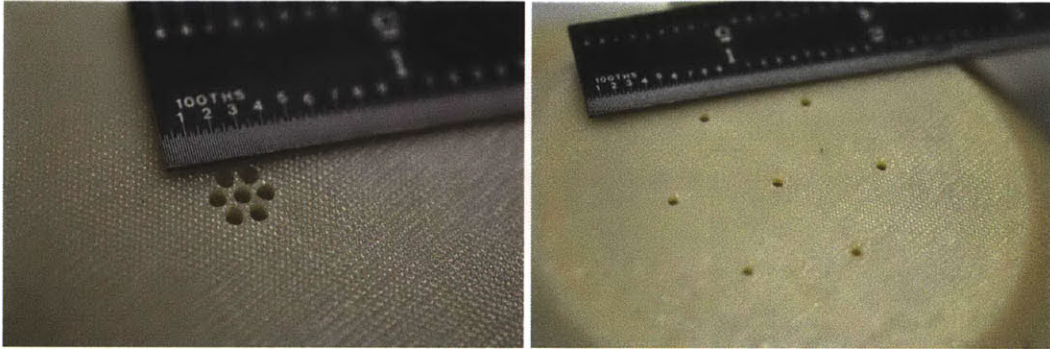Figure D-3: Vortex rings and jet formation using a rigid body synthetic jet.

Figure D-4: Multiple apertures spaced one diameter apart

Figure D-5: 3D print of cavity and apertures for a multiaperture synthetic jet.

(a) tightly packed apertures   (b) loosely packed apertures

Figure D-6: Synthetic jets with multiple apertures with different aperture spacing.
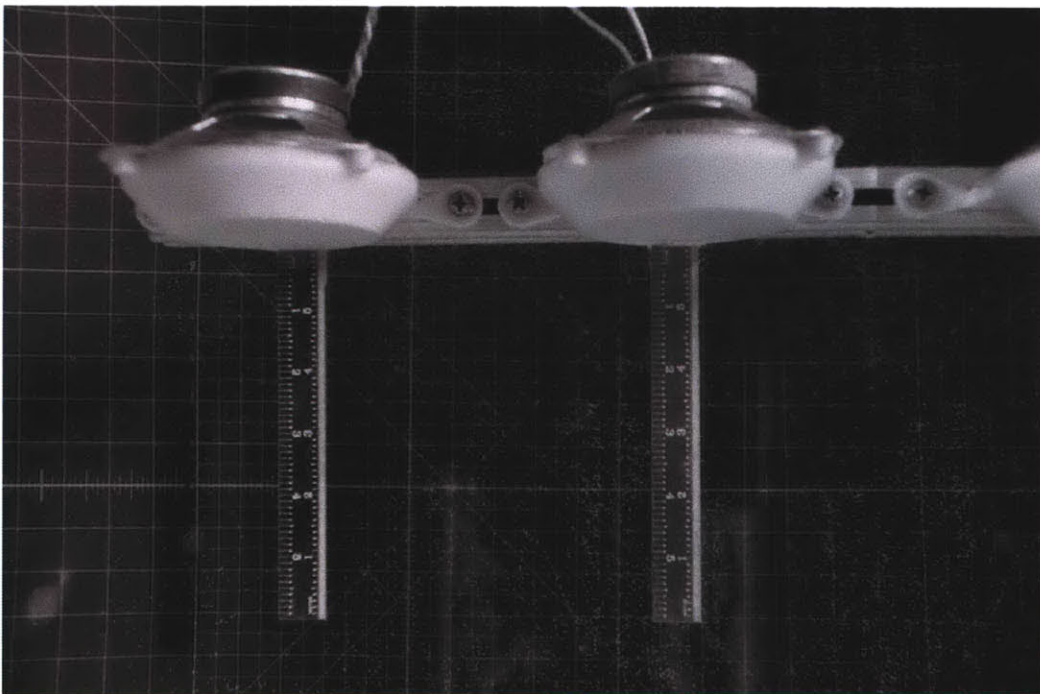
Figure D-7: Multiple apertures spaced one diameter apart.
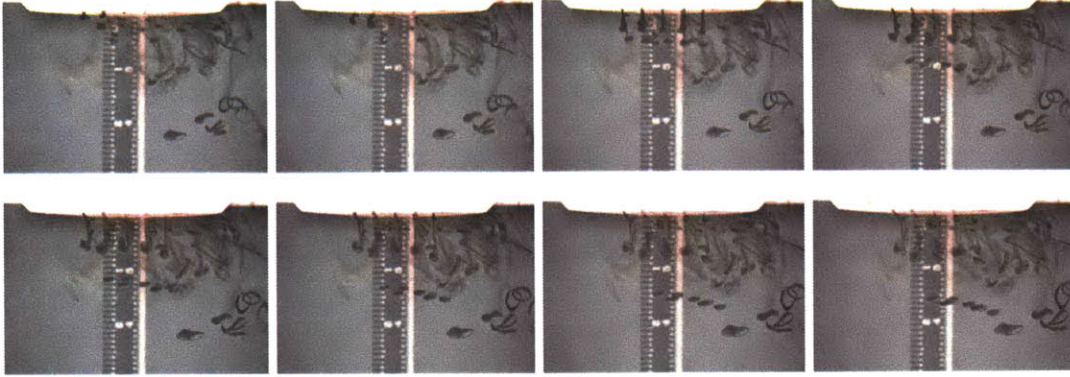
Figure D-8: Vortex rings created by loosely spaced apertures.
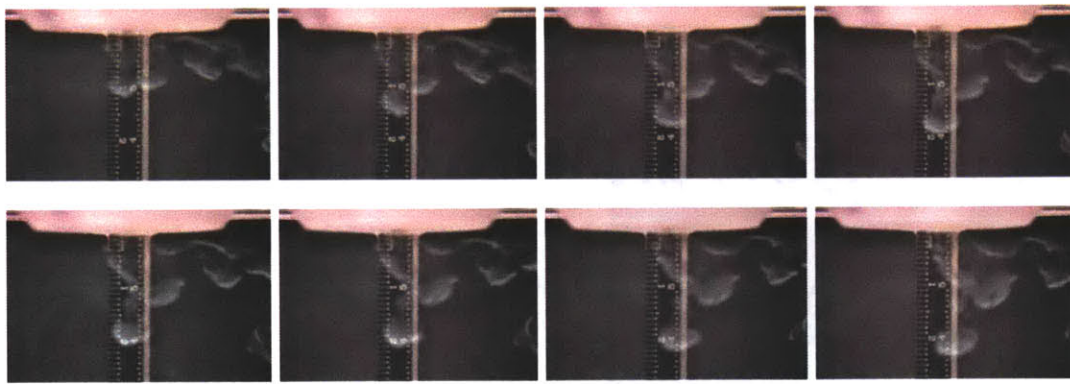
Figure D-9: Vortex rings created by closely spaced apertures.

D90 camera. The data plotted in figure 3-8 were captured with 24 frames per second 720 pixel high definition video and analyzed post experiment for precise readings.

Although the speaker coil is driven "instantaneously" by a sharp transition of the drive signal, the mechanics of the physical system have a slower response time. By using frame rate of the camera and distance traveled, the mean velocity of the jet could be calculated. The relationship of volume displaced to peak voltage of the drive signal was measured by ejecting fluid into a graduated cylinder sealed about the orifice.

Figure D-10: Setup to determine volume ejected as related to voltage.

Appendix E

An Asynchronous Routing Layer -

Asynchronous Packet Automata (APA)

Asynchronous Packet Automata is a routing algorithm for spatially distributed nodes assigned to a regular grid. It was first described as part of an extension of CBA's *Internet 0* coupled with an instrumentation reporting need in an unrelated project. The protocol was refined and fully defined for implemented in the "fault tolerant" demonstration (section 5.3).
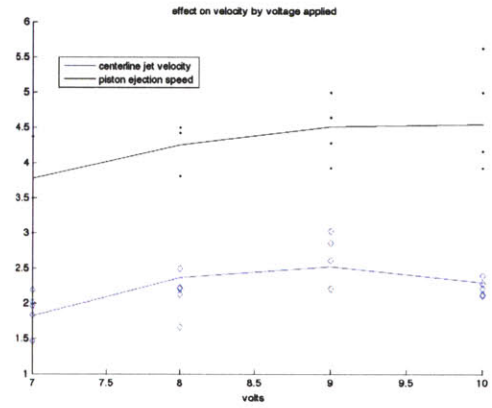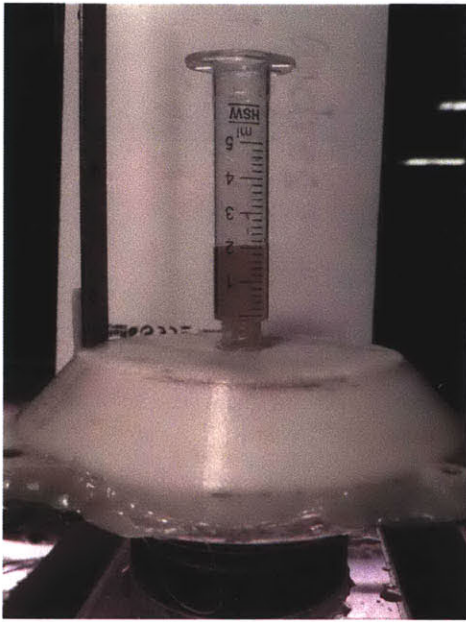
An APA packet consists of the *delivery path*, *return path*, and *payload*.

The delivery path is a list of travel directions in the order they are to be taken. As a travel direction is taken, the corresponding element on the list is removed from the delivery path and the source from which the packet arrived is added to the return path. When there are no travel directions in the delivery path, the remainder of the payload is processed for input to the control law program.

In addition to the cardinal travel directions *north*, *south*, *east*, and *west* (denoted with numbers 0-3 clockwise from north), the system includes three special directions: *self* (%), *all*, and *debug port*. In particular, all provides a mechanism for detecting which neighbors are present, which allows the system to periodically and dynamically map the array.

A consequence of the asynchronous design is each node does not have to buffer an entire packet instead only maintaining a constant amount of state, in this case,

the direction of travel and the current section within the packet. The communication scheme relies on a backpressure mechanism that blocks other nodes from sending bytes to it until it is ready. In the current implementation this is provided by request to send and clear to send signals from the UART, but many similar mechanism are available in other low level communication protocols.

Appendix F

A Cost Analysis of Many Small vs. a Few Big

There are several technical reasons why it may be advantageous to use many small distributed actuators rather than one very large actuator. It may be a matter of debate whether a "conformal" approach can have the same aggregate yield on national wind farm scales. Technical differences aside, we can all agree that some number of small turbines could be deployed together to generate an equal rated capacity as a (very) large turbine. In this section, I assume that the technical features of large and small turbines are identical and present a cost analysis comparing the purchasing strategy for turbines in unlimited and limited capital cases . Without relying on better or more clever "widgets" in either case, I show that fungible, easily scalable units can have a positive cost and time to acquisition impact.

For some motivation, I imagine that I am advising a locality or nation on an acquisition scheme for wind turbines to create an electric grid that does not yet exist. This imaginary country is the benefit of foreign goodwill and an initial gift will seed the energy production program. The Ministry of Energy knows that the energy demands will grow over time and wishes to implement a program that includes a capacity for self-sustainability and growth. There are two competing proposals that differ by the size of the turbine. In the programmable surfaces context the size difference between conventional turbines and conformal energy node is extreme; for this analysis the turbines are a factor of 10 apart.

The *large turbine proposal* makes a very large purchase of one turbine at the outset whereas the *small turbines proposal* makes a large purchase of enough small turbines to equal the total production capacity of the larger turbine. In reality the purchases should be sized to meet the estimated demand plus margin and since the operation ranges and failure rates differ with the turbines the simple production capacity approximation used here should be further refined. In both cases, the plan is to use the revenue from energy sales for operational costs and continue purchasing and installing more of the same sized turbines over time to meet the expected growth in demand.

Should the Minister of Energy invest in a steady smooth growth of smaller cheaper turbines or bank on large expensive turbines?

Treating the analysis as a straightforward investment, I evaluate the net present

value of two project proposals. I use standard assumptions of a discount rate of 15%, a system lifetime of 20 years, and that there is infinite market for the generated energy.

The project with smaller turbines is planned with a slow addition of turbines over time and thus more insensitive to electrical price volatility, our initial evaluation assumes all goes well as planned and the electrical energy price grows at a fixed 1.4% for the entire 20 years. Average costs, output ratings, and system efficiencies were compiled from a National Renewable Energy Labortory's 2006 report on wind turbine cost scaling models and quotes from a commercial wind turbine company (see appendix F.1 and F.2).

Generally speaking, if an investor has unlimited capital, he should by the bigger windmill project which gets more capacity online the fastest. As a straightforward investment, the largest possible windmill yields greater net present value over the lifetime of the turbine and because it generates a large capacity, the returns are faster and the investment is repaid sooner.

So long as all goes well.

Figure F-1: *"This turbine's 28-ton nacelle and 3-blade rotor assembly crashed to the ground scattering debris several hundred feet from the structure. Approximately 20-gallons of heavy oil spilled from the unit when its fluid reservoirs were damaged. The 11-turbine Searsburg, [VT] facility was brought online in 1997 and [...] the Zond Z-P40-FS turbines had an expected lifespan of 30-years."* IWAG Press Release dated October 2008, retrieved April 2011.

The risk involved with a system composed of only one turbine could be greater because any delays, damage or downtime halts revenue while a system composed of several turbines with one or more faults can continue to generate output.

However, in some cases a large loan with a good interest rate may be difficult to come by. Perhaps our imaginary nation must trade the energy infrastructure investment with investments in education, health, information and road infrastructure. In these

cases the amount of start up capital becomes much more important. The modular nature of smaller turbines means that a smaller array can be purchased initially and the system upgraded as more funds are available through revenue earnings.

Our imaginary nation has fixed startup capital allowance and an imperative for the fastest possible capacity growth from revenue. We start with an equal initial investment sufficient to purchase one large turbine and proceeds from energy sales are reinvested in additional turbines. Although the smaller turbines were more expensive per kWh, the smaller turbines were unit-wise cheaper so they could be acquired faster than the large turbines. The early adoption of these additional turbines resulted in years of smooth growth in energy capacity while the large turbine system capacity remained the same. Inspecting the total cost per year shows that in the limited capital case, a strategy of faster expansion through the purchase of smaller turbines is worse in capital efficiency. However, the time constant of expansion is smaller and can more readily adapt to price volatility and deliver more energy sooner. At the end of 20 years, in one analysis the strategy with smaller turbines generated nearly 9% more total capacity simply because the more affordable smaller turbines were able to come online sooner.

The results graphed in Figure F-2 and F-3 compare the deployments[1] where I found at least one reasonable condition when the approach of many-smaller acquisitions yielded a better result. These results are fragile and were highly sensitive to the assumptions about actual power produced, operating costs and risks, and the volatility of prices. In many cases, purchasing the larger turbine seemed much more straightforward for faster returns but the analysis can't capture those nation-building intangibles like local capacity. What's best is, after all, dependent on what is being optimized.

Without regard for risks (an arguably foolhardy approach), most results favored bringing as much generating capacity online as possible as quickly as possible without regard for the technology to accomplish it. Penalizing larger loans with larger interest rates (in the cases where the initial loan had to be repaid) was strongly subject to the

---

[1] I presume that there are no efficiency benefits or detriments with the use of the smaller turbines; for some this is charitable allowance while for others this is a pessimistic assumption.
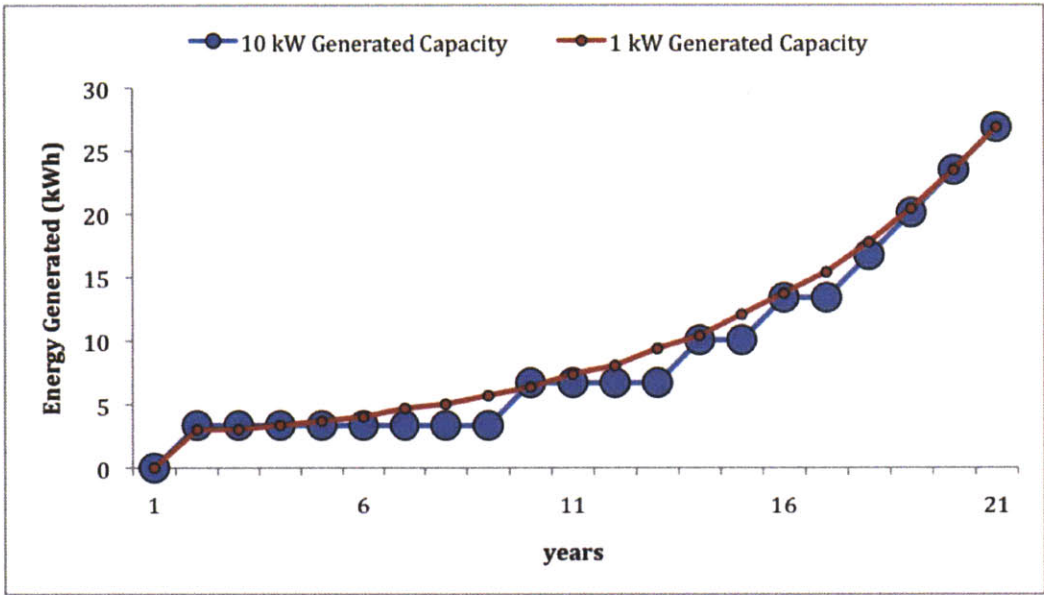
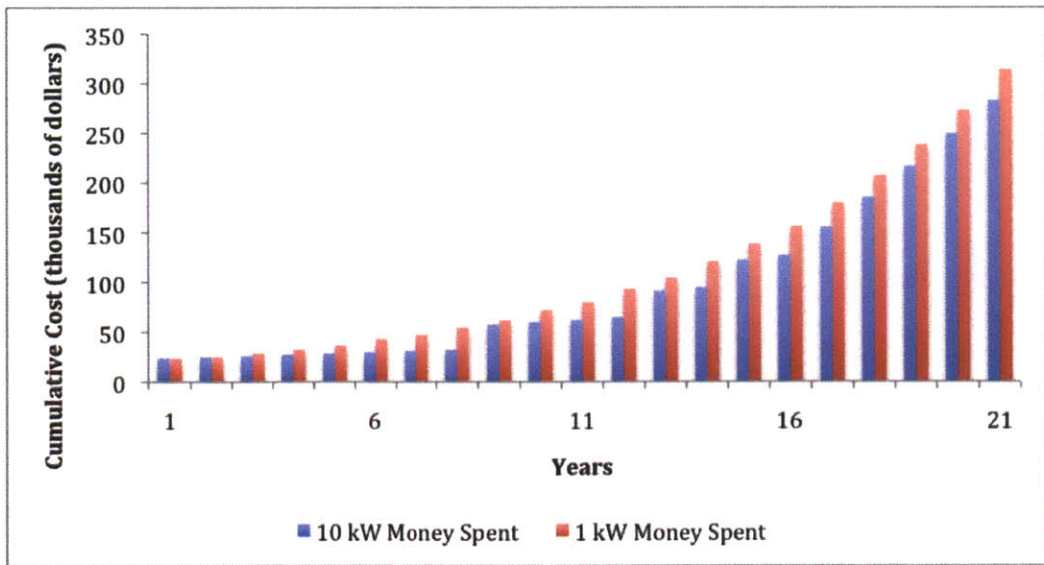Figure F-2: Comparison of Energy Generated over Time

Figure F-3: Comparision of Cumulative Cost over Time

117

details of interest, discount, and revenue rates. The analyses did not compare technologies, i.e., it did not take into account my unproven assertion that a larger number of smaller turbines can be installed more adaptably to the terrain and allowed to independently match very localized wind speed and direction, thus increasing the available generating time, nor the observation that smaller units are less costly to replace in the case of failure.

Our imaginary nation not only wants to provide electrical energy but build a different kind of capacity – human and resource capital. The higher operating costs and faster, more regular growth of the system with smaller turbines supports local skilled labor and provides regular opportunities to for workers operate the systems through its life cycle. Smaller turbines are also imagined to be less heroic to construct than massive turbines so a local supply chain for new and replacement parts could be developed. The policy implications from this conclusion are interesting beyond technical and financial terms.

F.1   1 kW Wind Turbine - Data Sheet and Quote

Manufacturer's Data Sheet with Quote. (2011)

Product Sheet

1 KW Hummer Wind Turbine (Off-Grid)

Dear Valued Customer,

- All products shown in this price list are covered by the manufacturer's warranties. We will gladly assist you with processing warranty claims for items purchased from us. We can also assist you with any replacement parts or accessories you may need to order
- We specialize in all sizes of wind turbines from micro & small sized wind turbines of 200Watt -10KW suitable for cabins, boats, residential & rural homes and small businesses up to larger sized industrial wind turbines sized from 20KW - 1.5 MW
- Larger sized wind turbines are custom-made for you to meet your unique specifications.
- We'll provide you with a FREE energy assessment to determine your needs & then put together a comprehensive package for you.
- Volume Discounts are available: Qty 10 (3%), Qty 20 (5%), Qty 50 (10%) & Qty 100 (15%).
- If purchasing multiple items, please contact us for a combined shipping quote. Multiple items will be charged shipping based on the total weight and the destination.

Wind Turbines (Up to 20 KW) Ship For FREE To Nearest Sea Port Dock in Canada!

Shipping Options (Canada):

1. In-store Pick-up – No shipping charges.
2. Ship Direct – Shipped direct to your door.
3. Dock Pick-up – Pick up at your nearest sea port dock **FOR FREE!** (Direct from MFR)
4. Custom Quote by email based on total weight of shipment & your location Contact Us by email.

Shipping Options (US):

1. Ship Direct – Shipped direct to your door.
2. Custom Quote by email based on total weight of shipment & your location Contact Us by email.

World Wide Shipping

•••

Wide Range Selection

•••

Great Service

•••

Installation Service

•••

Fast Turnaround

•••

For further information on any of the listed products please contact sales@mywindpowersystem.com

1 Kw Hummer Wind Turbine (Off-Grid)

1000 Watt (1KW) Wind Turbine (OFF-GRID)

Includes: Wind Generator, Inverter/Controller, Invert and 8m Tower

*Please note: Batteries are NOT included.

Complete system   US $2,672.00   click on price to convert to your currency

*Can add up to 500 watts of solar panels to this wind-solar hybrid system!
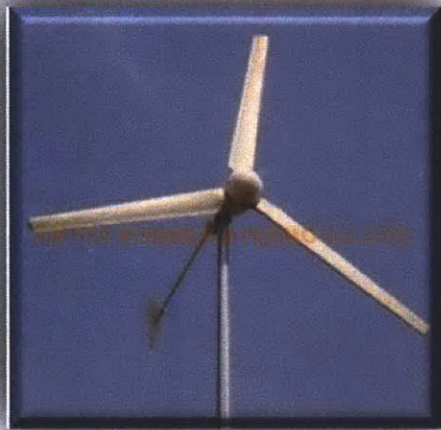
1Kw Hummer Inverter/Controller
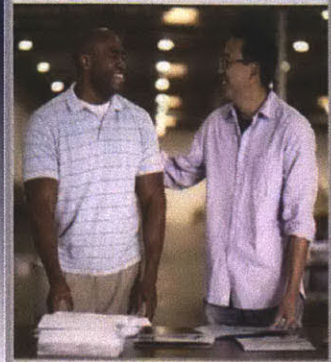
1 Kw Hummer Wind Turbine

tail wing | yaw shaft cover
tail pole | yaw shaft | generator
grid-tied inverter | off-grid inverter
blades | tower pin | pedestal | guy tower

Technical Specification:

Wind speed(m/s)	3	4	5	6	7	8	9	10	12	14	20
Power(W)	40	120	260	400	550	792	1050	1300	1892	2000	1530
Voltage(V)	50	50	52	57.14	61.1	66	70	76.5	86	90.9	80.53
Current(A)	0.8	2.4	5	7	9	12	15	17	22	22	19

Hummer 1000W Wind generator
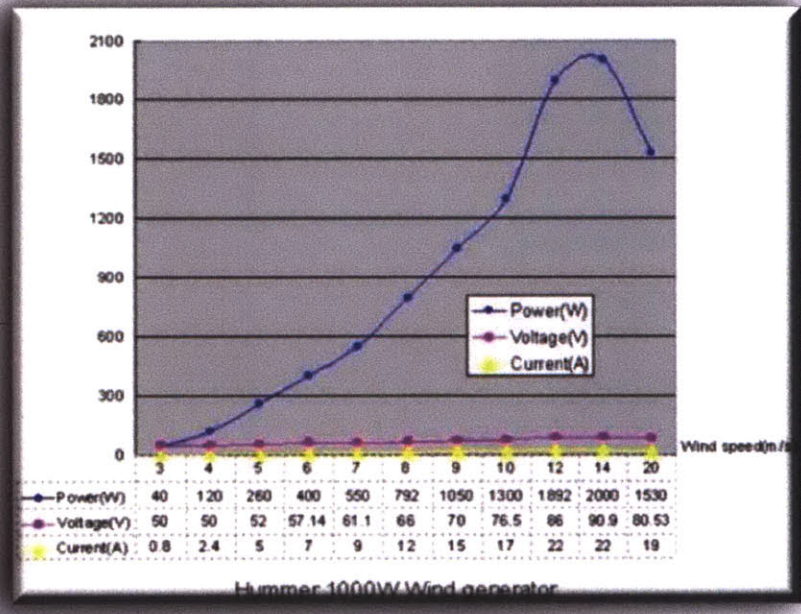
1m/s = 3.6 KM/H = 2.25 MPH
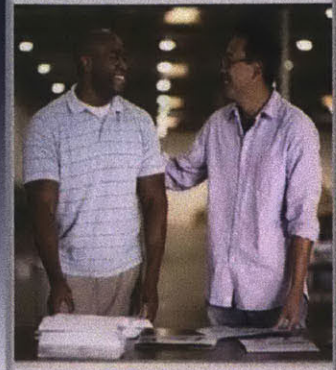
Technical Specification:

Power Data	1000W
Rated Output (W)	1000
Max output	2000
Charge Voltage(V)	DC 60V
Numbers of blade	3
Blade material	GRP
Blade diameter (m)	3.1
Start up wind speed (m/s)	3.0
Rated wind speed (m/s)	9.0
Rated rotate speed (r/min)	500
Wind Utilize Ratio (Cp)	0.42
Generator Efficiency	>0.8
Pole Diameter(mm)	Φ90
Tower Height (m)	8
Generator weight (kg)	15
Battery 12V 150Ah/200Ah (Batteries not included)	5 pcs

- Warranty Incl : 2 years for generator, 1 year for all other parts.
- *Optional 1 Year Extended Warranty (on generator) - $61.00 USD

Individual Component Prices :

- Hybrid Controller / Inverter - $ 963.39.00 USD
- 8M Guy Tower - $641.00 USD

NOISE INDEX: MODEL H3.1-1000W   LAeq=30 dBA 5m behind turbine@5m/s gusting

Parts and Accessories:

- Hummer wind turbine includes the body, tower plus accessories, and controlling units.
- Body includes: rotor blades, generator, yaw shaft, nose cone, tail pole, tail wing, etc.
- Tower and accessory: pole, nut, pedestal, guy wire, anchor, and cable, etc.
- controlling unit: controller ,inverter and load dumping. The generator, blades, nose cone,
- shaft, tail pole, tail wing, tower, anchor, etc are all spray-painted, galvanized and antisepticised.

Generator:

- This generator is the most advanced in the world, which has four patents.
- It is extremely light and small, high in efficiency--more than 0.78 of utilization ratio.

MyWindPowerSystem.com
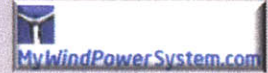
All Products Fully Warranted

Expert Advice

Free Estimates

World Wide Shipments

- Low in energy consumption, noise and speed-up wind speed (3m/s for 1000w).
- Swift running: hummer generator runs 1.5 - 3 times faster than other types of generators under equal conditions due to lightness, high efficiency and low resistance. As a result it can output more power than others.
- Swift charging: due to high efficiency and low wind start-up, the running time of hummer generator will be longer than conventional ones, and that is why it can charge batteries faster than others.

Hybrid Off-grid Controller/Inverter:

Control System:

- The power efficiency has been highly improved by using IGBT.
- With the automatic program optimization of MPPT the generator capacity is highly improved.
- LCD indicates information simultaneously.
- Real-time working power curve can be seen from the PC interface.
- Several optional communication interface includes power line carrier, RS485, wireless data transmission.
- Comprehensive protection function with highly reliability
- Wide AC voltage range
- Freely set working curve chart
- Simple, reliable and special plug connection

Rotor blade:

- Blades can typically be made of glass fiber reinforced plastic or aluminum alloy.
- The Hummer blade is designed by aerodynamic experts according to the airscrew structure and the wind power utilization ratio enhances up to 0.78.
- Most turbine blades have weak endurance through gale force type winds, they break easily in low temperature, the usable time in gale area is usually no more than 3 years, etc, Hummer has designed a new wind turbine blade, which can bear gale force winds.
- The hummer wind blade's successful application prolongs the entire wind turbine's service life to 10-15 years more. With the auto-deflection tech, it operates stable-quietly and soundlessly, and also brings enormous convenience for use and replacement.

Nose cone:

- The nose cone is made of reinforced aluminum alloy.
- It's located in front of blades to reduce the wind resistance. The generator is enclosed in the nose cone, which is favorable for heat dispersion.
- **Protection cover:** It is located between the blades and nose cone, and is made of reinforced aluminum alloy to further reduce the wind resistance and protect the generator.
- **Yaw shaft:** It is made of superior steel to integrate blades, the generator, tail pole, tail wing and tower. Inside the yaw shaft there are slip rings to prevent the cable from twisting.
- **Tail pole:** It is light with high intensity and made of manganese steel.
- **Tail wing:** It is made of stainless steel, inflexible, auto-deflection in high wind condition, reliable and sharp in speed limitation.
- **Tower:** It is made of carbon steel, with several sizes of outer diameter and height. They are anticorrosion, as well as UV-proof.
- **Guy wires & anchors:** Guy wire adopts button structure, and arrow like anchor, so it is much easier for installation
- **Surface coating & protection:** All the parts are static molded and then galvanized, so they are anticorrosion, UV-proof, crashworthy, fastness and will be fresh all year round.
- All the parts are made of high quality aluminum alloy and superior steel, which can be used in the temperature ranging from -45°C to 45°C, in the surroundings of high wet, sand salt or frost areas.

For further information please contact sales@mywindpowersystem.com
MyWindPowerSystem.com
- 23 Gatton Road
- Bristol BS2 9TF
- United Kingdom
- Tel.:+44 (0) 7962 420898
- Web www.MyWindPowerSystem.com
-
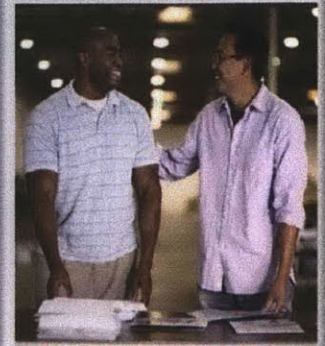
World Wide
Shipping

•••

Wide Range
Selection

•••

Great Service

•••

Installation
Service

•••

Fast Turnaround

•••

F.2 10 kW Wind Turbine - Data Sheet and Quote

Manufacturer's Data Sheet with Quote (2011)

Product Sheet

10KW Hummer Wind Turbine (Off-Grid)

Dear Valued Customer,

- All products shown in this price list are covered by the manufacturer's warranties. We will gladly assist you with processing warranty claims for items purchased from us. We can also assist you with any replacement parts or accessories you may need to order
- We specialize in all sizes of wind turbines from micro & small sized wind turbines of 200Watt -10KW suitable for cabins, boats, residential & rural homes and small businesses up to larger sized industrial wind turbines sized from 20KW - 1.5 MW
- Larger sized wind turbines are custom-made for you to meet your unique specifications.
- We'll provide you with a FREE energy assessment to determine your needs & then put together a comprehensive package for you.
- Volume Discounts are available: Qty 10 (3%), Qty 20 (5%), Qty 50 (10%) & Qty 100 (15%).
- If purchasing multiple items, please contact us for a combined shipping quote. Multiple items will be charged shipping based on the total weight and the destination.

Wind Turbines (Up to 20 KW) Ship For FREE To Nearest Sea Port Dock in Canada!

Shipping Options (Canada):

1. In-store Pick-up – No shipping charges.
2. Ship Direct – Shipped direct to your door.
3. Dock Pick-up – Pick up at your nearest sea port dock **FOR FREE!** (Direct from MFR)
4. Custom Quote by email based on total weight of shipment & your location Contact Us by email.

Shipping Options (US):

1. Ship Direct – Shipped direct to your door.
2. Custom Quote by email based on total weight of shipment & your location Contact Us by email.

World Wide Shipping

•••

Wide Range Selection

•••

Great Service

•••

Installation Service

•••

Fast Turnaround

•••

For full information on any of the listed products please contact sales@mywindpowersystem.com

MyWindPowerSystem.com and the MyWindPowerSystem logo are trademarks of MyWindPowersystem.com in the US and other countries

10KW Hummer Wind Turbine (Off-Grid)

(Hybrid: Wind & Solar)

10,000 Watt (10KW) Wind Turbine (OFF-GRID)

Includes: Wind Generator, Inverter/ Controller, and 14m Guyed Tower

*Please note: Batteries are NOT included.

Complete system US $22,069.00 click on price to convert to your currency

*Can add up to 3500 watts of solar panels to this wind-solar hybrid system!

- Individual Component Prices (Off-grid):
- Generator - $13,058.25 USD
- Hybrid Controller / Inverter - $9867.17 USD
- 14M Guy Tower - $3753.89 USD
- 14M Free Standing Tower - $7745.00 USD

- 2 Year Warranty on the generator and 1 Year on parts
- *Optional 1 Year Extended Warranty (on generator) - $451.52USD

All Products Fully Warranted
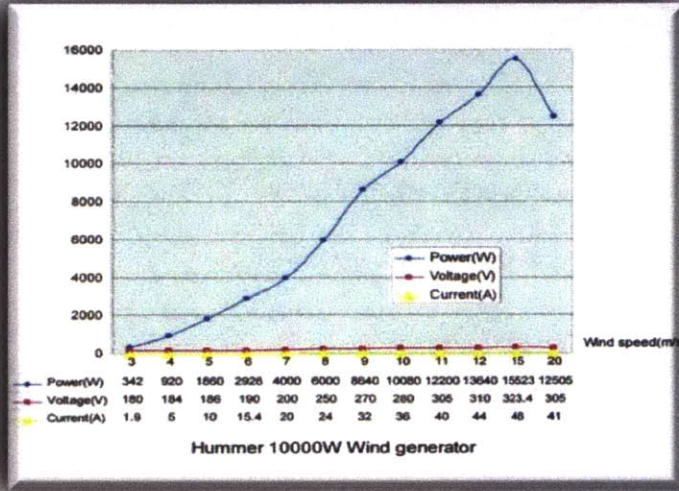
●●●

Expert Advice

●●●

Free Estimates

●●●

World Wide Shipments

●●●

10 KW Hummer Wind Turbine

Technical Specification:

	3	4	5	6	7	8	9	10	11	12	15	20
Power(W)	342	920	1860	2926	4000	6000	8640	10080	12200	13640	15523	12505
Voltage(V)	180	184	186	190	200	250	270	280	305	310	323.4	305
Current(A)	1.9	5	10	15.4	20	24	32	36	40	44	48	41

Hummer 10000W Wind generator

1m/s = 3.6 KM/H = 2.25 MPH

Model:	10,000W
Rated Output (W):	10000
Max output:	15000
Charge Voltage(V):	DC 300V
Numbers of blade:	3
Blade material:	GRP
Blade diameter (m):	8
Start up wind speed (m/s):	3
Rated wind speed (m/s):	10
Rated rotate speed (r/min):	180
Wind Utilize Ratio (Cp):	0.42
Generator Efficiency:	>0.8
Pole Diameter(mm):	Φ360
Tower Height (m):	14
Generator weight (kg):	150
12V 150Ah or 200Ah Battery (Batteries not included):	25 pcs

All Products Fully Warranted

●●●

Expert Advice

●●●

Free Estimates

●●●
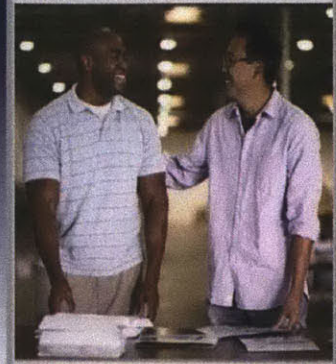
World Wide Shipments

NOISE INDEX:

MODEL H8.0-10000W   LAeq=34 dBA 5m behind turbine@5m/s gusting

Generator & Inverter:

Direct Drive Permanent Magnetic Generator

- Unique Design with Independent Intellectual Property
- Handsome-Looking
- Super Light Super Efficient with Low Rated Wind Speed
- Generator Placed Inside Nose Cone
- Widely Used in Same & Medium Scale Wind Farms, Residential, Commercial Areas

Hummer Off-Grid Inverter

- Specially Designed for Hummer Wind Turbine
- CPU Smart Control
- Highly Efficient & Reliable
- Compatible for Direct Linking with Solar Panels
- True Pure Sine Wave Output
- Stronger Compatibility for Driving Loads
- Multi Protection Against Overheat, Overcharge, Overdischarge, Overload etc.

For further information please contact sales@mywindpowersystem.com

- MyWindPowerSystem.com
- 23 Gatton Road
- Bristol BS2 9TF
- United Kingdom
- Tel.:+44 (0) 7962 420898
- Web: http://www.MyWindPowerSystem.com

All Products Fully Warranted

•••

Expert Advice

•••

Free Estimates

•••

World Wide Shipments

•••

THIS PAGE INTENTIONALLY LEFT BLANK

Bibliography

[1] Control of turbulent flow separation by synthetic jets. pages 1–9, May 2011.

[2] Assad Al Alam, Ather Gattami, and Karl Henrik Johansson. 13th International IEEE Conference on Intelligent Transportation Systems. In *2010 13th International IEEE Conference on Intelligent Transportation Systems - (ITSC 2010)*, pages 306–311. IEEE, 2010.

[3] A Alvarez-Calderon. A study of the aerodynamic characteristics of a high-lift device based on a rotating cylinder and flap, 1961.

[4] Alberto Alvarez-Calderon. CONVERTIPLANE AND APPARATUS THEREOF. April 1965.

[5] Alberto Alvarez-Calderon. VTOL AND THE ROTATING CYLINDER FLAP. *Annals of the New York Academy of Science*, 107(1):249–255, August 2006.

[6] J Beal. Cells Are Plausible Targets for High-Level Spatial Languages. In *Self-Adaptive and Self-Organizing Systems Workshops, 2008. SASOW 2008. Second IEEE International Conference on*, pages 284–291, 2008.

[7] William Joseph Butera. *Programming a paintable computer.* PhD thesis, libproxy.mit.edu, February 2002.

[8] Louis N Cattafesta III and Mark Sheplak. Actuators for Active Flow Control. *Annual Review of Fluid Mechanics*, 43(1):247–272, January 2011.

[9] D. R. Cichy, J W Harris, and J K MacKay. Flight Tests of A rotating Cylinder Flap on a North American Rockwell YOV-10 Aircraft. Technical report, North American Rockwell Corporation, November 1972.

[10] Thong Q. Dang and Peter R. Bushnell. Aerodynamics of cross-flow fans and their application to aircraft propulsion and flow control. *Progress in Aerospace Sciences*, 45:1–29, 2009.

[11] George de Bothezat. The General Theory of Blade Screws. *First Memoir. National Advisory Committee for Aeronautics. Preprint from Fourth annual report.*, January 1919.

[12] E de la Rosa Blanco, C A Hall, and D Crichton. Challenges in the Silent Aircraft Engine Design. In *45th AIAA Aerospace Sciences Meeting and Exhibit*, pages 1–20, January 2007.

[13] Alan H. Epstein. Distributed Propulsion: New Opportunities for an Old Concept. Technical report, December 2007.

[14] L Fingersh and M Hand. Wind turbine design cost and scaling model. ... *Laboratory Technical Report*, 2006.

[15] RE Froude. On the part played in propulsion by difference in pressure. *Transactions of the Institution of Naval Architects*, pages 390–423, 1889.

[16] Mohamed Gad-el Hak and D M Bushnell. Separation Control: Review. *Journal of Fluids Engineering*, 113(1):5–30, January 1991.

[17] N Gershenfeld, D Dalrymple, K Chen, A Knaian, F Green, E Demaine, S Greenwald, and P Schmidt-Nielsen. Reconfigurable Asynchronous Logic Automata (RALA). In *Proceedings of the 37th annual ACM SIGPLAN-SIGACT symposium on Principles of programming languages*, pages 1–6, January 2010.

[18] Neil Gershenfeld, kailang chen, and david allen dalrymple. Asynchronous Logic Automata. (12/422979).

[19] K Gilpin, A Knaian, and D Rus. Robot pebbles: One centimeter modules for programmable matter through self-disassembly. In *Robotics and Automation (ICRA), 2010 IEEE International Conference on*, pages 2485–2492, 2010.

[20] Ari Glezer and Michael Amitay. SYNTHETIC JETS. *Annual Review of Fluid Mechanics*, 34:503–529, 2002.

[21] AS Gohardani and G Doulgeris. Challenges of future aircraft propulsion: A review of distributed propulsion technology and its potential application for the all electric commercial aircraft. *Progress in Aerospace Sciences*, 2010.

[22] Cesare A. Hall, Emily Schwartz, and James I. Hileman. Assessment of Technologies for the Silent Aircraft Initiative. In *Journal of Propulsion and Power*, pages 1153–1162. Stanford Univ, Stanford, CA 94305 USA, 2009.

[23] J. I. Hileman, Z. S. Spakovszky, M. Drela, M. A. Sargeant, and A. Jones. Airframe Design for Silent Fuel-Efficient Aircraft. In *Journal of Aircraft*, pages 956–969. MIT, Dept Aeronaut & Astronaut, Gas Turbine Lab, Cambridge, MA 02139 USA, 2010.

[24] RD Joslin and CL Streett. Spatial Direct Numerical Simulation of Boundary-Layer Transition Mechanisms: Validation of PSE Theory. *Theoretical and Computational Fluid . . .*, 1993.

[25] Ronald D Joslin, Gordon Erlebacher, and M Y Hussaini. Active Control of Instabilities in Laminar Boundary Layers—Overview and Concept Validation. September 1996.

[26] HD Kim and GV Brown. Distributed turboelectric propulsion for hybrid wing body aircraft. *9th International Powered Lift . . .* , 2008.

[27] Hyun Dae Kim. Distributed Propulsion Vehicles. In *27TH INTERNATIONAL CONGRESS OF THE AERONAUTICAL SCIENCES*, pages 1–11. NASA Glenn Research Center, June 2011.

[28] AN Knaian. Design of programmable matter. 2008.

[29] Y Kubo. Suppression of wind-induced vibrations of tall structures through moving surface boundary-layer control. *Journal of Wind Engineering and Industrial Aerodynamics*, 61(2-3):181–194, July 1996.

[30] P F Linden. The efficiency of pulsed-jet propulsion. *Journal of Fluid Mechanics*, 668:1–4, 2011.

[31] Vernard E Lockwood and Linwood W McKinney. Lift and Drag Characteristics at Subsonic Speeds and at a Mach Number of 1.9 of a Lifting Circular Cylinder with a Fitness Ratio of 10. Technical report, Langley Research Center, December 1959.

[32] JKL MacKay. Boundary layer control device for tilt rotor configuration. (5236149), 1993.

[33] Norman Margolus. CAM-8: a computer architecture based on cellular automata. Technical report, December 1993.

[34] W McCarthy. Programmable matter. *Nature*, 2000.

[35] S Mittal. CONTROL OF FLOW PAST BLUFF BODIES USING ROTATING CONTROL CYLINDERS. *Journal of Fluids and Structures*, 15(2):291–326, February 2001.

[36] V J Modi, F Mokhtarian, T Yokomizo, G Ohta, and T Oinuma. Bound vortex boundary layer control with application to V/STOL airplanes. *Fluid Dynamics Research*, (1-4):225–230, September 1988.

[37] Vinod J Modi and Ayhan Akinturk. Effect of Momentum Injection on Drag Reduction of a Barge-like Structure. In *Proceedings of The Twelfth (2002) International Offshore and Polar Engineering Conference*, pages 295–302. University of British Columbia, May 2002.

[38] VJ Modi. Moving surface boundary-layer control: A review. *Journal of Fluids and Structures*, 11(6):627–663, 1997.

[39] VJ Modi, F Mokhtarian, MSUK FERNANDO, and T Yokomizo. Moving Surface Boundary-Layer Control as Applied to 2-Dimensional Airfoils. *Journal of Aircraft*, 28(2):104–112, 1991.

[40] VJ Modi, SR Munshi, G Bandyopadhyay, and T Yokomizo. High-performance airfoil with moving surface boundary-layer control. In *Journal of Aircraft*, pages 544–553. Univ British Columbia, Dept Mech Engn, Vancouver, BC V6T 1Z4, Canada, 1998.

[41] VJ Modi and ML Seto. On the dynamics and control of fluid-structure interaction instabilities. ... *of the International Offshore and Polar* ... , 1997.

[42] VJ Modi, E SHIH, B YING, and T Yokomizo. Drag Reduction of Bluff-Bodies Through Momentum Injection. *Journal of Aircraft*, 29(3):429–436, 1992.

[43] VJ Modi and T Yokomizo. On the Boundary-Layer Control Through Momentum Injection - Studies with Applications. *Sadhana-Academy Proceedings in Engineering Sciences*, 19:401–426, 1994.

[44] F Moktarian and V J Modi. Fluid Dynamics of Airfoils with Moving Surface Boundary-Layer Control. *JOURNAL OF AIRCRAFT / AIAA*, 25(2):163–169, February 1988.

[45] S R Munshi, V J Modi, and T Yokomizo. Fluid dynamics of flat plates and rectangular prisms in the presence of moving surface boundary-layer control. *sciencedirect.com*, 79, January 1999.

[46] Valery L Okulov and Jens N Sørensen. Refined Betz limit for rotors with a finite number of blades. *Wind Energy*, 11(4):415–426, July 2008.

[47] LaTunia G Pack and R D Joslin. Overview of Active Flow Control at NASA Langley Research Center. *Smart Structures and Materials 1998: Industrial and Commercial Applications of Smart Structures Technologies / SPIE*, 3326:202–213, 1998.

[48] Adnan Qayoum, Vaibhav Gupta, P K Panigrahi, and K Muralidhar. Influence of amplitude and frequency modulation on flow created by a synthetic jet actuator. *Sensors and Actuators A: Physical*, 162(1):36–50, July 2010.

[49] WJM Rankine. On the mechanical principles of the action of propellers. *Transactions of the Institution of Naval Architects*, pages 13–39, 1865.

[50] AK Sehra and W Whitlow. Propulsion and power for 21st century aviation. *Progress in Aerospace Sciences*, 2004.

[51] Khurshid Shahid, S. L. Lan, and M. Sun. Aerodynamic Forces of Micro Rotors at Low Reynolds Number. In *PROCEEDINGS OF THE INTERNATIONAL CONFERENCE ON MECHANICAL ENGINEERING AND MECHANICS*, pages 869–874, November 2007.

[52] Barton L Smith and Ari Glezer. The formation and evolution of synthetic jets. *PHYSICS OF FLUIDS*, 10(9):2281, 1998.

[53] O. Stalnov, A. Kribus, and A. Seifert. Evaluation of active flow control applied to wind turbine blade section. *Journal of Renewable and Sustainable Energy*, 2(6):, 2010.

[54] Kelly R Sutherland. *Form, function and flow in the plankton: Jet propulsion and filtration by pelagic tunicates*. PhD thesis, April 2010.

[55] T TOFFOLI and N MARGOLUS. Programmable Matter - Concepts and Realization. *Physica D*, 47:263–272, 1991.

[56] E Torenbeek and H Wittenberg. *Flight Physics: Essentials of Aeronautical Disciplines and Technology, with Historical Notes*. Springer, 1 edition, July 2009.

[57] V T Truong. Drag reduction technologies. Technical report, Aeronautical and Maritime Research Laboratory, Australia, June 2001.

[58] Frank M White. *Fluid mechanics*. McGraw-Hill Science/Engineering/Math, 2003.

[59] D You and P Moin. Active Control of Flow Separation Over an Airfoil Using Synthetic Jets. pages 1–11, May 2011.